
**Optimising biomass and peridinin production
in the immobilised cultivation of the
dinoflagellate *Symbiodinium voratum***



Inaugural - Dissertation
zur Erlangung des Doktorgrades
der Mathematisch-Naturwissenschaftlichen Fakultät
der Universität zu Köln

vorgelegt von
Dorothee Langenbach
aus Bonn

September 2016

Berichterstatter: Prof. Dr. Michael Melkonian
(Gutachter) Prof. Dr. Burkhard Becker

Tag der mündlichen Prüfung: 24.10.2016

Abstract

Dinoflagellates are a natural resource for unique secondary metabolites and pigments, which have great potential in the application in biomedical drug development, cosmetics and aquaculture. However, biotechnological cultivation of dinoflagellates in the common suspension-based closed photobioreactors (PBRs) has been proven to be problematic due to the sensitivity of the cultures against the associated shear forces. To overcome these and other constraints of suspension systems immobilised cultivation of the dinoflagellate *Symbiodinium voratum* is performed using a Twin-Layer porous substrate biofilm reactor (TL PSBR). In this thesis, the optimisation of the production of biomass and anti-oxidant peridinin, the main carotenoid of *S. voratum*, in TL PSBRs was investigated. In the optimisation process a maximal biomass productivity of 7.8 g m^{-2} was recorded at a light intensity of $600 \text{ } \mu\text{mol photons m}^{-2} \text{ s}^{-1}$ and 2 % CO_2 . Due to the persistent linear growth of the *S. voratum* biofilm a maximal biomass yield of 305 g m^{-2} was gained which is higher than in other biotechnological cultivated microalgae in the TL PSBR, like *Haematococcus pluvialis*. The peridinin production in *S. voratum* was enhanced by exposure of the biofilm to low light and high temperatures. While the peridinin yield (0.93 g m^{-2}) and productivity ($28.0 \text{ mg m}^{-2} \text{ d}^{-1}$) was highest at a light intensity of $100 \text{ } \mu\text{mol photons m}^{-2} \text{ s}^{-1}$, maximal peridinin concentration of 1.8 % of dry weight was obtained at $15 \text{ } \mu\text{mol photons m}^{-2} \text{ s}^{-1}$. Due to opposing conditions for biomass and peridinin production a two-step cultivation approach, composed of the combination of growth and peridinin enhancing phases was performed. Thereby, in this thesis, a maximal peridinin productivity of $51.4 \text{ mg m}^{-2} \text{ d}^{-1}$ was obtained. In addition up-scaling of the immobilised culture of *S. voratum* in a horizontal fleece-based TL PSBR, with a growth area of 2 m^2 , was shown to generate under comparable conditions as in the bench-scale experiment identical results. Therefore the TL PSBR presents an alternative biotechnological system for the large scale application of dinoflagellates.

Zusammenfassung

Dinoflagellaten stellen eine natürliche Quelle für einzigartige Sekundärmetabolite und Pigmente dar, die großes Potential in der Verwendung für biomedizinische Produkte, Kosmetika und Aquakulturen von Fischen und Meeresfrüchten haben. Allerdings hat sich die biotechnologische Kultivierung von Dinoflagellaten in den gängigen suspensions-basierten geschlossenen Photobioreaktoren (PBRs) als schwierig herausgestellt, da die Kulturen sehr empfindlich gegenüber den dort bestehenden Scherkräften sind. Zur Überwindung dieser und anderer Limitationen in Suspensionssystemen wurde eine immobilisierte Kultivierung des Dinoflagellaten *Symbiodinium voratum* an Hand des "Twin-Layer porous substrate biofilm reactors" (TL PSBR) vorgenommen. In dieser Arbeit wurde die Produktion von Biomasse und Peridinin, dem anti-oxidanten Hauptcarotenoid von *S. voratum*, im TL PSBR optimiert. Die maximale Biomasseproduktion von $7,8 \text{ g m}^{-2}$ wurde bei einer Lichtintensität von $600 \text{ } \mu\text{mol photonen m}^{-2} \text{ s}^{-2}$ und 2% CO_2 verzeichnet und aufgrund des konstanten linearen Wachstums des *S. voratum* Biofilms wurde ein maximaler Biomasseertrag von 305 g m^{-2} erreicht. Die Produktion von Peridinin in *S. voratum* wurde durch den Einsatz von geringem Licht und hoher Temperatur gesteigert. Während der Ertrag an Peridinin ($0,93 \text{ g m}^{-2}$) und die Produktivität ($28.0 \text{ mg m}^{-2} \text{ d}^{-1}$) bei einer Lichtintensität von $100 \text{ } \mu\text{mol photonen m}^{-2} \text{ s}^{-2}$ am höchsten war, wurde die maximale Peridinkonzentration von $1,8 \%$ bei $15 \text{ } \mu\text{mol photonen m}^{-2} \text{ s}^{-2}$ erreicht. Aufgrund der gegensätzlichen Bedingungen für optimale Biomasse und Peridinin Produktion wurde eine zweistufige Kultivierungsstrategie entwickelt, bestehend aus einer Wachstumsphase der Biomasse und einer sich anschließenden Akkumulationsphase des Peridinins. Damit wurde die maximale Peridininproduktivität von $51,4 \text{ mg m}^{-2} \text{ d}^{-1}$ in dieser Arbeit erreicht. Zusätzlich wurde durch Hochskalieren der immobilisierten Kultur von *S. voratum* in einem horizontalen Fleece-basierten TL PSBR, mit 2 m^2 Wachstumsfläche, identische Ergebnisse zu den Experimenten im Labormaßstab erzielt. Dies zeigt die Eignung des TL PSBRs als alternatives biotechnologisches System für die Massenkultivierung von Dinoflagellaten.

TABLE OF CONTENTS

1	Introduction	1
1.1	Dinoflagellates	1
1.1.1	<i>Symbiodinium voratum</i>	2
1.2	Peridinin	3
1.3	Potential applications of dinoflagellates	4
1.4	Biotechnological cultivation systems	7
1.5	Cultivation in suspension	7
1.5.1	Open ponds	8
1.5.2	Closed photobioreactors (PBRs)	9
1.5.3	Fermenters and heterotrophic growth	9
1.6	Immobilisation of microalgae	10
1.6.1	Twin-Layer porous substrate biofilm photobioreactors	11
1.7	Mass production of dinoflagellates	12
1.8	Aim of the thesis	13
2	Materials and Methods	15
2.1	Algae Culture and Conditions	15

2.1.1	Culture media	15
2.2	Bench-scale Twin-Layer PSBR	18
2.2.1	Harvesting in bench-scale	20
2.2.2	Experimental design and information	20
2.3	Up-scaling of the Twin-Layer PSBR	21
2.3.1	Vertical TL PSBR	21
2.3.2	Horizontal TL PSBR	22
2.3.3	Harvesting in up-scale TL PSBR	23
2.4	Cross-sectioning of the biofilm	24
2.5	Pigment analysis	24
2.5.1	Preparation of the peridinin standard	24
2.5.2	High-performance liquid chromatography (HPLC)	25
2.6	Spectrophotometric method for pigment analysis	26
2.7	Data analysis	27
3	Results	29
3.1	Light Experiments	29
3.1.1	First light experiment (Exp. L1)	29
3.1.2	Second light experiment (Exp. L2)	31
3.2	Effect of the inoculation density (Exp. D)	33
3.3	CO ₂ Experiments (Exp. C)	37
3.3.1	f/2 Medium (Exp. CF)	37
3.3.2	ASP 12 Medium (Exp. CA)	38
3.4	Summary of light and CO ₂ data	43
3.5	Temperature experiments (Exp. T)	46

3.6	Two-Step Approach (Exp. TS)	51
3.7	Media Experiment for up-scale systems (Exp. M)	56
3.8	Up-scaling of the Twin-Layer PSBR	58
3.8.1	Performance of <i>S. voratum</i> in the vertical up-scale TL PSBR	58
3.8.2	Performance of <i>S. voratum</i> in the horizontal up-scale TL PSBR	60
3.8.3	Paper as substrate layer	60
3.8.4	Fleece as substrate layer	63
3.9	Comparison of the investigated up-scale TL PSBRs	66
3.10	Photometric analysis of peridinin	67
4	Discussion	69
4.1	Application of dinoflagellates in biotechnology	69
4.2	Performance of <i>S. voratum</i> in the bench-scale Twin-Layer PSBR	70
4.2.1	Reproducibility of the TL experiments	70
4.2.2	Investigation of the lag phase	71
4.2.3	Effect of biofilm physiology	71
4.3	Optimisation of the bench-scale Twin-Layer PSBR	74
4.3.1	Effect of light	74
4.3.2	Effect of light in combination with CO ₂	74
4.3.3	Effect of temperature	76
4.3.4	Two-step approach	78
4.3.5	Media application in up-scale cultivation systems	79
4.4	Conclusions from the bench-scale Twin-Layer PSBR	80
4.5	Up-scaling of the <i>S. voratum</i> cultivation in the Twin-Layer PSBR	82
4.5.1	Comparison of the applied materials	84

4.5.2	Market potential of peridinin	85
4.5.3	Biotechnological application of <i>S. voratum</i>	87
4.6	Spectral reconstruction for peridinin analysis	88
5	Conclusions and Outlook	91
6	Appendix	93
	List of Tables	101
	List of Figures	103
	References	107

1 Introduction

1.1 Dinoflagellates

While the term dinoflagellates describes a variety of morphologies and lifestyles, dinoflagellates in general are unicellular organisms with a size of 10 to 100 μm and occur in plankton, benthos, as symbionts or even as parasites [Graham et al., 2009]. Thereby, dinoflagellates occupy fresh water, brackish and marine habitats [Fritsch, 1945; Tobias and Lariree, 2013]. With regard to feeding strategies dinoflagellates are very diverse and have been described to be photoautotroph, as well as heterotroph, even within one species [Taylor, 1980; Burkholder et al., 2008; Jeong et al., 2014b]. Since 50% of all dinoflagellate taxa are heterotrophic protists [Kofoid and Swezy, 1921; Schnepf and Elbrächter, 1992], species have been studied and described under zoological as well as botanical aspects and nomenclature [Spector, 1984]. The first record of dinoflagellates dates back to the 18th century, when a bioluminescent organism, now known as a member of the genus *Noctiluca*, was described by M. Baker [1753]. The basis of dinoflagellate taxonomy has been laid a few years later by O.F. Müller, who described the first dinoflagellate species [Müller, 1773].

The name dinoflagellate translates to the Greek word *dinò*, to whirl, and the latin word *flagellum* meaning whip. This refers to the typical morphology and movement of the cells. Most dinoflagellates possess, in at least one stage of their life cycle, two distinct flagella [Fritsch, 1945; Graham et al., 2009]. One is curled around the middle of the cell, called transverse flagellum, and one arises from the posterior end and moves like a whip [Taylor, 1980]. As a result from this arrangement the cells spin in a rotational fashion. A further special characteristic of dinoflagellates is the nucleus, called dinokaryon, in which the chromosomes are almost permanently condensed and possess no histones [Taylor, 1980; Fensome et al., 1993].

Dinoflagellates are most commonly known for two phenomena which are closely related to human health. First their ability to produce massive algal blooms, called brown or red tides [Anderson, 1995], and secondly the generation of toxins which are related to fish and shellfish poisoning [Bowden, 2006; Garthwaite, 2001]. These two effects can also occur simultaneous, which constitutes a serious risk for human and animal health [Anderson, 1995; García Camacho et al., 2007]. The effect of dinoflagellate toxins range from diarrhoea, severe nerve damage to even death [Bowden, 2006; Rodriguez-Navarro et al., 2007]. While these toxins have been studied and characterised for decades, new ones are still being discovered today [Holland et al., 2012; Garthwaite, 2001]. Well known representatives for toxic dinoflagellates are species of the genus *Alexandrium* and *Amphidinium* [Lippemeier et al., 2003; Parker et al., 2002; Kobayashi, 2008]. However, toxicity only occurs in a minority of dinoflagellates. It has been estimated, that from the known 5000 species of marine phytoplankton, 300 are able to form algal blooms [Daranas et al., 2001; Tobias and Lariree, 2013], while only 40-60 dinoflagellate species are reported to produce marine toxins [Smayda, 1997; Graham et al., 2009]. One of the non-toxic species is *Symbiodinium voratum*, which is the subject of this study.

1.1.1 *Symbiodinium voratum*

As the name implies the genus *Symbiodinium* has been first described as a ubiquitous endosymbiont for marine corals or other hosts [Freudenthal, 1962]. Nowadays *Symbiodinium* is one of the best studied symbionts and a main field of interest to investigate global warming and the consequential effect of coral bleaching [Takahashi et al., 2009]. This is of key importance since coral reefs are a unique ecosystem and have been estimated to economically support over 100 million people [WWF Australia et al., 2009]. Based on this symbiotic interaction and the colouration of the corals, symbiotic dinoflagellates, as *Symbiodinium*, were described as Zooxanthella (Greek zoon, animal; xanthos, yellow) [Freudenthal, 1962; Jeffrey, 1968], a generic term that is still in use today [Gottschling and McLean, 2013].

Even though the phylogeny of dinoflagellates is still under revision [Sausen, 2016], the genus *Symbiodinium* has been associated to the order Suessiales [Murray et al., 2005]. Interestingly, to date only two dinoflagellate genomes have been sequenced, while the first obtained genome was gained from the symbiont *Symbiodinium minutum* [Shoguchi et al., 2013] and the second one from *Prorocentrum minimum* [Ponmani et al., 2016].

However, besides symbiotic living organism of the genus *Symbiodinium*, the species *Symbiodinium voratum* has been described as a free-living dinoflagellate [Jeong et al., 2014a]. As known for dinoflagellates in general, also *Symbiodinium* is mixotroph and can exist photoautotroph or even heterotroph [Jeong et al., 2012, 2014a]. Their ability to feed phagotrophically on bacteria is expressed in the species name *voratum*, which is Latin for vorare, to engulf. *S. voratum* represents an economical interesting source of pigments, as it contains various carotenoids, from which the xanthophyll peridinin is the most interesting one.

1.2 Peridinin

Due to the ubiquitous abundance of dinoflagellates and diatoms, their main carotenoids peridinin and fucoxanthin [Johansen et al., 1974], are among the most abundant pigments of the world [Strain, 1976; Sugawara et al., 2007]. However, in contrast to fucoxanthin, peridinin occurs exclusively in dinoflagellates [Johansen et al., 1974; Bustillos-Guzman et al., 2004]. While the first isolation of peridinin was made by Schütt in an algal bloom of the genus *Peridinium* [Schütt, 1890], the first description dates back to 1935. In that year I. M. Heilbron declared the finding of a new lipid-soluble carotenoid, or lipochrome, called sulcatoxanthin from the sea anemone *Anemonia sulcata* [Heilbron et al., 1935]. However, this pigment was later shown to be identical with peridinin and originated from the symbiotic algae within the anemone [Strain et al., 1944].

Already in the same publication it has been stated, that peridinin is moderately resistant to oxidation [Strain et al., 1944]. Furthermore, peridinin was shown to

function inhibitory on lipid oxidation [Barros et al., 2001] and has been described as an anti-inflammation agent in mice [Onodera et al., 2014]. In addition to the anti-oxidant and anti-inflammatory capacities peridinin also possesses anti-cancerous properties, as it was shown to induce apoptosis in human colon cancer cells [Sugawara et al., 2007; Yoshida et al., 2007].

The main function of peridinin in dinoflagellates is to absorb light in the blue-green spectrum, as part of membrane bound light-harvesting complexes (LHCs) and soluble peridinin-chlorophyll *a*-protein complexes (PCPs) [Haidak et al., 1966], to close the green-gap of chlorophyll. PCPs have been investigated due to their highly efficient energy transferring properties early on [Haxo et al., 1976; Hata and Hata, 1982] and are still of interest now [Alexandre et al., 2007; Polívka et al., 2007; Kanazawa et al., 2014]. In 1989 the US patent on the PCP complex as a fluorescent label was accepted, which is especially suitable for diagnostic assays [Recktenwald, 1987]. The advantage of using the PCP in immunolabeling like fluorescence-activated cell sorter (FACS) is that the complex is due to the anti-oxidative properties of peridinin very stable and enhances the quality of the procedure by being water soluble, pH resistant and well separable from autofluorescence of the applied samples [Recktenwald, 1987; Haxo et al., 1976]. Therefore it is a high quality compound of the dinoflagellate *S. voratum* with a current value of 80-95 US \$ mg⁻¹ [Santa Cruz Biotechnology, catalogue nr.: sc-359908, Dallas, U.S.A., www.scbt.com, August 2016; AAT Bioquest, Sunnyvale, U.S.A., catalogue nr.: 2559, www.aatbio.com, August 2016]. However, a prerequisite for the production of peridinin and its associated products lies in the biotechnological cultivation of dinoflagellates.

1.3 Potential applications of dinoflagellates

Biotechnology of microalgae relies mostly on the utilisation of suspension-based cultivation systems, which have been proven to be problematic for the mass cultivation of dinoflagellates [Shah et al., 2014; Sullivan et al., 2003]. Therefore, the biotechnological

application of dinoflagellates is currently limited, even though their potential and their products have been studied intensively on laboratory scale.

As dinoflagellates are among the most important primary producers occurring in marine phytoplankton [Field, 1998; Graham et al., 2009], dinoflagellate biomass has high potential for the application in aquaculture, aiming on natural production of fish, molluscs and crustaceans. Due to presence of the polyunsaturated fatty acids (PUFAs), Eicosapentaenoic acid (EPA) and Docosahexaenoic acid (DHA), in dinoflagellates [Fuentes-Grünewald et al., 2013, 2009], the utilisation of dinoflagellate biomass can further enhance the quality of the obtained aquaculture products. For example the species *Symbiodinium microadriaticum* was shown to possess the second highest percentage [per dry weight] of total fatty acids and best growth in a screening of five different dinoflagellates [Mansour et al., 1999]. The aqua-farming of fish relies on the upbringing of larvae on microalgae which are subsequently used in the live feed of fish hatcheries. Therefore a further indication for the potential in aqua-farming is the ability of larvae to feed on the dinoflagellate species *Gymnodinium splendens* [Rodriguez and Hirayama, 1997]. Furthermore, high value aquaculture such as oyster and shellfish farming might benefit from feeding on dinoflagellate biomass directly. This was demonstrated in a study on the feed of bivalves on marine phytoplankton containing dinoflagellates which meet the nutritional requirements of the used filter feeder *Mytilus edulis* very well [Budge et al., 2001]. Overall aquaculture seems to be a promising market for the application for dinoflagellates since it has been estimated that 30 % of the global algal production is currently used in animal feed [Becker, 2007]. Besides the growing demand in aquaculture, the application of microalgae, as "super foods", for human consumption has steadily gained recognition in the last years.

In addition, in the last decade a increased demand for alternative fuels has lead to an exploitation of dinoflagellate biomass and lipids for potential fuel production [Fuentes-Grünewald et al., 2013, 2009]. While only the species of *Alexandrium minutum* and *Karlodinium veneficum* are applied in this field, in total 62 different kinds of dinoflagellates were found to possess valuable lipids, emphasising the unused

potential of dinoflagellate cultures [Fuentes-Grünewald, 2015; Fuentes-Grünewald et al., 2009; Kneeland et al., 2013].

Apart from the total biomass it is very common to extract natural compounds and secondary metabolites from dinoflagellates. The properties of dinoflagellate toxins, even though they are known to cause extensive harm for humans, have been shown to have beneficial applications. For example neosaxitoxin was identified to be a local anaesthetic and gonyautoxin is used in the treatment of anal fissures in medical trials [Garrido et al., 2005; Gallardo Rodriguez et al., 2007]. Also from the most prominent toxic algae of genus *Amphidinium* multiple compounds, called amphidinolide and amphidinols, have been identified as candidates for anti-fungal or anti-cancer drugs [Kobayashi, 2008; Echigoya et al., 2005]. Extracts from *Symbiodinium* sp., such as symbiodinolide and symbioramide, were shown to function as a Ca^{2+} ATPase activator or Ca^{2+} channel-opening agent and possess anti-leukaemic activity [Yoshida et al., 1992; Kita et al., 2007]. In different studies two undefined species of *Symbiodinium* were found to contain mycosporine-like amino acids (MAAs), which are known to have photo-protective properties [Banaszak et al., 2006; Bandaranayake, 1997]. Due to this, it can function as a UV absorbing agent in the cosmetic industry in make-up and sunscreen. In addition anti-inflammatory compounds, for example symbiospirols, symbioimine and neosymbioimine, from the symbiotic *Symbiodinium* sp. have been isolated [Kita et al., 2007, 2004, 2005; Tsunematsu et al., 2009]. Due to their functionality the application osteoporosis treatment was proposed [Kita et al., 2004]. Also carotenoids, like peridinin, are extracted from dinoflagellates which are utilised in biological and biophysical research [Carbonera et al., 2014; Schulte et al., 2010; Johansen et al., 1974; Bjørnland, 1990].

In summary, biomedical science is the best studied application for dinoflagellates so far, related to the fact that with the current technologies only small amounts of dinoflagellate cultures can be produced [Gallardo Rodríguez et al., 2010]. This makes their extracts a high value niche product and limits the current research on dinoflagellates to high cost consumables like drugs or cosmetics.

1.4 Biotechnological cultivation systems and their relevance for dinoflagellates

A core requirement for the exploitation of microalgae as a resource for commercial production lies in their biotechnological cultivation. As a consequence products become only available when a suitable mass cultivation technique has been identified. Since there is no such system for the majority of dinoflagellates available, their industrial applications are currently limited. This stands in clear contrast to macroalgae. These algae occur naturally in such quantities, that their biomass can directly be collected from their habitat. Due to this, coastal regions like France and Japan have a long history in using macroalgae for human consumption and application of their biomass and extracts in a variety of products, such as cosmetics. However, given that this is not an agricultural system, they have to be regarded as a naturally limited resource. Therefore the major downfall of macroalgae is, that with increasing demand, the supply of marine products becomes scarce. A current example is the high requirements for agar from the Rhodophyta *Gelidium*, which cannot be fulfilled [Callaway, 2015]. This underlines that the utilisation of an algal products for commercial applications is dependent on their availability and a controllable biotechnological cultivation system. Since the majority of microalgae is water-borne, the mass cultivation of microalgae is almost exclusively dependent on suspension.

1.5 Cultivation in suspension

In contrast to macroalgae, habitats from microalgae can be simulated by the usage of specialised growth media, enabling the cultivation of microalgae. The capability of microalgae cultivation enables the preservation of single species and strains, which is a prerequisite of the biotechnological exploitation of the resource microalgae. However, while small suspension cultures are efficient for culture maintenance, the application of liquid cultures in mass cultivation and biomass production is not trivial. With an increase of the culture volume the light penetration into the suspension becomes

limiting. Thereby algae close to the water surface of the medium obtain most of the light and grow, while further shading the underlying cells and hindering optimal growth in a suspension culture. Besides light, CO₂ is one of the most important limiting factors for microalgae growth, especially at high light intensities or densely grown cultures. To increase light and gas diffusion, cultures often have to be aerated or mixed. While mixing not only enhances the costs for mass cultivation, it also generates mechanical stress for the cultured algae. As a consequence only robust algae can be grown in such mass production systems, limiting the effective use of microalgae. A further disadvantage of suspension cultures is harvesting the microalgae. To achieve the separation of cells and water, the culture has in general to be filtrated, sedimented and subsequently centrifugated or spray dried [Chen et al., 2011; de la Noüe and Basseres, 1989; Bínová et al., 1998; Brennan and Owende, 2010]. Therefore the harvesting of microalgae from any suspension-based culturing system is always dependent on high input of energy and effort [Uduman et al., 2010].

1.5.1 Open ponds

Cultivation of microalgae in suspension has traditionally been achieved in larger scale by the application of open pond systems. The main advantage of the open ponds is the technical simplicity, since they are only composed of a artificial pond with a cartwheel or aeration system for culture mixing. Due to this design, open ponds have only been commercially realised for the production of two extremophile algae, *Arthrospira (Spirulina) platensis* and *Dunaliella salina*. The cyanobacteria *Arthrospira (Spirulina) platensis* presents the most prominent application of microalgae in the market of food supplement and health product [Radmann et al., 2007; Markou and Georgakakis, 2011]. Already Incas and Aztecs used *Arthrospira (Spirulina) platensis* grown in ponds as food source. However, these microalgae can only be grown in open suspension systems due to their niche ability [Del Campo et al., 2007]. The culture naturally grows at a pH of 9-11 and brackish water, hindering contamination to rise up and ensuring a selective growth of *Arthrospira (Spirulina) platensis*. The same holds true for *Dunaliella salina*, a known source for β carotene [Wegmann and Metzner,

1971]. The culture can be predominately grown in open ponds [Hejazi et al., 2004; Morowvat and Ghasemi, 2016] due to its high salt tolerance [Avron and Ben-Amotz, 1992].

However, a freshwater pond with regular medium and conditions in general is not controllable. Air- and waterborne contaminations can enter the system and are not removable once they have settled in the medium. Thus the cultivation of desirable freshwater algae like *Haematococcus pluvialis* is not performed in open ponds, but rather in closed photobioreactors. With regard to the cultivation of dinoflagellates, open ponds are not realised since the cultures are sensitive to the associated turbulences and shear forces [Dixon and Syrett, 1988; Sullivan et al., 2003].

1.5.2 Closed photobioreactors (PBRs)

In general closed photobioreactors (PBRs) rely on a stack of glass tubing and thus make more efficient use of area and light. Due to this they are technically more complex and since they are based on suspension the associated problems regarding contamination, shear stress and harvesting are persistent. Nevertheless these types of culturing systems are also applied in aquaculture and production of food supplements [Michels et al., 2014; López-Rosales et al., 2015; Leupold et al., 2013; Ugwu et al., 2008; Slegers et al., 2013]. Commercially realised systems for closed PBRs are currently operated for the production of *Haematococcus* in large scale systems in Israel and Portugal [Borowitzka, 1995; Carvalho et al., 2006]. For the application of dinoflagellates the species *Alexandrium minutum* and *Karlodinium veneficum* have been reported to be maintained in a bubble column photobioreactor [Fuentes-Grünwald et al., 2013].

1.5.3 Fermenters and heterotrophic growth

In order to overcome the common disadvantages in suspension cultures the focus of research has been shifted to immobilised and heterotrophic cultivation [Ogbonna et al., 1995; Shi et al., 1999; Liu et al., 2013]. Especially in biotechnological fields like biofuels or biohydrogen production the reports on growth of algae in fermenters has

been increasing [Wan et al., 2016; Liu et al., 2013; Shi et al., 1999; Ogbonna et al., 1995; Perez-Garcia et al., 2011]. In case of heterotrophic growth the ability of microalgae to switch from fixation of gaseous CO₂ to using organic carbon from the environment as energy source and for the production of light-independent metabolites, such as amino acids and lipids, is required. Additionally the requirements on the algae are to be fast growing in light-limited condition and resistance to mechanical stress [Gladue and Maxey, 1994]. The growth of heterotrophic dinoflagellates in fermenters for the production of biomass and lipids has been patented [Kyle et al., 1998] and has mainly been described for the species *Cryptocodinium cohnii* [Ganuza et al., 2008]. However, since the production of pigments is a light coupled process, this cultivation method cannot be applied in this project. Furthermore the technical setup of fermenters and operational cost of these stainless steel reactors is very high and often not profitable for algae cultivation.

1.6 Immobilisation of microalgae

An immobilisation is given when the cell is hindered, in natural or artificial way, to move independently in the liquid phase [Tampion and Tampion, 1987]. Traditionally the immobilisation is realised by enclosing algae in beads or gels, a technique that has been used for over 30 years [Chevalier and de la Noüe, 1985; Robinson et al., 1985; Tam and Wong, 2000; Mallick, 2002]. The aim is to facilitate access to algal products without harvesting of the algae itself. Even though research on entrapment of algae continues [Zeng et al., 2012], this approach does not solve the limitations in gas and light diffusions. In addition an up-scaling seems to be difficult due to the elaborate immobilisation technique. However, already in the late 19th century, the more evident way of immobilisation microalgae as a biofilm has been described [Beijerinck, 1890; Klebs, 1896]. Nevertheless, the approach was not pursued until the late seventies, when the work on attached biofilm reactors has been revisited [Hansford et al., 1978]. The described system of a rotating algal "disc" relies on at least temporary submerging of the cells in media, which increases detachment of the biomass into the bulk medium and lowers the productivity of the systems. These

systems are still studied today [Sebestyén et al., 2016; Blanken et al., 2014; Gross and Wen, 2014], but due to the submerging the algae culture is not immobilised and grows in the medium. In a horizontal orientation, the submerged biofilm systems are also referred to as algal turf scrubber (ATS) [Craggs et al., 1996] and have been studied with respect to waste water treatment with microalgae [Roeselers et al., 2008; Boelee et al., 2011, 2014; Mulbry et al., 2008; Wilkie and Mulbry, 2002]. A strict separation of medium and algae cells has been achieved by the application of the Twin-Layer (TL) system [Melkonian and Podola, 2003]. For algae cultivation the system is referred to as a TL porous substrate bioreactor (TL PSBR).

1.6.1 Twin-Layer porous substrate biofilm photobioreactors

The Twin-Layer technology is based on the combination of two layers, which enable the growth of algae apart from the bulk medium. Algae are applied on a fine porous substrate layer, which is supplied with medium by the underlying source layer. Requirements for the substrate layer are that the pores are large enough to allow a diffusion of micro- and macro nutrients while preventing the penetration of any cells larger than 1 μm . Thus the substrate layer functions as a barrier against contamination. The source layer has to be strongly hydrophilic to collect and transport the culture medium without washing off the attached biofilm. The theoretical groundwork for this technology had been developed by the work group of Professor Melkonian for Bio and Environmental Technology of microalgae, at the University of Cologne [Melkonian and Podola, 2003]. It was further on developed for algae immobilisation and culturing from small to up-scale with a multitude of freshwater and marine cultures [Nowack et al., 2005; Shi, 2005; Naumann, 2003; Benstein et al., 2014]. By immobilising the cells a monoalgal biofilm is established and so the culture surface is increased, resulting in an effective gas diffusion and enhancement of CO_2 supply to the cells. Since no aeration, mixing or agitation of the biomass is necessary, these type of biofilm photobioreactors provide a cost and energy efficient way to culture microalgae [Ozkan et al., 2012; Schnurr et al., 2016; Gross et al., 2015]. It has been estimated, that the current TL PSBR requires a volume of 36 - 250 L to produce 1 kg of

algae biomass, in comparison 2000 - 2850 L are needed in open pond systems [Podola et al., 2016].

With regard to harvesting, no centrifugation is needed, due to the low water content (70 - 85 %) of the biomass [Podola et al., 2016]. The maximal surface productivity of the system was recorded to be $31 \text{ g m}^{-2} \text{ d}^{-1}$ at $1000 \text{ } \mu\text{mol photons m}^{-2} \text{ s}^{-2}$ and the addition of CO_2 with the alga *Halochlorella rubescens* [Schultze et al., 2015]. Furthermore the setup of the Twin-Layer is technically fairly simple and the materials can be chosen according to the requirements. Thus the Twin-Layer has been studied for applications with environmental [Shi, 2005]; [Li, 2011] or commercial purposes, like aquaculture [Naumann, 2003; Naumann et al., 2013]. The Twin-Layer system makes it possible to cultivate multiple algae in parallel on limited space and provides stable cultivation conditions [Naumann et al., 2013]. Apart from the Twin-Layer PSBR and the work at the University of Cologne the principle has been applied for *Botryococcus braunii* [Cheng et al., 2013], *Acutodesmus obliquus* [Ji et al., 2014b] and *Pseudochlorococcum* sp. [Ji et al., 2014a]. To summarise, the greatest advantage of the Twin-Layer technology is that the limitations of suspension cultures in respect to light and gas diffusion, the omitting of shear stresses as well as the problematic harvesting can be overcome. With respect to the immobilisation of dinoflagellates it has been shown, that the species *S. voratum* has been successfully cultivated on a paper-based biofilm reactor and achieved a surface production rate of $11 \text{ g m}^{-2} \text{ d}^{-1}$ [Benstein et al., 2014]. However, no growth data on a glass fiber substrate layer in bench- and up-scale cultivation have been recorded.

1.7 Mass production of dinoflagellates

The first dinoflagellate cultures were established in the late 19th century [Stein, 1883] and the cultivation of the species *Gymnodinium fucorum* was initially reported on by Küster [1907]. Nowadays the maintenance of dinoflagellates is performed in suspension within classical culture vessels or tubular reactors in order to produce biomass or biomedical products like toxins [Fuentes-Grünwald et al., 2013; Wang

et al., 2015; Gallardo Rodríguez et al., 2007]. With these cultivation systems, only low concentrations of biomass and desired compounds could be obtained [Hu et al., 2006; Gallardo Rodríguez et al., 2010]. When an attempt for the up-scaling of cultures was performed the productivities were reduced in larger cultures [Beuzenberg et al., 2011; García Camacho et al., 2007]. Moreover the sensibility of most dinoflagellates to shear stress and turbulences which are associated to large scale cultivation in suspension, hinder the up-scaling of cultures further [Sullivan et al., 2003; Karp-Boss et al., 2000; Gibson and Thomas, 1995]. For the fragile alga *Protoceratium* a successful up-scale of the culture has been recorded, but only from a volume of 2 L to 15 L [Camacho et al., 2011]. Thus reports on the large scale production of dinoflagellates are scarce due to a lack of specialised cultivation systems [Shah et al., 2014]. Given this, dinoflagellate products are often obtained from natural sources, such as algal blooms, host organisms like corals or filter feeders [Rosic and Dove, 2011; Carlos et al., 1999; Warner and Berry-Lowe, 2006; Jeffery and Haxo, 1968]. The immobilisation of *S. voratum* in a simple biofilm PSBR has been shown to be a potent alternative for the cultivation of dinoflagellates [Benstein et al., 2014] and was therefore the focus of this thesis.

1.8 Aim of the thesis

The aim of the thesis was to further study the cultivation of the dinoflagellate *S. voratum* on the Twin-Layer PSBR. The focus was set on identifying the optimal culture conditions for the growth of *S. voratum* and finally the production of the highly valuable peridinin. The optimisation process was performed in a series of bench-scale TL PSBR experiments, with the aim to identify the effect of abiotic factors and media on the growth and peridinin accumulation of the biofilm. Furthermore the cultivation of the dinoflagellate *S. voratum* in different up-scale TL PSBRs was investigated and compared to bench-scale PSBRs in order to test whether the TL PSBR is a suitable mass cultivation system for *S. voratum*.

2 Materials and Methods

2.1 Algae Culture and Conditions

The dinoflagellate *Symbiodinium voratum* CCAC 0047, was obtained from the Culture Collection of Algae (CCAC). The strain had been isolated from phytoplankton samples collected on the Ille de Batz in Brittany, France, by Professor M. Melkonian in 1997. Therefore it is considered a free living strain.

The stock and back up cultures were grown at a light intensity of 50 $\mu\text{mol photons m}^{-2} \text{s}^{-1}$ in a 16 °C climate chamber. Prior to an experiment the cultures were scaled up to 500 mL, 1 - 2 L and subsequently 6 L Erlenmeyer flasks. The culture bottles containing 1 L or more were aerated with 2 % CO_2 and maintained in a 23 °C culture chamber in order to enhance algae growth further. The illumination in the climate chambers was based on fluorescent lamps (L36W/640i energy saver cool white and L58W/956 BioLux fluorescent lamps, Osram, Munich, Germany). All cultivations were performed with ASP 12 medium. The composition of the medium is given in the following section. For the pilot scale experiments, larger quantities of cultures were required. Thus the cultures were scaled from 2 L to 10 L glass vessels and were maintained with 2 % CO_2 and 23 °C. As light intensity in the 23 °C chamber 200 $\mu\text{mol photons m}^{-2} \text{s}^{-1}$ was applied. 3 - 5 days before each experiment the culture was refreshed with ASP 12 medium to obtain optimal growth conditions.

2.1.1 Culture media

The suspension cultures have been maintained in the medium ASP 12. If different media have been applied in for the experiments, it is stated within the correlating section. The composition of all applied media is given here.

Table 2.1: ASP 12 Medium

Stock Solution	Addition		Final
	for 1 L Stock	for 1 L medium	concentration
HEPES	238.1 g	3 mL	3.00 mM
NaCl		28 g	479.00 mM
KCl	60.0 g	11.6 mL	9.40 mM
MgSO ₄ × 7 H ₂ O		7 g	28.40 mM
MgCl ₂ × 6 H ₂ O		4 g	19.70 mM
CaCl ₂ × 2 H ₂ O	370.0 g	4 mL	10.00 mM
NaNO ₃	100.3 g	1 mL	1.18 mM
K ₃ PO ₄ × 3 H ₂ O	12.5 g	1 mL	47.00 µM
Na ₂ -Glycerophosphate	6.85 g	1 mL	31.70 µM
Na ₂ SiO ₃ × 9 H ₂ O	28.42 g	5.3 mL	528.00 µM
NTA (Titriplex I)	10.00 g	10 mL	523.00 µM
Vitamins		1 mL	
Trace metal solution		1 mL	

[McLachlan, 1973], modified after [McFadden and Melkonian, 1986]

The preparation of the trace metal and vitamin solutions is given in [McLachlan, 1973] and the homepage of the culture collection (www.ccac.uni-koeln.de). For one litre ASP 12 medium the according amount of the stock solutions was diluted in 1 L bidistilled water. The pH was set to 8.3 with NaOH and NaCl.

The original medium f/2 [Guillard and Ryther, 1962] is based on natural seawater but the medium in this thesis was prepared by a substitution with an artificial sea salt replacement, Tropic Marine Meersalz Classic (Tropic Marine, Wartenberg Deutschland). The measured pH was 8.3 and since the medium is not buffered, the pH was not

Table 2.2: Artificial f/2 Medium

Stock Solution	Addition for 1 L Stock [g]		For 1 L medium
Tropic Marine			36 g
NaNO ₃	75		1 mL
NaH ₂ PO ₄ × H ₂ O	5		1 mL
Trace metal solution			1 mL
Vitamins			1 mL

altered. In up-scale applications the f/2 medium was prepared with the commercial stock solution AlgaBoost (f/2 concentrate 200x, Wallaroo, Australia).

Seawater modifications

Selected experiments, see section 3.7, were conducted using natural seawater obtained from the Biologische Anstalt in Helgoland (Alfred-Wegener-Institut Helgoland) as basis for f/2 medium. The required stocks were added up to 1 L of medium as listed in table 2.2. The obtained seawater had a pH of 8.1. Overall three modifications of the seawater have been made, whereas 1 L of seawater was utilised as basis, the compositions are given in the following tables 2.3 - 2.5.

Table 2.3: SW1 Medium

Stock Solution	Addition for 1 L Stock [g]	For 1 L medium
Seawater		
NaNO ₃	100.3	1 mL
K ₃ PO ₄	12.5	1 mL

Table 2.4: SW2 Medium

Stock Solution	Addition for 1 L Stock [g]	For 1 L medium
Seawater		
MgSO ₄		7 g
NaNO ₃	100.3	1 mL
K ₃ PO ₄	12.5	1 mL
Na ₂ -Glycerophosphate	6.85	1 mL
Na ₂ SiO ₃ × 9 H ₂ O	28.42	5.3 mL
NTA (Titriplex I)	10.00	10 mL
Trace metal solution		1 mL
Vitamins		1 mL

In the third seawater modification the liquid fertiliser Salozene NPK (Liquid with micronutrients, Sandepan chimica s.r.l, Viadana, Italy) was used (Tab. 2.5). The applied amount was chosen to match the phosphate concentration of ASP 12. Furthermore it provides nitrogen in the form of urea. Since the fertiliser does not contain iron the trace metal solution was added to the SW3 medium.

Table 2.5: SW3 Medium

Stock Solution	For 1 L medium
Seawater	
Fertiliser	0.5 mL
Trace metal solution	1 mL

2.2 Bench-scale Twin-Layer PSBR

In order to apply the theoretical principle of the Twin-Layer, as it is described in section 1.6.1, into technical application the Bio and Environmental Technology group of Professor Melkonian, in cooperation with the workshop of the Biological Institute, has designed a bench-scale TL PSBR. The setup was established by Shi et al. [2007] and more information on the design are given by Schultze et al. [2015].

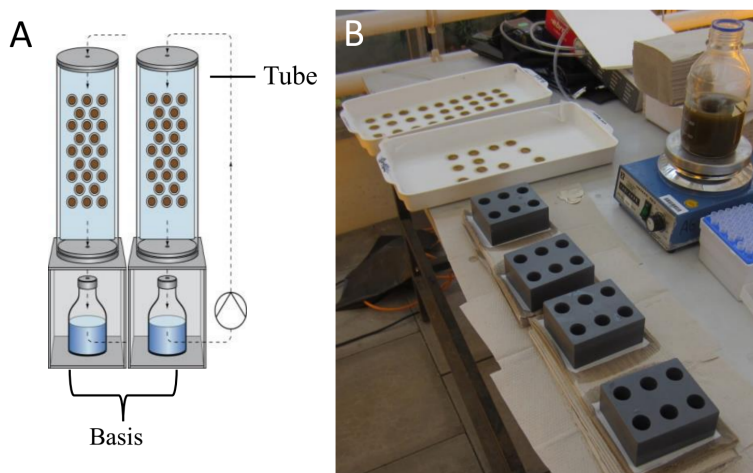


Figure 2.1: The bench-scale Twin-Layer PSBR. **A** Schematic drawing of the bench-scale TL PSBR [modified from [Schultze et al., 2015]]. **B** Inoculation setup for *S. voratum*.

As it is shown in the schematic drawing in figure 2.1 the bench-scale system consists of a PVC basis (30 cm x 30 cm) and transparent vertical tubes made of PMMA (Height: 50 cm, 12 cm in diameter). In this thesis glass fibre (80 g m², Isola AS, Eidanger, Norway) was chosen as substrate layer and commercial printing paper (Kölner Stadtanzeiger, 45 g m², obtained from DuMont Schauberg, printing plant, Cologne, Germany) was determined as substrate layer. In the setup a strip of glass fibre (65 cm x 10 cm), was applied to the top of the tube, which holds the substrate

layer. In case of the bench-scale TL experiments the biofilm grows on small discs of paper (diameter of 25 mm) in order to improve the handling and harvesting of the system. The medium was supplied via PVC tubing (Raulair E, Rehau AG + Co, Rehau, Germany) which was connected to a peristaltic pump (Ismatec, Cole-Parmer GmbH, Wertheim, Switzerland) by pump tubing (Spetec, Erding, Germany). The circulation of the medium was performed at a flow rate of 4.5 - 5.5 mL min⁻¹. The air was provided through an inlet at the basis of the reactor by aquarium pumps (Schego Prima, Schemel & Goetz GmbH & Co KG, Offenbach am Main, Germany). If additional CO₂ was provided to the system it was mixed with pressured air to a concentration of 2 % and a flow rate of 1 L min⁻¹. As the light source in all TL PSBR experiments sodium discharge lamps (SON-T AGRO 400W, Philips, Hamburg, Germany) were chosen. The light dark cycle for all experiments was set to 14/10 hours. While the outdoor green house has integrated time switches, the light cycle in the indoor green house was established by external timers (Theben Timer 26, Theben, Haigerloch, Germany). The tubes were arranged in front of the sodium discharge lamps according to the wanted light intensity. The light was measured with a photometer (LI-250A, LI-COR, Lincoln, NE, USA). For the light and temperature experiment filters for the reduction of light were used (Filter type 209, 210; LEE, Germany) in order to obtain the wanted range of light irradiances.

To prevent leakage and technical malfunction, Twin-Layer systems were installed and put into operation one day prior to inoculation. The biofilm had been generated as described by Naumann et al. [2013]. In figure 2.1 B the set up for the inoculation of the paper discs is depicted for the culture of *S. voratum*. After the preparation of the biofilm the paper discs were placed on top of the wet glass fibre mat in the bench-scale Twin-Layer system. The medium was exchanged every three days to prevent nutrient limitations of the cultures. In case of evaporation of the medium due to high temperature or light the loss was replaced with distilled water.

2.2.1 Harvesting in bench-scale

The bench-scale TL PSBR was harvested by removing a minimum of three replicate filters from different locations of the glass fibre. Thus taking environmental effects into account. The so obtained filters were then washed with distilled water for at least two minutes in order to remove salt from the biomass. This procedure had previously been verified by a comparison to centrifuged and washed biomass and a well established ammonium bicarbonate treatment by Benstein [2010]. All methods were proven to be sufficient in the removal of salt from a *S. voratum* biofilm or biomass (data not shown). The washed biomass was freeze dried for at least an hour in the ALPHA 1 - 4 LSC lyophilisator (Martin Christ Gefriertrocknungsanlagen GmbH, Osterode am Harz) to gain the dry weight and to prepare the biomass for the peridinin extraction without destroying the pigments. The biomass was analysed gravimetrically. Therefore the initial weight of the filter was subtracted from the gained result. In general harvesting was performed after initially three days and subsequently every two days. If a tube was partially dried out, or the long term duration of the experiment did not allow harvesting every two days, the sampling interval was adapted accordingly.

2.2.2 Experimental design and information

With regard to optimising the process of biomass and peridinin production in the dinoflagellate *S. voratum* a series of bench-scale TL experiments were carried out. Initially abiotic culturing factors such as light, CO₂ and temperature have been investigated. Subsequently a two-step process and an additional medium experiment were carried out. The goal was to mutually increase biomass and peridinin production. Finally the dinoflagellate culture had been grown in pilot photobioreactors in order to compare the gained data to bench-scale TL PSBRs and inquire information on how to up scale the cultivation of *S. voratum*. In general the bench-scale TL experiments had been performed in the indoor green house of the Biozentrum in Cologne, which is fully temperature controlled and kept around 23 - 25 °C.

Due to the high space requirement the light experiments (Exp. L1 and L2) were maintained in the large outside green house within the botanical garden of the University of Cologne. The set up was surrounded by a protective black foil, preventing a surplus of light from the outside. The biomass was harvested every third day. The first light experiment was performed at an average temperature of 20.6 ± 7.6 °C. The second light experiment (Exp. L2) was conducted at 24.2 ± 8.2 °C. It has to be noted that in comparison to the initial light experiment the percentage of peridinin per biomass was four times higher in the beginning of the experiment due to the suspension pre-culture. For both setups the artificial f/2 medium was applied.

2.3 Up-scaling of the Twin-Layer PSBR

All up-scaling experiments were carried out in the outside green house within the botanical garden of the University of Cologne. The aeration in the facility was maintained by windows located at the top of the green house and was automatised via a temperature sensor set to 25 °C. However, if this was not sufficient, the temperature in the green house varied. Due to this data loggers (HOBO Pendant, Onset Computer Corporation, Bourne, U.S.A) had been placed with the experiments to record the temperature and light. The media in the up-scaling experiments were prepared with tap water, which was also applied in the replacement of evaporation losses.

2.3.1 Vertical TL PSBR

The vertical TL PSBR has been successfully applied in the cultivation of microalgae by Naumann et al. [2013] and Shi et al. [2014]. In this thesis a proof of concept on the up-scaling of *S. voratum* in a vertical Twin-Layer system composed of paper and glass fibre is presented. The experiments were conducted in cooperation with B. Podola and B. Piltz. The up-scale TL PSBR was set up in the outdoor green house in April 2014 with a culture area of 1.5 m². On average an irradiation of 130 $\mu\text{mol photons m}^{-2} \text{s}^{-1}$ was recorded and the temperature on the layer was 27.3 ± 9.7 °C. As medium f/2 had been applied which was provided in a 150 L medium tank connected

to the reactor via irrigation drippers (Netafim Ltd., Tel Aviv, Israel). The medium was filtered by two modules with 200 and 100 μm pore size. The pre-culture was kept at 100 $\mu\text{mol photons m}^{-2} \text{s}^{-1}$ in 20 L Stedim bags (Sartorius AG, Göttingen, Germany) using artificial f/2 medium and was aerated via an aquarium pump. For the inoculation the suspension was concentrated to 500 mL and the biomass was then applied to the substrate layer by a spraying bottle (Gloria, Typ 133, Witten, Germany). The density of the inoculation has been determined by the placement of polycarbonate filters on the cultivation area prior to the spraying. Afterwards the filters were removed and processed as in the bench-scale TL experiments (Section 2.2.1). During harvesting samples from the top, middle and bottom of the TL PSBR were taken for each measurement.

2.3.2 Horizontal TL PSBR

The basic principle of the Twin-Layer was originally described as a horizontal system for microtiter plates by Nowack et al. [2005]. It has been applied in bench-scale systems by [Ji et al., 2014a; Zhang et al., 2014]. In this thesis it was scaled up to a horizontal PSBR of 2 m^2 , as shown in figure 2.2. The pre-culture was grown at 23 °C in aerated 10 L glass vessels. For the inoculation 30 L of cultures were concentrated up to 500 mL and the substrate layer was inoculated with a sponge.



Figure 2.2: Horizontal up-scale TL PSBR used in the immobilised cultivation of *S. voratum*. The growth area was 1 m^2 per side. The declination of the system is 13°.

As medium ASP 12 has been used, which was exchanged every four days. The evaporated water was replaced in accordance to the salinity of the medium (Salinity meter, pHenomenal, C03100L, VWR, Darmstadt, Germany). In total two reactors with different substrate layers were set up.

Paper-based horizontal PSBR

The first reactor was build up with paper as substrate layer and an underlying glass fibre sheet. The size of the surface was 100 cm x 100 cm. The set up was mirrored to two sites, referred to as left and right (see section, 3.8.3). Both sides were connected to the same medium supply and exposed to the same irradiance. On average the applied light intensity was $100 \pm 10 \mu\text{mol photons m}^{-2} \text{s}^{-1}$ and the temperature was $23.0 \pm 5.1 \text{ }^\circ\text{C}$.

Fleece-based horizontal PSBR

To further study and improve the construction of the up-scale system a fleece material, sawascreen 88AG010106 (60 g m^{-2}) was investigated. The material was developed and custom made for the Twin-Layer system (Sandler, Schwarzenbach/Saale, Germany). In total two compositions of the horizontal set up were compared. First to gain comparable results to the bench-scale TL PSBRs the Twin-Layer has been constructed by the combination of the fleece material with the glass fibre. Secondly the fleece is assembled only with the grid as source layer in order to simplify the setup. The light intensity during the experiment was $115 \pm 10 \mu\text{mol photons m}^{-2} \text{s}^{-1}$. The average temperature was $26.5 \pm 2,3 \text{ }^\circ\text{C}$. The results of the fleece-based PSBR are given in section 3.8.4.

2.3.3 Harvesting in up-scale TL PSBR

When working with the up-scale TL PSBR the biomass was harvested by scraping off the biofilm from a defined area. The obtained biomass was collected in 40 mL of distilled water. Subsequently the biomass was centrifuged for 10 min at $500 \times g$. The supernatant was discarded and the pellet was washed with distilled water again in order to remove salt residues from the biomass. After the second centrifuga-

tion (10 min, 500 × g), the pellet was vacuum-filtrated on polycarbonate filters and lyophilised. The biomass was analysed gravimetrically, as described in section 2.2.1.

2.4 Cross-sectioning of the biofilm

For a better visualisation of the algae biofilm cross-sections have been prepared for some of the performed experiments. This procedure was originally developed for the analysis of plant tissue, but has been established for immobilised microalgae by Kiperstok [2016]. In theory the biofilm is embedded in a preserving agent containing carbowax, which structurally protects the biofilm. For this purpose small pieces of the filter (3 × 3 mm²) were cut from the biofilm with a razor blade. Since paper was too thick to obtain clean cuts additionally three polycarbonate filters (47 mm, Nucleopore, Whatman, GE Healthcare Europe GmbH, Freiburg, Germany) were kept in the bench-scale TL PSBRs. These biofilm blocks were embedded in Tissue-Tek (Sakura Finetek U.S.A Inc., Torrance, CA, USA) and frozen at -30 °C. From the embedded samples 90 - 70 µm sections were produced via a cryostat microtome (HM500, Microm International, Walldrof, Germany). The sections were cut at -16 °C and subsequently photos were taken with a light microscope (Olympus, Hamburg, Germany).

2.5 Pigment analysis

2.5.1 Preparation of the peridinin standard

For the chromatographic quantification of the peridinin concentrations a calibration standard was required. The here used method for the isolation of peridinin was established as originally described by [Jeffrey, 1968] and was applied on *S. voratum* by Benstein et al. [2014]. Since the preparation of a standard requires high amounts of biomass a 6 L culture of the strain *Symbiodinium voratum* (CCAC 0047) had been maintained with aeration and 2% CO₂ supply. After 3 weeks the culture was dense enough for the pigment extraction as described in Benstein et al. [2014]. For estab-

lishing a calibration curve the spectrum of the peridinin extract in methanol was recorded photometrically (UV-2450, Shimadzu, Duisburg, Germany). The concentration was calculated by applying the volumetric absorption coefficient for peridinin: $E_{1\%}^{1\text{cm}}: 1360$ as recommended in the publication by Jeffery and Haxo [1968]. The calibration standard was prepared as described by Benstein et al. [2014].

2.5.2 High-performance liquid chromatography (HPLC) of dinoflagellate pigments

The samples were analysed by HPLC, which was carried out according to the original method of Rogers and Marcovich [2007] and which has been applied for *S. voratum* by Benstein et al. [2014]. The separation of pigments by liquid chromatography is based on the affinities of polar pigments to interact with mobile and stationary phase of column and solvents under high pressure. The separation of pigments arises according to their polarity and interaction with a reverse phase C 18 column (Spherisorb ODS-2, 5 μm particle size, 250 mm x 4.0 mm ID, packed by Dionex, Techlab, Braunschweig, Germany). In general the HPLC is build up by three components: the high pressure pump (L-6200 Intelligent Pump, Merck Hitachi, Darmstadt, Germany) designed to regulate and control the solvents, the detector (L-4200 UV-Vis detector, Merck Hitachi) which records the chromatographic information and converts it into electrical voltage and the LC system for the sample throughput. Within the LC system the applied reagents are brought together where the pre-column (Waters; Spherisorb ODS-2, Particle size 5 μm , 10 mm x 4.0 mm ID, packed by Dionex, Techlab, Braunschweig, Germany) and the C18 column are located. The analysis was performed with 100 μL extract, which was applied with a Hamilton syringe and let into the pressurized solvent stream via a reodyne injection valve. The linkage of the valve and pre-column was formed by a 50 μL sample loop, which supports a stable and reproducible sampling. The analysis of the pigments was carried out at a wavelength of 436 nm with the following three solvents as described by Rogers and Marcovich [2007]. Solvent A: 80:20 methanol: 0.5 M ammonium acetate (pH 7.2), solvent B: 80:20 acetonitrile: water, solvent C: ethyl acetate. In figure 2.3 a typical chromatogram of

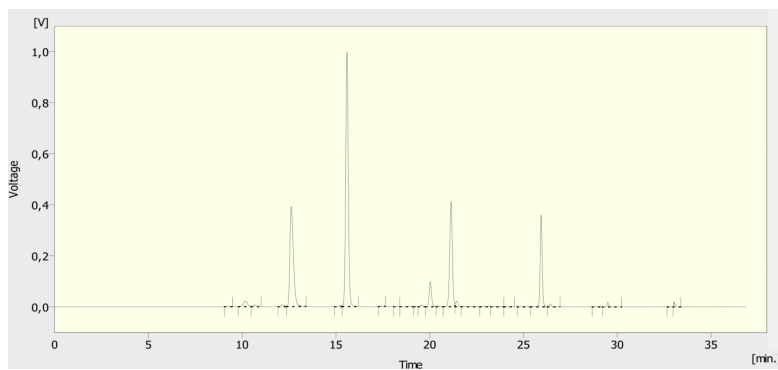


Figure 2.3: Chromatogram of *S. voratum*. Presented are the peaks of the pigments in the order they are eluted from the column: Chlorophyll *c*, peridinin, diadinoxanthin and chlorophyll *a*.

S. voratum is depicted. The data analysis had been performed by the Clarity software (Version 3.0.2.244).

2.6 Spectrophotometric method for pigment analysis

To find an alternative to the time- and cost-intensive procedure of HPLC for the determination of peridinin a spectrophotometric method was investigated.

In the visible wavelength regime *S. voratum* shows a strong absorption band as a result of the contribution of all its pigments. To differentiate each contribution individually the spectrum reconstruction method (SRCM) has been applied. This approach is more robust than the classical utilization of single wavelength equations for pigment determination [Naqvi et al., 1997]. More details on the method are given by Naqvi et al. [2004]. The approach makes use of reconstructing the total absorption spectrum of a pigment mixture by a linear combination of the single absorption spectra of all its contributing pigments [Naqvi et al., 2004]. The simulation is performed by linear least-squares fitting. In order to establish the method all contributing single spectra of the pigments present in *S. voratum* were required. Thus 1 L of suspension culture was concentrated and extracted in MeOH over night at -30 °C. The separation of pigments was performed by thin layer chromatography (TLC) as described by Benstein et al. [2014]. The gained extracts of the single pigments were analysed photometrically from 400 - 700 nm (UV-2450, Shimadzu, Duisburg, Germany). In total four main pigments of *S. voratum* were isolated and applied for the spectral reconstruction (Fig. 2.4 A).

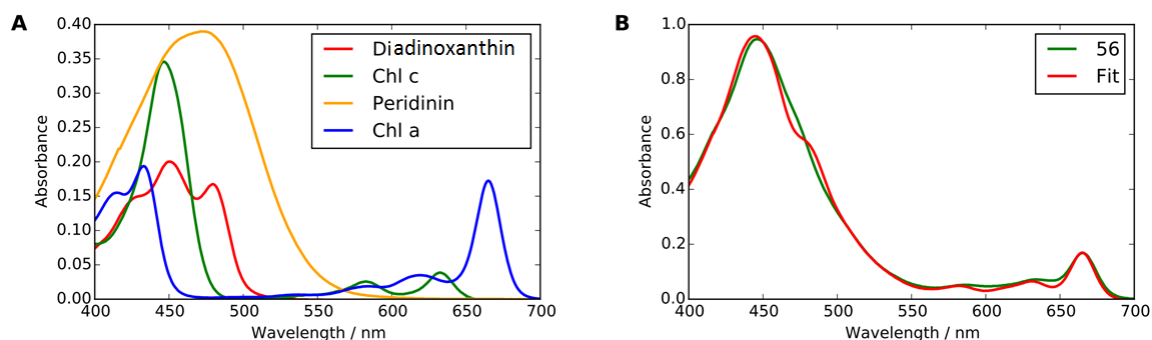


Figure 2.4: Measured and simulated absorption spectrum of *S. voratum* by the spectral reconstruction method. Presented are the single spectra **A** scaled according to their contribution. Measured total spectrum of a *S. voratum* biofilm (**B**, green line) in comparison to the fitted curve (**B**, red line) from the spectral reconstruction.

The software Phyton x,y (version 2.7.10.0) and the development environment spyder² (version 2.3.5.2) were employed to fit the single spectra to a simulated total spectrum. The used script is given in the appendix, chapter 6. In order to improve the linear combination the wavelength of 660 - 675 nm are fitted by the single spectrum of chlorophyll *a* only, since this is the predominant constituent. The wavelength of 400 - 550 nm are fitted by all other isolated pigments for an optimal fit.

For the actual photometrical analysis of a sample the alga pellet or biofilm is extracted in 5 mL MeOH over night at -30 °C and analysed photometrically from 400 - 700 nm. From the curve fit the concentration of peridinin can be retained in $\mu\text{g mL}^{-1}$. Overall 100 samples were analysed and employed in the evaluation of the method. To enhance the reliability of the method data from most experiments of this thesis have been applied. Therefore variations, in abiotic factors which can have an effect on the pigment composition, such as light, CO₂ content, temperature and media were included.

2.7 Data analysis

The data given in the shown figures represent the mean and standard deviation (SD) of a minimum of 3 replicates ($n = 3$). Data were recorded and gathered with Microsoft Excel 2013. Biomass and peridinin accumulation rates were obtained by fitting a linear

regression if the R^2 was > 0.90 . Statistic analysis was done via ANCOVA for comparing of slopes, one-way ANOVA and Tukey's multiple comparison test. The data are considered to be statistically different at a p-value < 0.05 . The asterisks indicate the threshold of the significance level. p-value < 0.001 , extremely significant, ***; p between 0.001 and 0.01, very significant, **; p between 0.01 and 0.05, significant *.

Considering the one-way ANOVA, when two or more samples are not distinguishable they are marked as one group (a). However, if one of the group members is found to be statistically identical with another but the others of the group are not, the corresponding label (ab) is given. For the statistics Graph Pad Prism 5 (GraphPad Software Inc. La Jolla, USA) was applied.

3 Results

3.1 Light Experiments

3.1.1 First light experiment (Exp. L1)

Light is the most crucial factor for an photoautotrophic organism. Therefore the effect of light intensity on the *S. voratum* biofilm was analysed first. For this purpose bench-scale Twin-Layer PSBRs with artificial f/2 medium have been set up (Section 2.2.2).

As shown in figure 3.1, algae biomass in dry weight (dw) per area [g m^{-2}] is increased linearly for all the shown light intensities over a time period of 27 days. However, a lag phase within the first three days of the experiment can be observed. Thus the linear fit has been adjusted accordingly. At 0 and $5 \mu\text{mol photons m}^{-2} \text{s}^{-1}$ no biomass increase has been recorded (data not shown). The growth rate P_B of the biofilm increases with the light intensity up to $200 \mu\text{mol photons m}^{-2} \text{s}^{-1}$ (Fig. 3.1 E), where the maximal

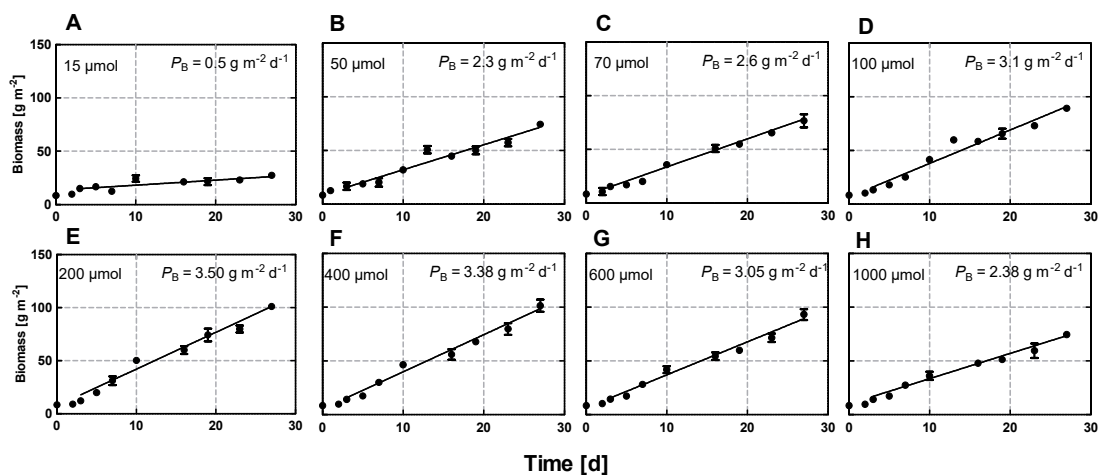


Figure 3.1: Biomass growth of *S. voratum* in dependence of the light intensity. [μmol] indicates light intensity in $\mu\text{mol photons m}^{-2} \text{s}^{-1}$. Shown are mean \pm SD for $n = 3$ and the correlating linear regression. P_B = Biomass growth rate from the linear fit in $\text{g m}^{-2} \text{d}^{-1}$.

biomass production P_B of $3.5 \text{ g m}^{-2} \text{ d}^{-1}$ has been recorded. Hereafter the growth rate P_B decreases (Fig. 3.1 F - H). A saturation of the growth over 27 days has not been recorded for any of the light intensities.

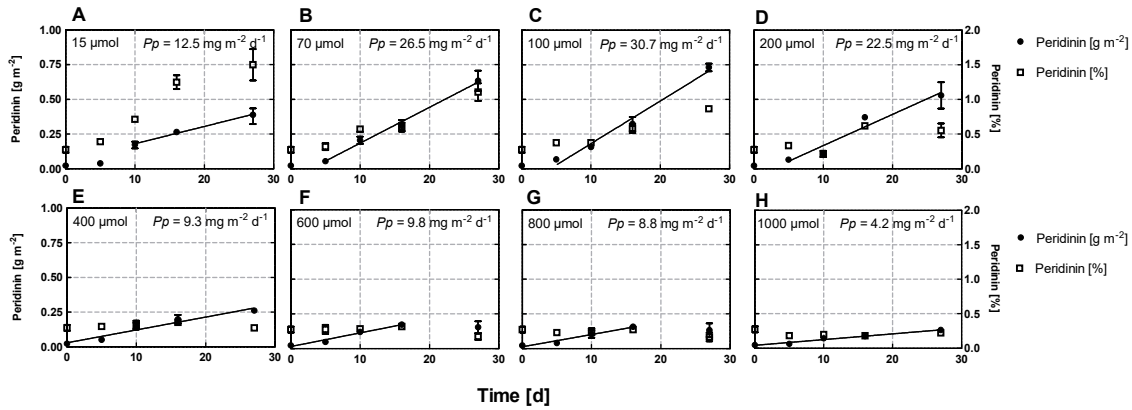


Figure 3.2: Peridinin production of *S. voratum* in dependence of the light intensity. Indicated by the closed circles (\bullet) is the absolute peridinin per area [g m^{-2}], while the open squares (\square) represent the relative peridinin concentration per dw biomass [% of dw]. [μmol] indicates light intensity in $\mu\text{mol photons m}^{-2} \text{ s}^{-1}$. Shown are mean \pm SD for $n = 3$ and the correlating linear regression. P_P = Peridinin productivity from the linear fit in $\text{mg m}^{-2} \text{ d}^{-1}$.

As, shown in figure 3.2 A-D, the initial increase in peridinin amount per area at low light is minor. Thus, the results of the peridinin accumulation per area are consistent with the growth data and the same lag phase is observed. However, after ten days the amount of peridinin [g m^{-2}] is increasing linearly. The highest production of peridinin P_P is obtained at a light intensity of $100 \mu\text{mol photons m}^{-2} \text{ s}^{-1}$ with $30.7 \text{ mg m}^{-2} \text{ d}^{-1}$ (Fig. 3.2 C). Enhancing the light intensity above $200 \mu\text{mol photons m}^{-2} \text{ s}^{-1}$ strongly reduces the peridinin production rate P_P from $22.5 \text{ mg m}^{-2} \text{ d}^{-1}$ by 60 % down to $9.3 \text{ mg m}^{-2} \text{ d}^{-1}$ (Fig. 3.2 D, E). Further increase of the light intensity leads to a reduction of peridinin productivity P_P . The final peridinin amount per area at day 27 even decreases at high light (Fig. 3.2 F, G). The relative peridinin concentration per biomass [% of dw] has its highest increase at $15 \mu\text{mol photons m}^{-2} \text{ s}^{-1}$ (Fig. 3.1 A). At the lowest light conditions of $0 \mu\text{mol photons m}^{-2} \text{ s}^{-1}$ the concentration is stagnating and as the values from $5 \mu\text{mol photons m}^{-2} \text{ s}^{-1}$, do not surpass 1 % (Data not shown). Up to $100 \mu\text{mol photons m}^{-2} \text{ s}^{-1}$ the relative peridinin concentration [% of dw] is increasing over time (Fig. 3.2 A-C), while it decreases with further increase of the light intensity (Fig. 3.2 D, E). At very high light the peridinin concentration is

stagnating around 0.25 % of dw (Fig. 3.2 E-H). Overall it can be stated, that the peridinin production is strongly light dependent and more effective at low light conditions of 15 - 200 $\mu\text{mol photons m}^{-2} \text{s}^{-1}$.

3.1.2 Second light experiment (Exp. L2)

In order to ensure the reproducibility of the TL experiments and study the effect of light over five weeks, the light experiment in artificial f/2 has been repeated. The data for the biomass and peridinin production of the *S. voratum* biofilm have been recorded and are presented in figure 3.3 and 3.4.

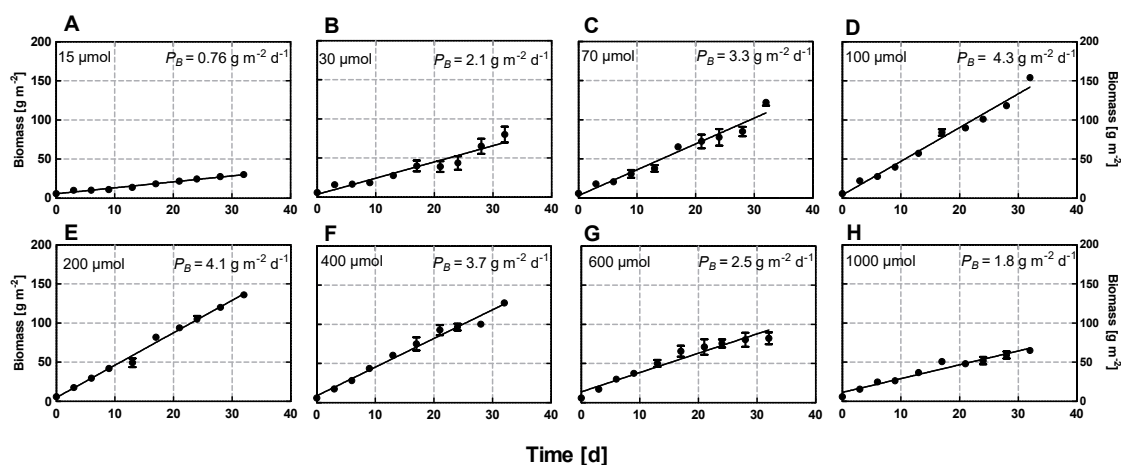


Figure 3.3: Biomass growth of *S. voratum* in dependence of the light intensity in the second light experiment (Exp. L2). Shown are mean \pm SD for $n = 3$ and the correlating linear regression. P_B = Biomass growth rate from the linear fit in $\text{g m}^{-2} \text{d}^{-1}$.

As in the previously described experiment (Exp. L1), growth in terms of biomass is following a linear trend in all applied light intensities (Fig. 3.1). The growth rates P_B range from 0.7 (Fig. 3.3 A) up to a maximum of $4.3 \text{ g m}^{-2} \text{d}^{-1}$ at $100 \mu\text{mol photons m}^{-2} \text{s}^{-1}$ (Fig. 3.3 D) and decrease with further increase of the light intensity (Fig. 3.3 E - H). In comparison to the first light experiment (Exp. L1), the maximal biomass production is 20 % higher (Fig. 3.1 E).

The pigment amount per area [g m^{-2}] is increasing linearly in all of the applied light intensities (Fig. 3.4). As in the previous experiment (Exp. L1), highest peridinin production P_P is recorded at $100 \mu\text{mol photons m}^{-2} \text{s}^{-1}$ with $23.7 \text{ mg m}^{-2} \text{d}^{-1}$ (Fig. 3.4 D)

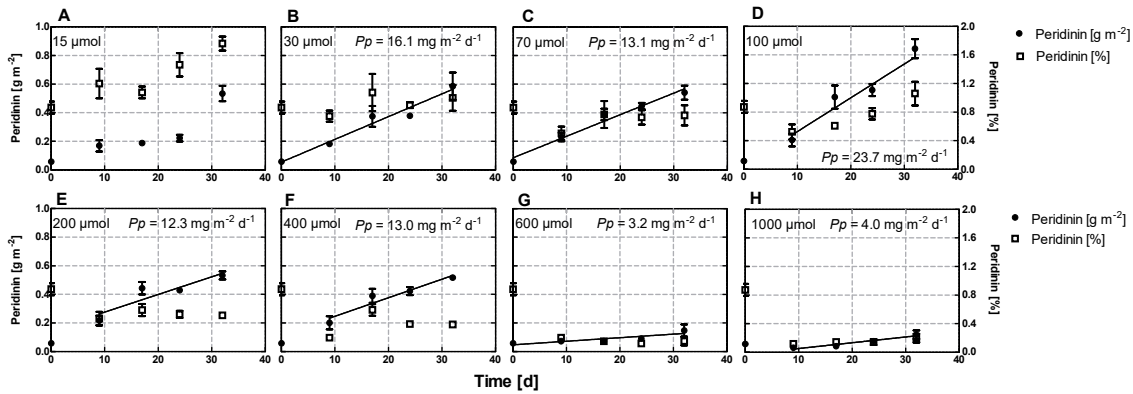


Figure 3.4: Peridinin production of *S. voratum* in dependence of the light intensity in the second light experiment (Exp. L2). Presented is the peridinin amount per area (●) and the peridinin concentration per biomass dw (□). Shown are mean ± SD for n = 3 and the correlating linear regression. P_p = Pigment productivity from the linear fit in $\text{mg m}^{-2} \text{d}^{-1}$.

and is decreasing at higher light intensities (Fig. 3.4 E - H). From the presented results a light dependence curve with respect to biomass and peridinin production has been generated. As depicted in figure 3.5 A, the biomass productivities of the light experiment show different maxima.

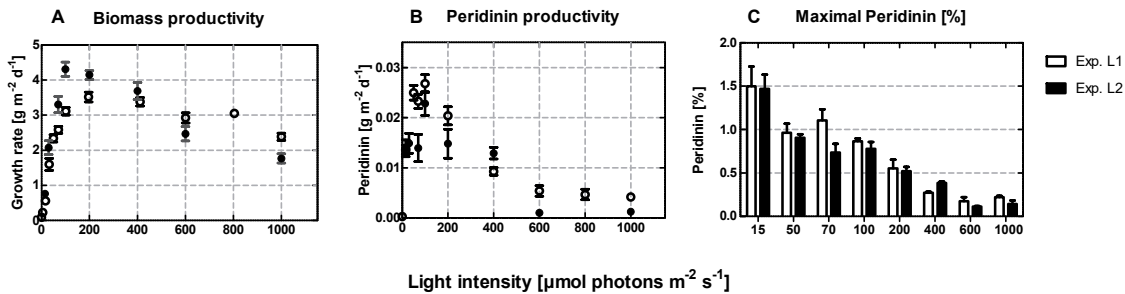


Figure 3.5: Comparison of biomass and peridinin productivity in dependence of the light intensity and the final concentration of peridinin per biomass [% of dw]. Shown are mean ± SD for n = 3 and the correlating linear regression. The clear circles represent data from the first light experiment (Exp. L1), the closed ones from the second light experiment (Exp. L2).

However, overall it can be stated, that growth is maximal at lower light intensities, between 100 and 200 $\mu\text{mol photons m}^{-2} \text{s}^{-1}$. Thus these light intensities have been focused on for optimal growth of the biofilm. When comparing the overall data of the two experiments for the peridinin productivity, the correlations follow the same trend, while the exact values vary slightly (Fig. 3.5 B). Furthermore, the different biomass production rates, within the two experiments, have no effect on the maximal peridinin

productivity. In addition also the maximal peridinin value per biomass [% of dw] are, except for the light intensity of $70 \mu\text{mol photons m}^{-2} \text{s}^{-1}$ (ANOVA, $p = 0.013$), not significantly different (Fig. 3.5 C).

Since the main focus of this thesis is laid on peridinin production, which is maximal at $100 \mu\text{mol photons m}^{-2} \text{s}^{-1}$, this light intensity is referred to as the optimum and has been used as control in the subsequent experiments.

3.2 Effect of the inoculation density (Exp. D)

From the first performed light experiment (Exp. L1), it has been evident that the biofilm is presenting an assimilation or lag phase after the inoculation (Section 3.1.1). To further analyse this phenomenon the inoculation density of the *S. voratum* biofilm in the bench-scale TL PSBRs has been altered from 5 to 10 g m^{-2} .

In lowest light condition of $45 \mu\text{mol photons m}^{-2} \text{s}^{-1}$ a biomass growth rate P_B of $3.1 \text{ g m}^{-2} \text{d}^{-1}$ is recorded (Fig. 3.6 A). At $100 \mu\text{mol photons m}^{-2} \text{s}^{-1}$ the biomass growth rate is further enhanced to $5 \text{ g m}^{-2} \text{d}^{-1}$, which represents an increase of

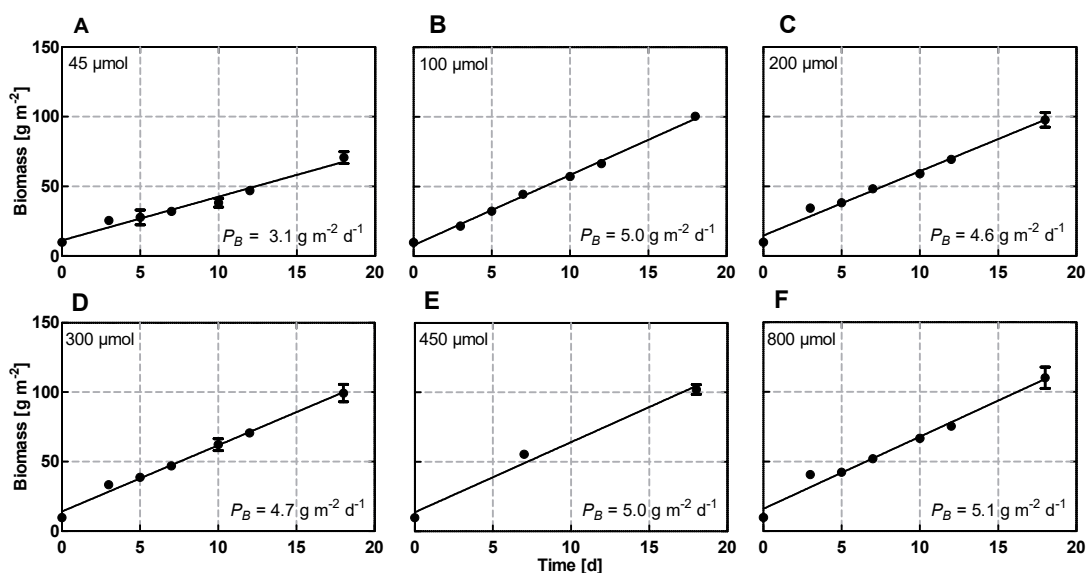


Figure 3.6: Biomass growth of the immobilised *S. voratum* culture inoculated with a higher biomass density in six different light conditions. Shown are mean \pm SD for $n = 3$ and the correlating linear regression. P_B = Biomass growth rate from the linear fit in $\text{g m}^{-2} \text{d}^{-1}$.

20 % to 40 % in comparison to the light experiments (Fig. 3.5 A). Interestingly, the light intensities of 100 to 800 $\mu\text{mol photons m}^{-2} \text{s}^{-1}$ generate similar growth rates independent from the applied illumination (Fig. 3.6 C - F), which are statistically not distinguishable (ANCOVA, $p = 0.175$). There is also no statistical difference in the maximal amount of biomass yield [g m^{-2}] at the different light intensities, except for the immobilised culture grown at 45 $\mu\text{mol photons m}^{-2} \text{s}^{-1}$ (Fig. 3.8 A). This diverges from the previously described findings (compare figure 3.1 and 3.3).

In summary, while biomass productivity P_B above 100 $\mu\text{mol photons m}^{-2} \text{s}^{-1}$ is not affected by the light intensity, it increases overall with the higher inoculation density. However, the maximal biomass productivity P_B with the lowest input of light, is recorded at a light intensity of 100 $\mu\text{mol photons m}^{-2} \text{s}^{-1}$ (Fig. 3.6 B).

As shown in figure 3.7, the peridinin amount [g m^{-2}] increases linearly over the duration of the experiment, the recorded R^2 fit of the productivity P_P is never lower than 0.98 in all the applied light radiations. Demonstrating, that with a thicker inoculated biofilm the productivity of peridinin P_P is linear from the start. It is notable, that the rate of pigment production P_P is not distinguishable in the light conditions of 45 - 400 $\mu\text{mol photons m}^{-2} \text{s}^{-1}$ (Fig. 3.7 A-E) and in contrast to the initial light

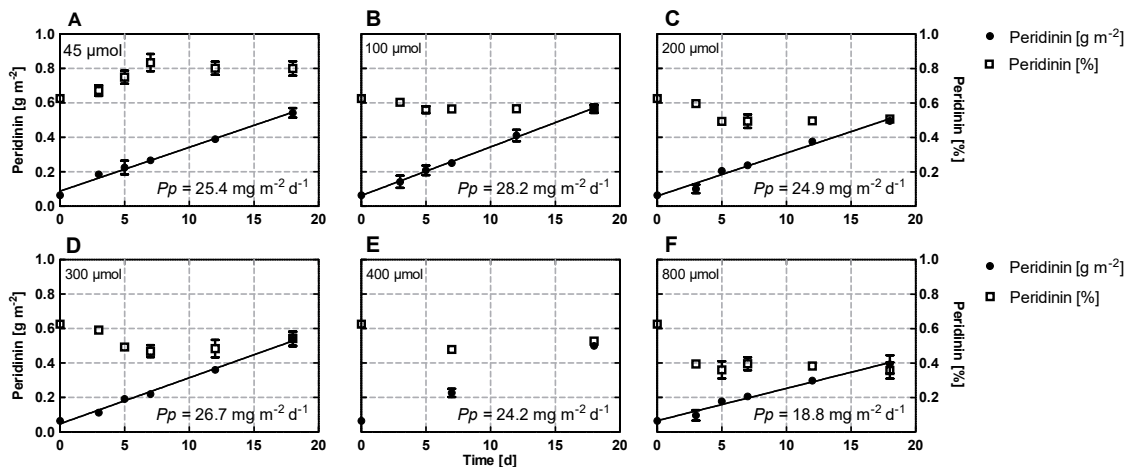


Figure 3.7: Peridinin production of the immobilised *S. voratum* culture inoculated with a higher biomass density in six different light conditions. Presented is the peridinin amount per area (\bullet) and the peridinin concentration per biomass dw (\square). Shown are mean \pm SD for $n = 3$ and the correlating linear regression. P_P = Peridinin productivity from the linear fit in $\text{mg m}^{-2} \text{d}^{-1}$.

experiment (Exp. L1, section 3.1.1) does not decrease until 800 $\mu\text{mol photons m}^{-2} \text{s}^{-1}$. The productivities P_P in both experiments at 100 $\mu\text{mol photons m}^{-2} \text{s}^{-1}$ were comparable at 28.2 and 30.7 $\text{mg m}^{-2} \text{d}^{-1}$, respectively (Fig. 3.7 B and 3.2 C). However, it is possible to double the production rate P_P at 800 $\mu\text{mol photons m}^{-2} \text{s}^{-1}$ (Fig. 3.7 F and 3.2 G). With regard to the relative concentration of peridinin per biomass [% of dw] it is initially increasing at the lowest light condition (Fig. 3.7 A), but is then, as recorded at 100 $\mu\text{mol photons m}^{-2} \text{s}^{-1}$, stationary (Fig. 3.7 B). In comparison to the first light experiments (Fig. 3.2 C), the peridinin concentration [% of dw] at 100 $\mu\text{mol photons m}^{-2} \text{s}^{-1}$ is reduced by 40 % (Fig. 3.4 D). At higher light intensities the concentration of peridinin in the biofilm [% of dw] is slightly reduced in the time course of the experiment (Fig. 3.7 C-F).

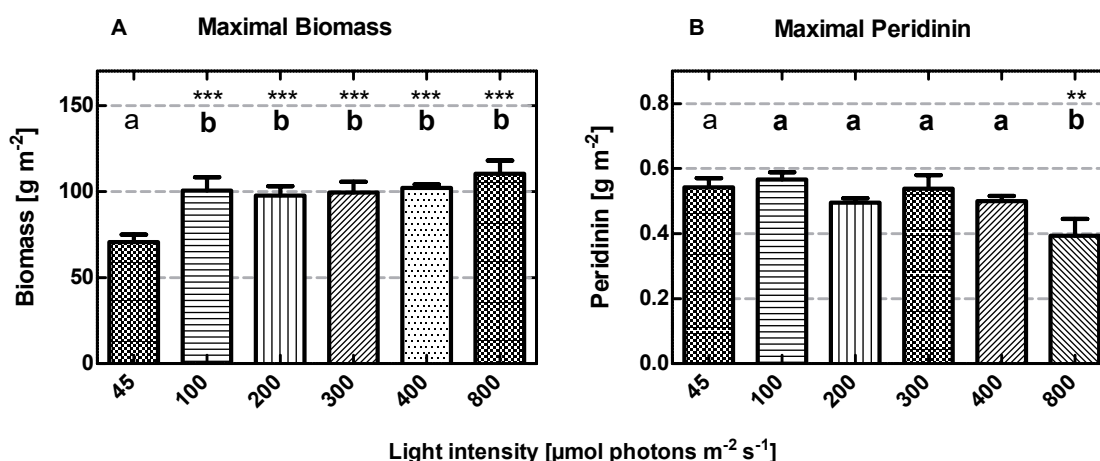


Figure 3.8: Maximal amount of biomass and peridinin per area [g m^{-2}] recorded in the experiment probing higher inoculation. Presented are the results from the final day (d18) of the experiment. Shown are mean \pm SD for $n = 3$. As statistical analysis a one-way ANOVA with Tukey's multiple comparison test has been performed.

Overall, by applying light intensities of 100 - 800 $\mu\text{mol photons m}^{-2} \text{s}^{-1}$ to the *S. voratum* biofilm with the inoculation density of 10 g m^{-2} , an equal amount of biomass per area (d18) is recorded (Fig. 3.8 A). When analysing the maximal amount of peridinin, no significant differences at the light intensities of 45 - 400 $\mu\text{mol photons m}^{-2} \text{s}^{-1}$ are found (Figure 3.8 B). In summary, as in previous experiments (Fig. 3.5 B), the maximal peridinin productivity P_P is determined at 100 $\mu\text{mol pho}$

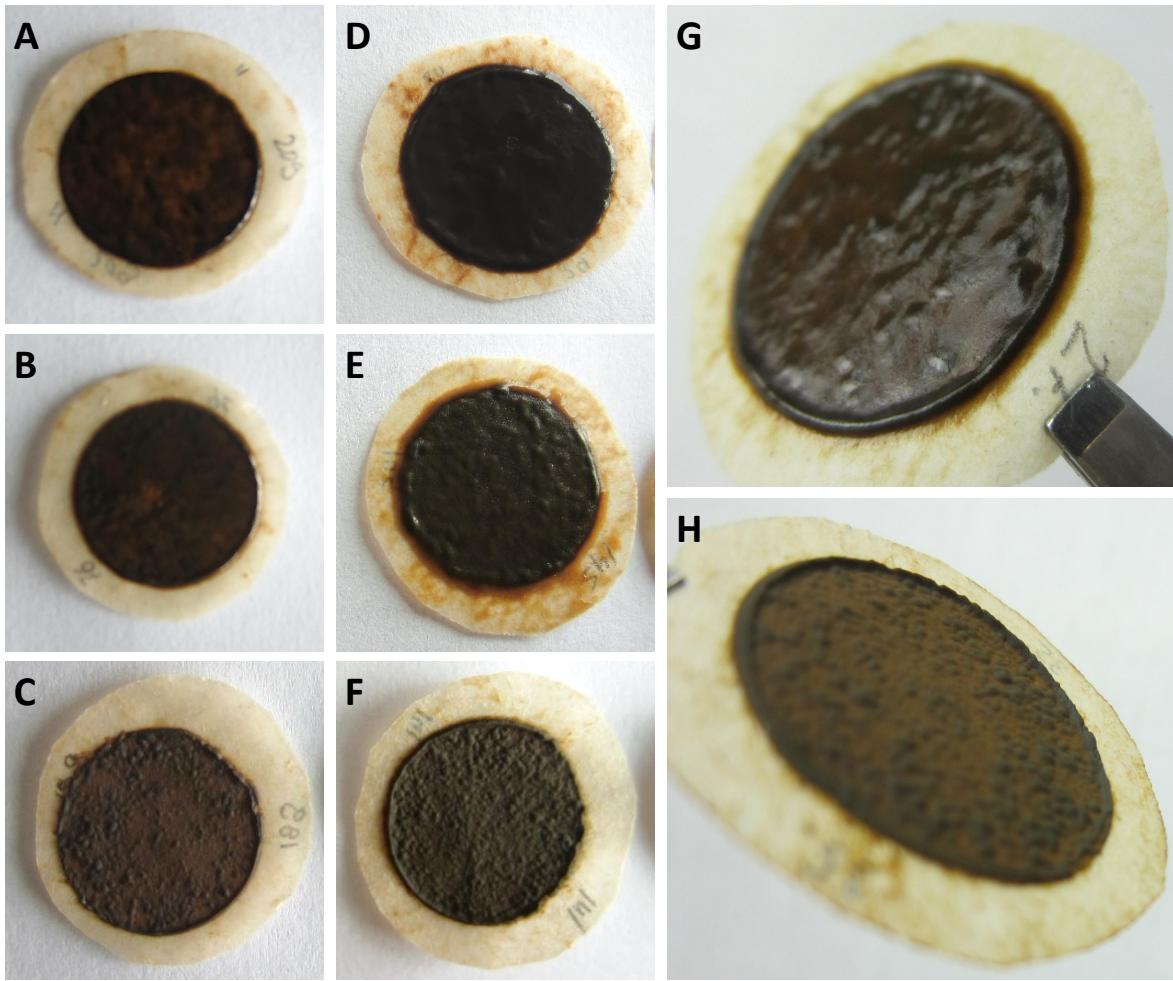


Figure 3.9: Documentation of the *S. voratum* biofilm inoculated with a density of 10 g m^{-2} . Presented are immobilised cultures grown at **A, D** $45 \text{ } \mu\text{mol photons m}^{-2} \text{ s}^{-1}$; **B, E, G** $100 \text{ } \mu\text{mol photons m}^{-2} \text{ s}^{-1}$ and $800 \text{ } \mu\text{mol photons m}^{-2} \text{ s}^{-1}$ **C, F, H**. The biofilms have been harvested on day 5 **A-C**; day 7 **G, H** and day 10 **D-F**.

$\text{tons m}^{-2} \text{ s}^{-1}$, while the concentration of peridinin in the biomass [% of dw] is reduced. Therefore the subsequent experiments have been set up with a density of 5 g m^{-2} .

Presented in figure 3.9 is a documentation of the *S. voratum* biofilm within the time course of the experiment. At day five the immobilised cultures have a density of 27.6, 32.3 and 42.3 g m^{-2} at 45, 100 and $800 \text{ } \mu\text{mol photons m}^{-2} \text{ s}^{-1}$, respectively. After the first few days the paper substrate layer is still visible in some areas of the inoculation area, especially in the thinnest at $45 \text{ } \mu\text{mol photons m}^{-2} \text{ s}^{-1}$ (Fig. 3.9 A). Whereas the filters in low light (Fig. 3.9 A, B) seem to be dark brown, the ones at $800 \text{ } \mu\text{mol photons m}^{-2} \text{ s}^{-1}$ appear lighter in colour (Fig. 3.9 C). This effect becomes more prominent with a longer duration of the experiment (Fig. 3.9 H, F).

On day 10 the colouration of the biofilm at the lowest light has become very rich in colour, they appear almost black as shown in figure 3.9 D. From the peridinin data, given in figure 3.7, it is known that the darker colouration is not caused by a higher absolute peridinin amount per area, but is due to a higher concentration of peridinin per biomass [% of dw]. The biofilm at $45 \mu\text{mol photons m}^{-2} \text{s}^{-1}$ is very smooth and uniform over the inoculated area (Fig. 3.9 A, D), while in the *S. voratum* biofilm at 100 and $800 \mu\text{mol photons m}^{-2} \text{s}^{-1}$ small accumulations of cells within the biofilm can be seen, which increase in number over time (Fig. 3.9 E, F). In contrast to the biofilm exposed to low light, the surface of the biofilm at the highest light intensity (Fig. 3.9 C, F, H) has no shine.

3.3 CO₂ Experiments (Exp. C)

Besides light, CO₂ is one of the most important limiting factors for the photosynthesis. Therefore, after investigating the relationship of light and culture productivity, the effect of CO₂ on the *S. voratum* biofilm was focused on. For the experiments two different media have been analysed with regard to the culture performance at ambient air and with additional CO₂.

3.3.1 f/2 Medium (Exp. CF)

In this experiment the *S. voratum* biofilms have been set up with ambient air and 2 % CO₂ in parallel over three weeks. As culture medium artificial f/2 has been supplied (Section 2.1.1). As shown in figure 3.10 A, B; at low light conditions, such as 100 and $300 \mu\text{mol photons m}^{-2} \text{s}^{-1}$, no significant differences in the growth kinetics P_B of ambient air and CO₂ supplied biofilms have been detected (ANCOVA, $p = 0.1857; 0.30$). At a light intensity of $600 \mu\text{mol photons m}^{-2} \text{s}^{-1}$ a significant increase of 23 % in the growth rate P_B from 3.1 to $4.5 \text{ g m}^{-2} \text{d}^{-1}$ is noted for biofilms supplied with 2 % CO₂ (Fig. 3.10 C, ANCOVA, $p < 0.001$). At $1000 \mu\text{mol photons m}^{-2} \text{s}^{-1}$ the biomass grows with $2.6 \text{ g m}^{-2} \text{d}^{-1}$ in ambient air and $3.0 \text{ g m}^{-2} \text{d}^{-1}$ in CO₂ rich

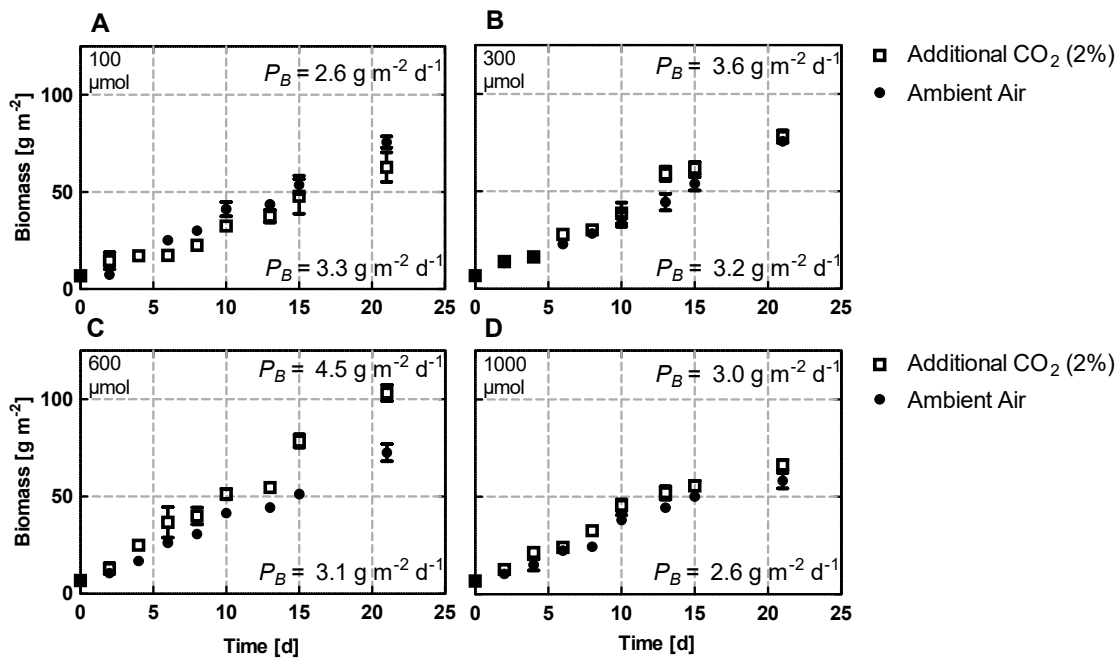


Figure 3.10: Biomass growth of the *S. voratum* biofilm on f/2 medium in 2 % CO₂ (□) and ambient air (●) over the duration of 21 days. In the top of a graph growth rate from CO₂ supplementation is given, while in the bottom growth rates from ambient air is presented. Shown are mean \pm SD for $n = 3$. P_B = Biomass growth rate from the linear fit in g m⁻² d⁻¹.

atmosphere (Fig. 3.10 D). Thus the supply of CO₂ only alters the growth rate at a light intensity of 600 $\mu\text{mol photons m}^{-2} \text{s}^{-1}$. By the analysis of the pH in the medium a decrease from 8.3 ± 0.29 to 6.4 ± 0.24 after an application of three days in the setups with CO₂ has been recorded. As a result the experiment has been repeated with the buffered medium ASP 12.

3.3.2 ASP 12 Medium (Exp. CA)

In order to get more insight to whether a more complex and buffered medium is beneficial for the production of peridinin in the *S. voratum* biofilm in the presence of CO₂, the experiment has been repeated, using the growth medium ASP 12 and a larger range of light intensities (Section 2.1.1).

In the comparison of the biofilm growth in ambient air and additional CO₂ the linearity of growth remains, while the growth rates P_B are altered (Fig. 3.11). CO₂ application in combination with the use of ASP 12 enhances the biomass productivity

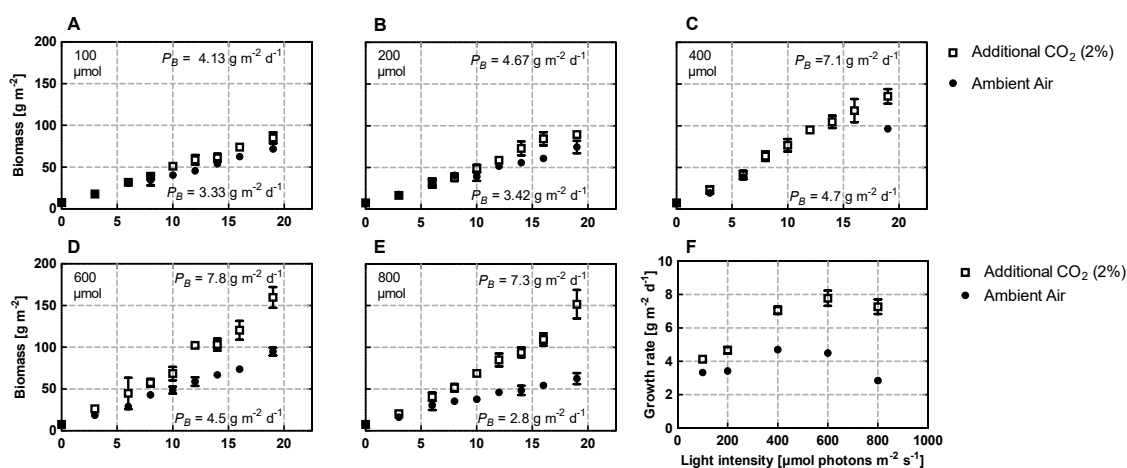


Figure 3.11: Biomass growth of *S. voratum* biofilm on ASP 12 medium at increasing light intensities in ambient air (●) and 2 % CO₂ (□). Shown are mean ± SD for n = 3. P_B = Biomass growth rate from the linear fit in g m⁻² d⁻¹. F Light curve with (□) and without (●) CO₂.

at all the applied light intensities. At low light conditions the effect is only minor (Fig. 3.11 A, B), but significantly different (ANCOVA, $p < 0.001$). The higher the irradiance, the stronger is the enhancing effect of CO₂ on biomass growth. At light conditions of 400 μmol photons m⁻² s⁻¹ the daily growth rate P_B is 1.5-fold increased at 600 μmol photons m⁻² s⁻¹. At the highest applied light intensity of 800 μmol photons m⁻² s⁻¹, the application of CO₂ leads to an 2.5 fold increase in biomass productivity. From the obtained light curve (Fig. 3.11 F), a clear change in the optimum of the biomass productivity by the addition of CO₂ is determined. The growth rate P_B at ambient air is maximal at 200 - 400 μmol photons m⁻² s⁻¹, while the maxima is shifted towards 600 μmol photons m⁻² s⁻¹ with the supplementation of CO₂. In ASP 12 the average pH was in the TL PSBRs with 2 % CO₂ 7.53 ± 0.40 .

In figure 3.12 the absolute peridinin amount and concentration at different CO₂ and light conditions is presented. As it has been reported before (Section 3.1), the increase in peridinin within the biofilm is progressing in a linear fashion. At the low light intensities (Fig. 3.12 A, C) the additional CO₂ lowers the production rate P_P of peridinin (Fig. 3.12 B, D). In case of 200 μmol photons m⁻² s⁻¹ even by 36% (Fig. 3.12 D). In contrast at the high applied light conditions (Fig. 3.12 E - H) the presence of 2 % CO₂ affects an increase of peridinin production. The increase at 600 μmol photons m⁻² s⁻¹ is 20 %, while it only reaches 4 % at 800 μmol photons m⁻² s⁻¹, respectively. Overall the start-

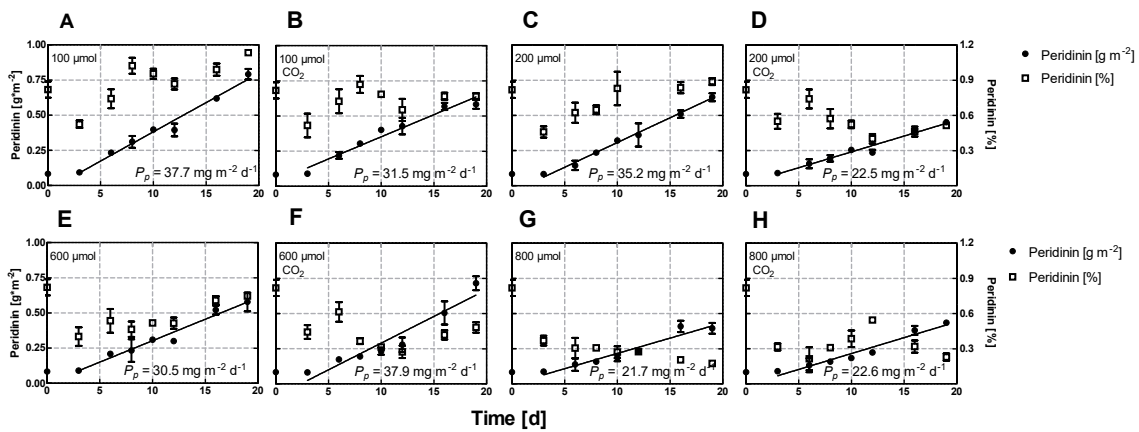


Figure 3.12: Pigment production of *S. voratum* biofilms grown on ASP 12 medium at ambient air and 2 % CO₂. Presented is the peridinin amount per area (●) and the peridinin concentration per biomass dw (□). Shown are mean ± SD for n = 3 and the correlating linear regression. P_p = Peridinin productivity from the linear fit in $\text{g m}^{-2} \text{d}^{-1}$.

ing value for the peridinin per biomass [% of dw] from the inoculation culture in suspension is very high (0.82 %) and decreases therefore in all setups within the first days of the experiment. After this initial drop the percentage of peridinin within the biofilm increases at lower light intensities in ambient air up to 1.13 % and 0.9 % at 100 and 200 $\mu\text{mol photons m}^{-2} \text{s}^{-1}$ respectively (Fig. 3.12 A, C). While at higher light or excess CO₂ the values never surpass 0.7 % (Fig. 3.12 E - H).

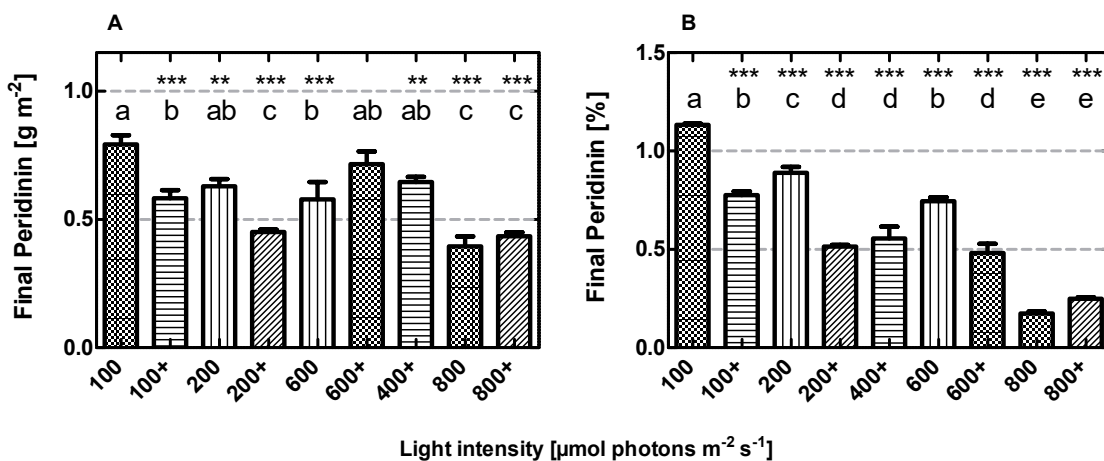


Figure 3.13: Results for the amount of peridinin per area and biomass recorded on the final day of the CO₂ experiment in ASP 12. (+) indicates the supply with 2 % CO₂. Mean ± SD, n = 3 are presented. As statistical analysis a one-way ANOVA with Tukey’s multiple comparison test has been performed. The labelled groups and asterisks indicate the significance in comparison to 100 $\mu\text{mol photons m}^{-2} \text{s}^{-1}$.

The maximal peridinin amount per area [g m^{-2}] (Fig. 3.13 A) at the final day of the CO_2 experiment with ASP 12 medium shows, that identical amounts of peridinin are recorded at $600 \mu\text{mol photons m}^{-2} \text{s}^{-1}$ light and the addition of CO_2 as well as $100 \mu\text{mol photons m}^{-2} \text{s}^{-1}$ without CO_2 (Fig. 3.13 A). The peridinin amount at $600 \mu\text{mol photons m}^{-2} \text{s}^{-1}$ is statistically not differentiable (group labeling ab) with the results obtained at $200 \mu\text{mol photons m}^{-2} \text{s}^{-1}$ with ambient air and $400 \mu\text{mol photons m}^{-2} \text{s}^{-1}$ with 2 % CO_2 (Fig. 3.12 A). Although the absolute amount of peridinin [g m^{-2}] is the same, the concentration per biomass [% of dw] shows a different result. As it is indicated in figure 3.13 B, the final concentration of peridinin per biomass [% of dw] is significantly highest at $100 \mu\text{mol photons m}^{-2} \text{s}^{-1}$ and ambient air. Interestingly, this value is 57 % higher than the data from $600 \mu\text{mol photons m}^{-2} \text{s}^{-1}$, which presented similar production rates P_p .

To get a better understanding of the immobilised growth of *S. voratum*, cross-section of the biofilm at two time points of the experiment have been performed (Section 2.4). In figure 3.14, a visualisation of the biofilm grown in different conditions, is depicted. The orientation of the biofilm is presented from top to bottom. In some samples the remnants of the substrate layer is still visible at the bottom (Fig. 3.14 B). In $600 \mu\text{mol photons m}^{-2} \text{s}^{-1}$ and CO_2 the complete biofilm is tightly packed with cells and only the uppermost layer seems lighter in colour (Fig. 3.14 A). The cultures grown at $800 \mu\text{mol photons m}^{-2} \text{s}^{-1}$ and ambient air (Fig. 3.14 B) appear less dense and show a bright top part of the biofilm. In comparison, the biofilm at $100 \mu\text{mol photons m}^{-2} \text{s}^{-1}$ is darker in colour and presents a differentiation of the biofilm into top, middle and bottom layer (Fig. 3.14 C). Close to the surface cells are loosely connected to each other, while the underlying layer has a higher cell density. At the bottom of the biofilm the cells are even more densely packed. Over time the separation of these three layers is maintained, while only the lowest layer has gained in size (Fig. 3.14 D) and is so dense that no light is passing through. In general the appearance of the biofilms reflect the findings of the biomass and peridinin analyses (Fig. 3.11, 3.12).

By comparing the two media it can be shown, that the biomass and peridinin productivity is reduced under the application of CO_2 in the f/2 medium (Fig. 3.15). As

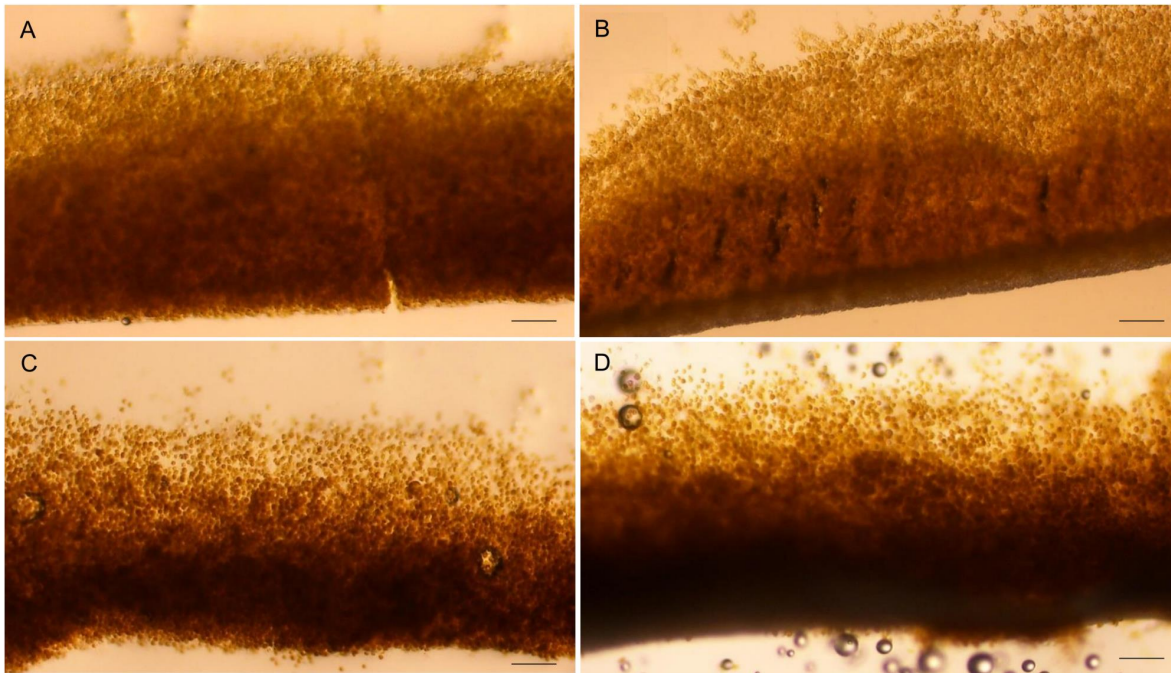


Figure 3.14: Biofilm cross-sections of *S. voratum* at different culture conditions and time points in the Exp. CA. All sections are 90 μm thick. **A** 600 $\mu\text{mol photons m}^{-2} \text{s}^{-1}$, 2 % CO_2 , day 9. **B** 800 $\mu\text{mol photons m}^{-2} \text{s}^{-1}$, ambient air, day 9. **C** 100 $\mu\text{mol photons m}^{-2} \text{s}^{-1}$, ambient air on day 9 and **D** day 19. The scale bar refers to 80 μm .

a summary for ASP 12 medium it can be stated, that high light intensities generate higher biofilm growth rates with CO_2 supply (Fig. 3.11), whereas peridinin production is unaltered or lowered by CO_2 , except for the light intensity of 600 $\mu\text{mol photons m}^{-2} \text{s}^{-1}$ (Fig. 3.12). Here a identical peridinin production was recorded as at 100 $\mu\text{mol photons m}^{-2} \text{s}^{-1}$ and ambient air (Fig. 3.12 A, F). Since the relative peridinin

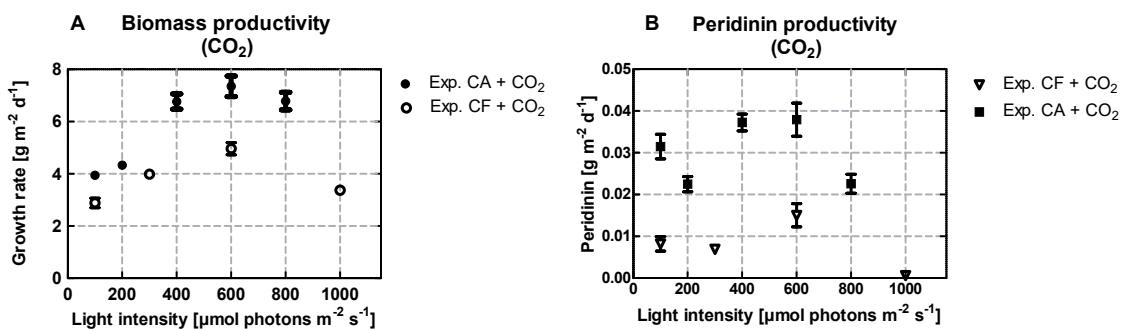


Figure 3.15: Biomass and peridinin production of the *S. voratum* biofilm in 2% CO_2 in dependence of the light intensity in f/2 and ASP 12. Exp. CF + CO_2 : Experiment with f/2, Exp. CA + CO_2 : Experiment with ASP 12. Mean \pm SD, $n = 3$ are presented.

concentration [% of dw] is by far highest in 100 $\mu\text{mol photons m}^{-2} \text{s}^{-1}$ without supplementary CO_2 (Fig. 3.12 B), it is persistently selected as the optimal condition for peridinin accumulations in the medium ASP 12.

3.4 Summary of light and CO_2 data

In this section a comparison of all gathered results from the experiments regarding light (Exp. L1, L2) (Section 3.1), inoculation density (Exp. D, section 3.2) and CO_2 (Exp. CF, Exp. CA, section 3.3) are given.

In figure 3.16 the biomass productivity per area and day P_B is correlated to the applied light intensity of all experiments. The direct comparison of all f/2 based experiments (Fig. 3.16 A) highlights the reproducible growth behaviour of the used system, with only slight variation. The growth rate P_B peaks at a light intensity between 100 and 200 $\mu\text{mol photons m}^{-2} \text{s}^{-1}$ and decreases with higher illumination. For further comparisons Exp. L1 is used as reference for the experiments performed in f/2. With the increase of the inoculation density (Fig. 3.16 B, Exp. D), the biomass productivity is stagnating above 100 $\mu\text{mol photons m}^{-2} \text{s}^{-1}$. Thus the higher inoculation density favours the biomass growth. The comparison of growth rates in different cultivation media (Fig. 3.16 C), indicates that the differences in medium does not affect the biomass growth rate at light intensities up to 200 $\mu\text{mol photons m}^{-2} \text{s}^{-1}$. Thereafter, the biofilm in ASP 12 medium and ambient air gains the highest biomass productivity at 400 $\mu\text{mol photons m}^{-2} \text{s}^{-1}$ with 4.7 $\text{g m}^{-2} \text{d}^{-1}$ and decreases subsequently. When considering the biomass productivity with CO_2 for both applied media, an increase in growth is detectable and the maximum is found at 600 $\mu\text{mol photons m}^{-2} \text{s}^{-1}$ (Fig. 3.16 D). However, the effect on the productivity is much more prominent with the utilisation of ASP 12. The maximal growth rate is 7.8 $\text{g m}^{-2} \text{d}^{-1}$ and therefore 2.5 times higher than the average growth rate at low light without CO_2 . To summarise, the best conditions for maximal biomass growth have been found at 600 $\mu\text{mol photons m}^{-2} \text{s}^{-1}$ and 2 % CO_2 in the medium ASP 12.

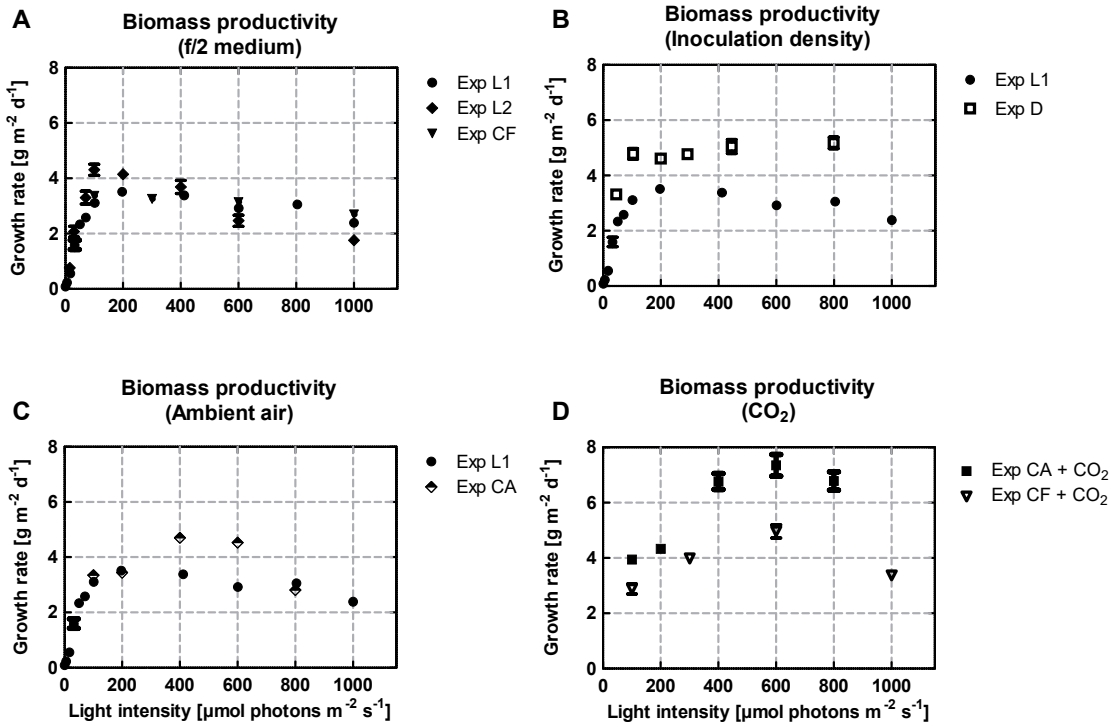


Figure 3.16: Summary of the biomass productivities of *S. voratum* in the TL PSBR. The growth rate is given in $\text{g m}^{-2} \text{d}^{-1}$. Compared are **A** experiments conducted in f/2 and ambient air; **B** Experiments on the *S. voratum* biofilm with different inoculation densities; **C** Experiments conducted in ambient air with f/2 and ASP 12 medium; **D** Experiments conducted with 2 % CO₂ with f/2 and ASP 12 medium. The labelling refers to the experiments on the *S. voratum* biofilm: Exp. L1 = first light experiment (Section 3.1.1), Exp. L2 = second light experiment (Section 3.1.2), Exp. D = experiment on inoculation density of the biofilm (Section 3.2), Exp. CF = ambient air reference from Exp. C with f/2 (Section 3.3.1), Exp. CA = ambient air reference from Exp. C with ASP 12 (Section 3.3.2), Exp. CF + CO₂: experiment with 2 % CO₂ and f/2, Exp. CA + CO₂: experiment performed with 2 % CO₂ and ASP 12. Data present mean \pm SD, $n = 3$.

In figure 3.17 an overview of the peridinin productivity P_P from the last presented results is given. When comparing the data from the experiments performed in f/2 (Fig. 3.17 A), the productivity curve consistently peaks at $100 \mu\text{mol photons m}^{-2} \text{s}^{-1}$. For further comparisons the light experiment Exp. L1 is set as reference in figure 3.17. The change in inoculation density does not alter the optimum for peridinin production either, even so the productivity is enhanced at the light intensities of $300 - 800 \mu\text{mol photons m}^{-2} \text{s}^{-1}$ in comparison to the light experiment (Fig. 3.17 B). From the medium experiments with ASP 12 and f/2 with ambient air, it can be concluded, that the peridinin production rate is maximal at the light intensity of $100 \mu\text{mol pho}$

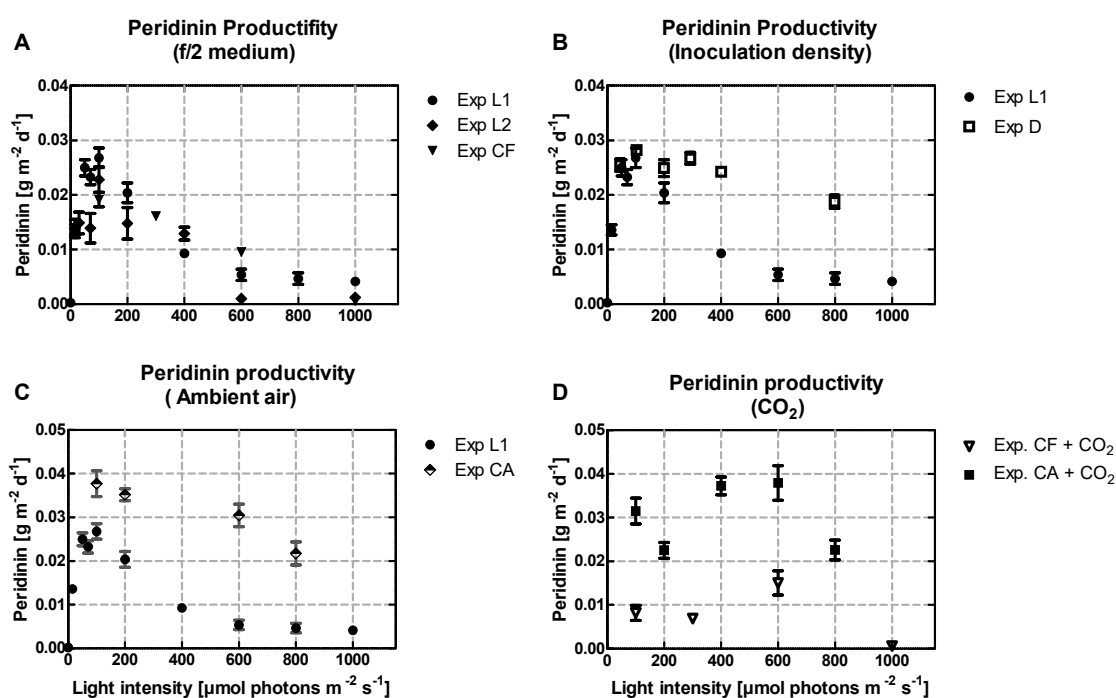


Figure 3.17: Summary of the peridinin production with *S. voratum* in the TL PSBR. The productivity is given in $\text{g m}^{-2} \text{d}^{-1}$. Compared are **A** experiments conducted in f/2 and ambient air; **B** Experiments on the *S. voratum* biofilm with different inoculation densities; **C** Experiments conducted in ambient air with f/2 and ASP 12 medium; **D** Experiments conducted with 2% CO_2 with f/2 and ASP 12 medium. The labelling refers to the experiments on the *S. voratum* biofilm: Exp. L1 = first light experiment (Section 3.1.1), Exp. L2 = second light experiment (Section 3.1.2), Exp. D = experiment on inoculation density of the biofilm (Section 3.2), Exp. CF = ambient air reference from Exp. C with f/2 (Section 3.3.1), Exp. CA = ambient air reference from Exp. C with ASP 12 (Section 3.3.2), Exp. CF + CO_2 : experiment with 2% CO_2 and f/2, Exp. CA + CO_2 : experiment performed with 2% CO_2 and ASP 12. Data present mean \pm SD, $n = 3$.

tons $\text{m}^{-2} \text{s}^{-1}$ as well. However, the supply of ASP 12 increases the peridinin production rate by 25% in comparison to the light experiment (Exp. L1, Fig. 3.17 C). In the application of CO_2 it becomes apparent, that the *S. voratum* biofilm has a lower peridinin productivity in f/2 medium, although the curve trends in both media are congruent. By applying ASP 12 and CO_2 the highest peridinin production of $37.9 \text{ mg m}^{-2} \text{d}^{-1}$ is recorded at $600 \mu\text{mol photons m}^{-2} \text{s}^{-1}$ (Fig. 3.17 C). Overall the maximal peridinin productivity with regard to the light intensity seems to be independent from supplied medium or inoculation density, since the productivity is persistently highest at the light intensity of $100 \mu\text{mol photons m}^{-2} \text{s}^{-1}$. The application of 2% CO_2 changes the response of peridinin production rate to light intensity,

leading to the maximal peridinin production at 600 $\mu\text{mol photons m}^{-2} \text{s}^{-1}$ under these conditions (Fig. 3.17 D). However, the production rate cannot be increased further and is identical with the set standard conditions at 100 $\mu\text{mol photons m}^{-2} \text{s}^{-1}$ and ambient air.

In summary the maximal peridinin production is achieved by the application of the medium ASP 12 at a light intensity of 100 $\mu\text{mol photons m}^{-2} \text{s}^{-1}$ in ambient air or 600 $\mu\text{mol photons m}^{-2} \text{s}^{-1}$ and 2 % CO_2 . However, due to the lower peridinin concentration per biomass, as presented in figure 3.12, the optimal production conditions for peridinin are found at 100 $\mu\text{mol photons m}^{-2} \text{s}^{-1}$ with ambient air and are 25 % higher in ASP 12, than in the reference (Fig. 3.17 A, Exp L1).

3.5 Temperature experiments (Exp. T)

As temperature has direct impact on cell metabolism and growth of microalgae the effect on the TL PSBR productivity has been considered as next factor. The experiment is designed in a way, that the cells of *S. voratum* are initially immobilised and pre-grown at low light (100 $\mu\text{mol photons m}^{-2} \text{s}^{-1}$, ambient air and 20 °C), as well as high light (600 $\mu\text{mol photons m}^{-2} \text{s}^{-1}$, 2 % CO_2 and 30 °C) for 12 days to insure a uniform composition of the biofilm. After this time the immobilised *S. voratum* biofilm have been exposed to various temperatures. As in the previous experiments, the focus is set on the analysis of biomass and peridinin production (Fig. 3.18 to 3.21). The cultured biofilms pre-grown at low light were transferred at day 12 to 32 and 25 °C with ambient air, respectively, while the biofilm pre-grown at high light were transferred to 36 °C and 2 % CO_2 . Additionally the biofilms from both, 100 and 600 $\mu\text{mol photons m}^{-2} \text{s}^{-1}$, were exposed to 16 and 4 °C. However, it has be noted, that to remain within realistic natural parameters these cold temperatures were exposed to lower light intensities and ambient air as well. The cultivation at 16 °C is carried out with 50 $\mu\text{mol photons m}^{-2} \text{s}^{-1}$ and 4 °C with 5 $\mu\text{mol photons m}^{-2} \text{s}^{-1}$, respectively. As a reminder of this stepwise procedure the samples are referred to 600/50, 600/5, 100/50 and 100/5 $\mu\text{mol photons m}^{-2} \text{s}^{-1}$, accordingly.

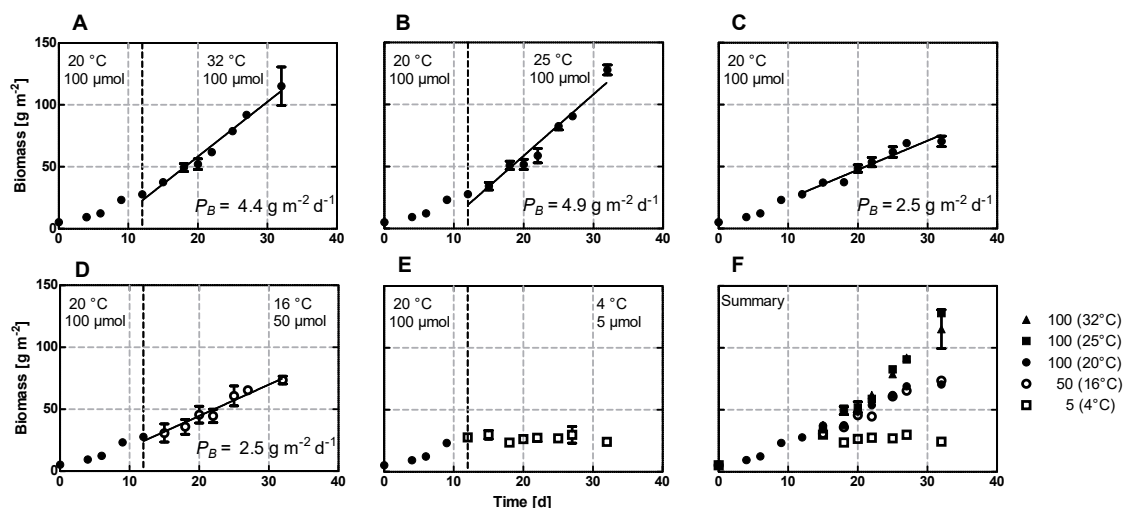


Figure 3.18: Impact of temperature on the growth rate of the *S. voratum* biofilm pre-grown at $100 \mu\text{mol photons m}^{-2} \text{s}^{-1}$. After the transfer on day 12 the biofilms were exposed to 32 and 25 °C as well as 16 and 4 °C with ambient air. Shown are mean \pm SD for $n = 3 - 6$ and the correlating linear regression. P_B = Biomass growth rate from the linear fit in $\text{g m}^{-2} \text{d}^{-1}$.

In figure 3.18 the biomass data from all biofilms pre-grown at $100 \mu\text{mol photons m}^{-2} \text{s}^{-1}$ are given. As it can be seen, the highest biomass growth rate P_B is recorded at a 25 °C (Fig. 3.18 B). In comparison to 20 °C (Fig. 3.18 C) an 50 % increase is gained. Further enhancing of the temperature leads to a decrease of growth rate compared to the condition at 25 °C (Fig. 3.18 A). However, at 32 °C the growth rate of *S. voratum* is still 30 % higher than at 20 °C. With $100/50 \mu\text{mol photons m}^{-2} \text{s}^{-1}$ and 16 °C the growth rate P_B has been maintained, while at $100/5 \mu\text{mol photons m}^{-2} \text{s}^{-1}$ 4 °C a stationary phase is reached (Fig. 3.18 D, E).

In summary, at a light intensity of $100 \mu\text{mol photons m}^{-2} \text{s}^{-1}$ the biomass growth rate of the *S. voratum* biofilm increases with temperature until 25 °C, where it peaks. Since the highest biomass growth rates have been shown to be at a light intensity of $600 \mu\text{mol photons m}^{-2} \text{s}^{-1}$ and additional CO_2 (as reference see section 3.3), the biofilm is additionally cultivated at this condition first and then exposed to different temperatures. The corresponding results are given in figure 3.19. By raising the temperature to 36 °C a decrease in biomass growth is observed (Fig. 3.19 A). However, at the standard conditions of 30 °C (Fig. 3.19 B) the biofilm grows with $7.6 \text{ g m}^{-2} \text{d}^{-1}$ ($R^2 = 0.99$), which corresponded to the expected reference data (Fig. 3.11).

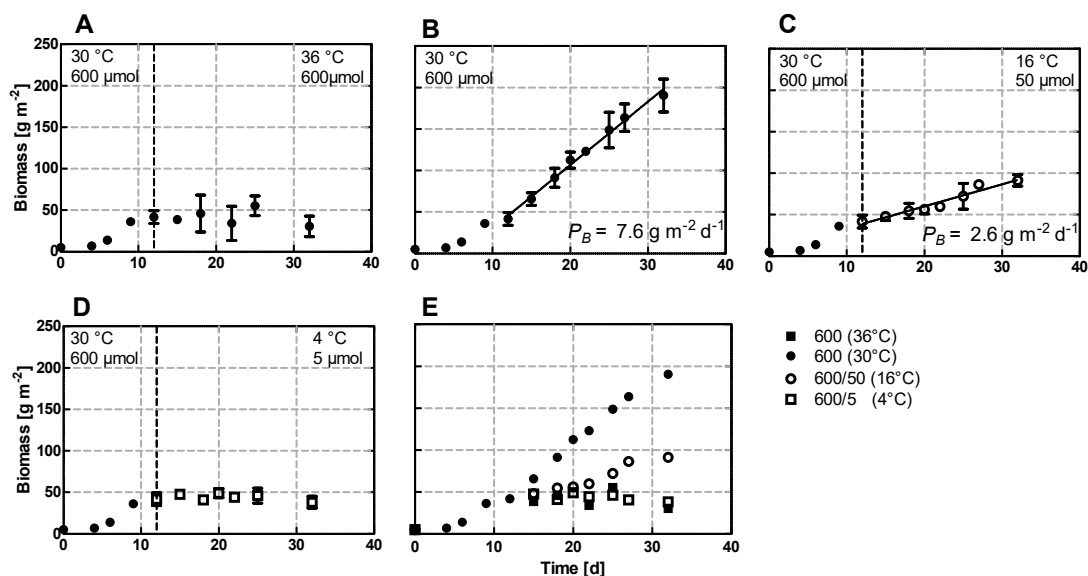


Figure 3.19: Impact of temperature on the biomass growth rate of the *S. voratum* biofilm pre-grown at $600 \mu\text{mol photons m}^{-2} \text{s}^{-1}$ and 2 % CO_2 . After the transfer on day 12 the biofilms were exposed to 36 °C and 2 % CO_2 as well as 16 and 4 °C with ambient air. Shown are mean \pm SD for $n = 3$ and the correlating linear regression. P_B = Biomass growth rate from the linear fit in $\text{g m}^{-2} \text{d}^{-1}$.

At lower light, temperature and ambient air the growth ceases (Fig. 3.19 C) and is stationary at 4 °C (Fig. 3.19 D). Therefore the determined temperature optimum in this experiment at $600 \mu\text{mol photons m}^{-2} \text{s}^{-1}$ is 30 °C.

In figure 3.20 the peridinin production over the time course of the experiment at $100 \mu\text{mol photons m}^{-2} \text{s}^{-1}$ is given. The maximal peridinin amount per area, 0.95 g m^{-2} , and the highest productivity P_P , $0.043 \text{ g m}^{-2} \text{d}^{-1}$, are obtained at a light intensity of $100 \mu\text{mol photons m}^{-2} \text{s}^{-1}$ and 32 °C, (Fig. 3.20 A). In addition, the productivities P_P of the data from 25 and 32 °C are not significantly different (Fig. 3.20 F) and on average 30 % higher than at 20 °C. Overall with the decrease of the temperature and irradiance, the productivity P_P is unaltered (Fig. 3.20 D, F).

The data for the pigment production in the biofilms of *S. voratum* initially grown at $600 \mu\text{mol photons m}^{-2} \text{s}^{-1}$ and 2 % CO_2 are illustrated in figure 3.21. As shown in figure 3.21 B and C, only by the exposure to 30 and 16 °C a linear increase in peridinin can be achieved. The highest productivity is recorded at $600/50 \mu\text{mol photons m}^{-2} \text{s}^{-1}$ and 16 °C with $0.037 \text{ g m}^{-2} \text{d}^{-1}$ ($R^2 = 0.99$) (Fig. 3.21 C).

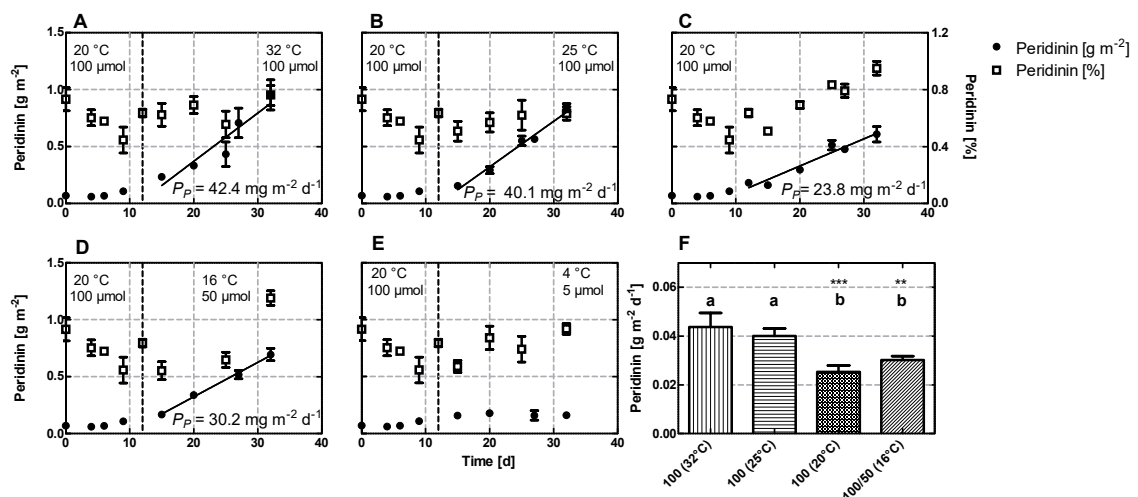


Figure 3.20: Impact of temperature on the peridinin production of the *S. voratum* biofilm pre-grown at $100 \mu\text{mol photons m}^{-2} \text{ s}^{-1}$. After the transfer on day 12 the biofilms were exposed to 32 and 25 °C as well as 16 and 4 °C with ambient air. Presented is the peridinin amount per area (●) and the peridinin concentration per biomass dw (□). Shown are mean \pm SD for $n = 3$ and the correlating linear regression. P_P = Peridinin productivity from the linear fit in $\text{mg m}^{-2} \text{ d}^{-1}$. F Comparison of P_P . As statistical analysis a one-way ANOVA with Tukey's multiple comparison test has been performed.

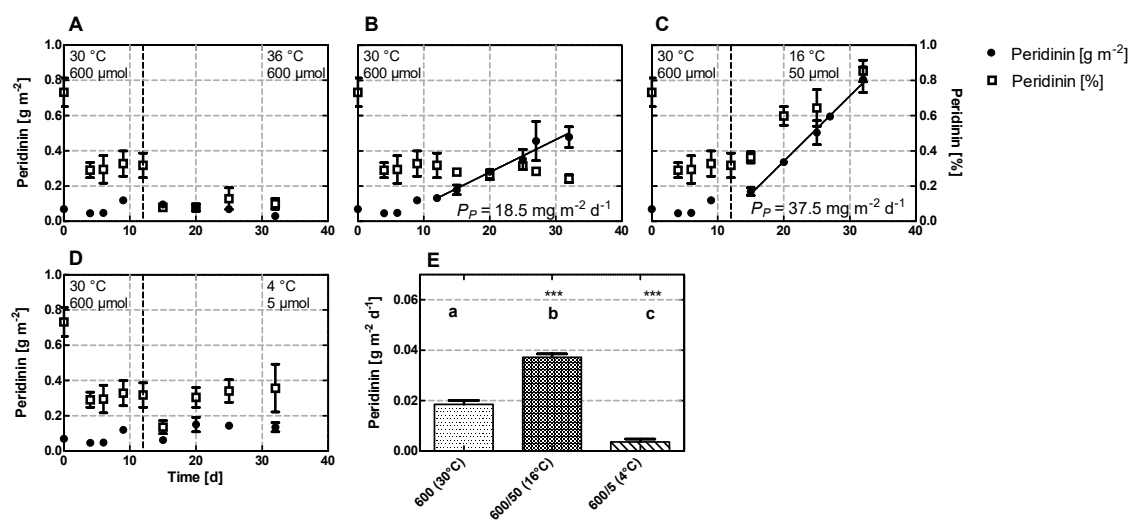


Figure 3.21: Impact of temperature on peridinin production of the *S. voratum* biofilm pre-grown at $600 \mu\text{mol photons m}^{-2} \text{ s}^{-1}$ and 2 % CO₂. After the transfer on day 12 the biofilms were exposed to 36 °C and 2 % CO₂ as well as 16 and 4 °C with ambient air. Presented is the peridinin amount per area (●) and the peridinin concentration per biomass dw (□). Shown are mean \pm SD for $n = 3$ and the correlating linear regression. P_P = Peridinin productivity from the linear fit in $\text{mg m}^{-2} \text{ d}^{-1}$. E Comparison of P_P . As statistical analysis a one-way ANOVA with Tukey's multiple comparison test has been performed.

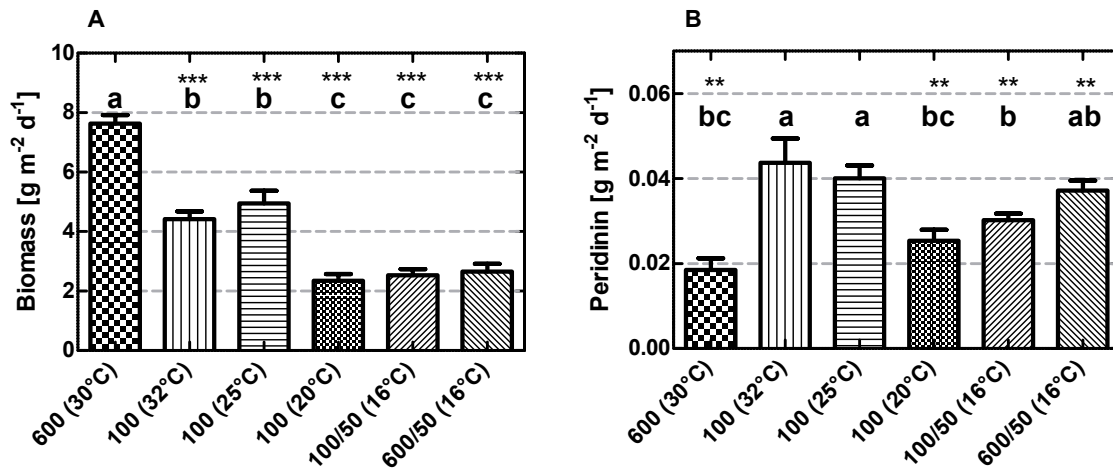


Figure 3.22: Biomass and peridinin productivity of an the *S. voratum* biofilm culture from the temperature experiment. In one setup the biofilm has been pre-grown 100 $\mu\text{mol photons m}^{-2} \text{s}^{-1}$, 20°C and ambient air, while the other is initially kept at 600 $\mu\text{mol photons m}^{-2} \text{s}^{-1}$, 30 °C and 2 % CO_2 . After 12 days the cultures at 100 $\mu\text{mol photons m}^{-2} \text{s}^{-1}$ were transferred to the shown conditions. On the x axis the applied light intensity and temperature is presented. Shown are mean \pm SD for $n = 3$. As statistical analysis a one-way ANOVA with Tukey's multiple comparison test was performed.

Thus, the transfer to low light and temperature increased the maximal amount of peridinin [g m^{-2}] by 40 % and doubled the productivity rate P_P in comparison to the biofilm grown continuous with 600 $\mu\text{mol photons m}^{-2} \text{s}^{-1}$ and 30 °C (Fig. 3.21 E).

Overall the highest biomass growth rate (Fig. 3.22 A), is noted at 600 $\mu\text{mol photons m}^{-2} \text{s}^{-1}$ 2 % CO_2 and 30 °C. At the irradiance of 100 $\mu\text{mol photons m}^{-2} \text{s}^{-1}$ the maximal biomass growth rate is gained at a temperature above 25 °C. In total the light intensity and temperature show to affect the biomass growth rate. Likewise the peridinin production is dependent on the applied temperature and increases with lower light conditions. As a result the peridinin production rate at 100 $\mu\text{mol photons m}^{-2} \text{s}^{-1}$ with 32 °C, 23 °C and 600/50 $\mu\text{mol photons m}^{-2} \text{s}^{-1}$ with 16 °C cannot be differentiated and are therefore marked as one group (a) (Fig. 3.22 B). Furthermore the data obtained in this experiment indicate, that the peridinin production rate is identical at the control conditions (100, ambient air and 600 $\mu\text{mol photons m}^{-2} \text{s}^{-1}$ with 2 % CO_2), which is in accordance to the previous findings (Fig. 3.12).

3.6 Two-Step Approach (Exp. TS)

A conclusion of the CO₂ experiment (Section 3.3) has been that the highest biomass growth rate does not correlate with the maximal pigment production. In addition it has been found that the light intensity significantly affect peridinin productivity (see Section, 3.1, 3.5). As a result a two-step experiment investigating the shift from growth enhancing to peridinin promoting conditions has been conducted. To maximise the biomass production in the first step and generate a thick biofilm prior to the second peridinin production step, biofilms have been grown at 600 $\mu\text{mol photons m}^{-2} \text{s}^{-1}$ and 2 % CO₂ (for references, see section 3.3, Fig. 3.16 D). In order to investigate the optimal time interval for the shift between the growth phase (600 $\mu\text{mol photons m}^{-2} \text{s}^{-1}$, 2 % CO₂) and the peridinin production phase (100 $\mu\text{mol photons m}^{-2} \text{s}^{-1}$ and ambient air), biofilms are pre-grown at 600 $\mu\text{mol photons m}^{-2} \text{s}^{-1}$ and 2 % CO₂ for one, two, three and four weeks, respectively, prior to the shift to 100 $\mu\text{mol photons m}^{-2} \text{s}^{-1}$. As control, biofilms have been grown in parallel at constant growth enhancing (600 $\mu\text{mol photons m}^{-2} \text{s}^{-1}$ and 2 % CO₂) and peridinin promoting conditions (100 $\mu\text{mol photons m}^{-2} \text{s}^{-1}$ and ambient air), respectively.

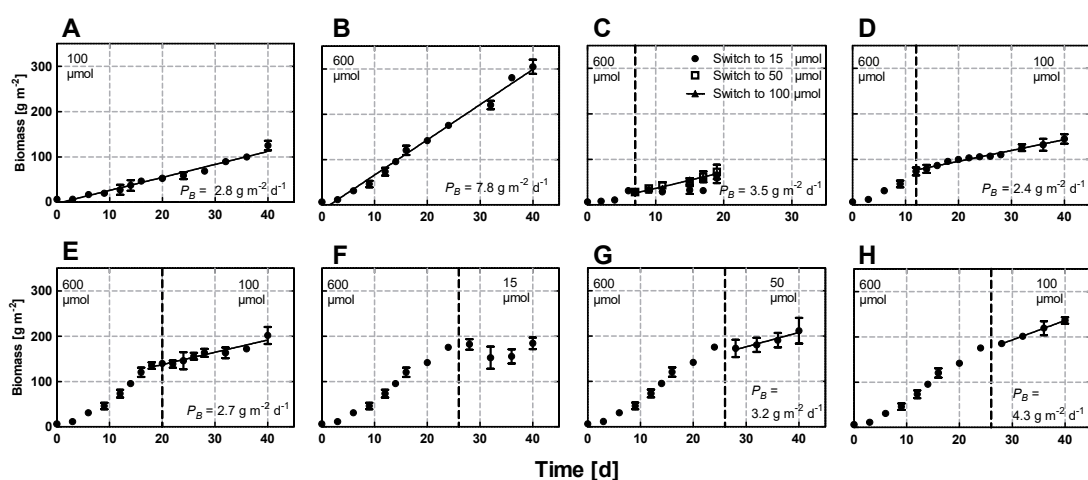


Figure 3.23: Growth of *S. voratum* biofilm in a two-step approach. The immobilised culture is grown at 600 $\mu\text{mol photons m}^{-2} \text{s}^{-1}$ and 2 % CO₂ and then shifted to 100 $\mu\text{mol photons m}^{-2} \text{s}^{-1}$. The time points are indicated by the dashed lines. Shown are mean \pm SD for $n = 3$ and the correlating linear regression. P_B = Biomass growth rate from the linear fit in $\text{g m}^{-2} \text{d}^{-1}$.

In general, elongation of the growth promoting phase has been found to enhance the biomass production during the peridinin producing phase (Fig. 3.23). The biofilm kept at $100 \mu\text{mol photons m}^{-2} \text{s}^{-1}$ is growing linear with a productivity P_B of $2.8 \text{ g m}^{-2} \text{d}^{-1}$. Over the whole experimental time course (40 d), the *S. voratum* biofilm illuminated with $100 \mu\text{mol photons m}^{-2} \text{s}^{-1}$ (Fig. 3.23 B) grows linear to maximal 125.4 g m^{-2} without reaching a stationary phase. The obtained growth rate is in accordance to previous results (Fig. 3.16). When grown solely at growth enhancing conditions (Fig. 3.23 A), the biofilm growth during the time course of the experiment (40d) is linear with maximal 304.8 g m^{-2} and does not reach a stationary phase. At the first time point of the light transfer the biomass has been exposed to 15, 50 and $100 \mu\text{mol photons m}^{-2} \text{s}^{-1}$. At 50 and $100 \mu\text{mol photons m}^{-2} \text{s}^{-1}$ the biofilm continues to increase linear as well ($R^2 = 0.96, 0.98$), but the growth rate is reduced by 50 % to 3.4 and $3.5 \text{ g m}^{-2} \text{d}^{-1}$, respectively, in comparison to high light conditions (Fig. 3.16 C). The slopes of the two light intensities are not distinguishable (ANCOVA, $p = 0.9878$). Immobilised cultures transferred to $15 \mu\text{mol photons m}^{-2} \text{s}^{-1}$ stop biomass accumulation, independent from the duration of the growth enhancing period (Fig. 3.16 C, F). In the shift after the second, third and fourth week (Fig. 3.16 D, E, G, H) the biomass growth always remains linear. The highest growth rate is gained at the switch in the fourth week with $4.3 \text{ g m}^{-2} \text{d}^{-1}$ (Fig. 3.16 H).

Under constant low light conditions the peridinin production P_P grows linear with $27.3 \text{ mg m}^{-2} \text{d}^{-1}$ (Fig. 3.24 A). The pigment concentration [% of dw] in the *S. voratum* biofilm is highest at $100 \mu\text{mol photons m}^{-2} \text{s}^{-1}$ at day 24 (1.16 %) and then decreases. The peridinin amount [g m^{-2}] in the biofilm cultivated at $600 \mu\text{mol photons m}^{-2} \text{s}^{-1}$ (Fig. 3.24 B) is maximal at day 32 and then is decreasing with time, this is also shown for the relative peridinin concentration [% of dw]. In both control conditions, constant growth promotion and pigment enhancement, the peridinin production rate P_P and amount per area [g m^{-2}] is similar until day 32 (Fig. 3.24 A, B). In the shift after one weeks (Fig. 3.24 C) the peridinin production remains linear and is identical with the control. The highest peridinin productivity ($P_P = 51.4 \text{ mg m}^{-2} \text{d}^{-1}$) is recorded when the biofilm is shifted after a biomass growth phase of two weeks (Fig. 3.24 D). In contrast at the switch after three weeks the peridinin accumulates

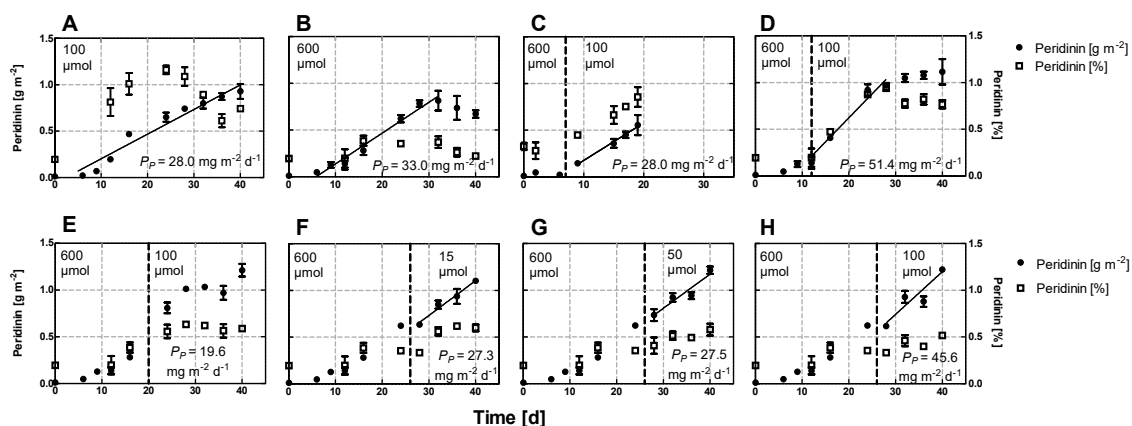


Figure 3.24: Pigment production of *S. voratum* biofilms in the two-step approach. Development of the peridinin per area (●) and peridinin per biomass (□) over the time course (40 days) of the experiment. The dashed line indicates a shift from growth promoting conditions ($600 \mu\text{mol photons m}^{-2} \text{s}^{-1}$, 2 % CO_2) to the peridinin productive phase ($100 \mu\text{mol photons m}^{-2} \text{s}^{-1}$, ambient air). Shown are mean \pm SD for $n = 3$ and the correlating linear regression. P_P = Peridinin productivity from the linear fit in $\text{mg m}^{-2} \text{d}^{-1}$.

slowly with $19.6 \text{ mg m}^{-2} \text{d}^{-1}$, but the fit is not linear ($R^2 = 0,74$) (Fig. 3.24 E). When considering the data which were gained by the shift in week four (Fig. 3.24 F, G, H) the production rate P_P matches the one from the control again. Shifting the biofilm after four weeks at growth enhancing conditions to $100 \mu\text{mol photons m}^{-2} \text{s}^{-1}$ even increases the productivity to $45.6 \text{ mg m}^{-2} \text{d}^{-1}$ ($R^2 = 0.9042$) (Fig. 3.24 H). The peridinin per biomass [%] from the two-step approaches is increasing when the biofilm is shifted in week one and four (Fig. 3.24 C, F, G, H). At the second and third time point (Fig. 3.24 D, E) the percentage of pigment is stagnating.

As it is shown in figure 3.25 A, the control at $100 \mu\text{mol photons m}^{-2} \text{s}^{-1}$ reaches a final peridinin amount of 0.93 g m^{-2} while the value in the biofilm at high light is significantly reduced at this time point of the experiment. Shifting of the immobilised *S. voratum* biofilm from growth promoting to peridinin producing conditions enhanced the pigment amount significantly in all approaches, compared to the 100 and 600 $\mu\text{mol photons m}^{-2} \text{s}^{-1}$ control (Fig. 3.25 A). With the exception of the shift after four weeks to $15 \mu\text{mol photons m}^{-2} \text{s}^{-1}$, the two-step approach generates a significantly higher absolute peridinin amount per area on the final day of the experiment. Overall the duration of the growth phase does not affect the final peridinin amount and a 22.5 % increase in comparison to $100 \mu\text{mol photons m}^{-2} \text{s}^{-1}$ is achieved. Since

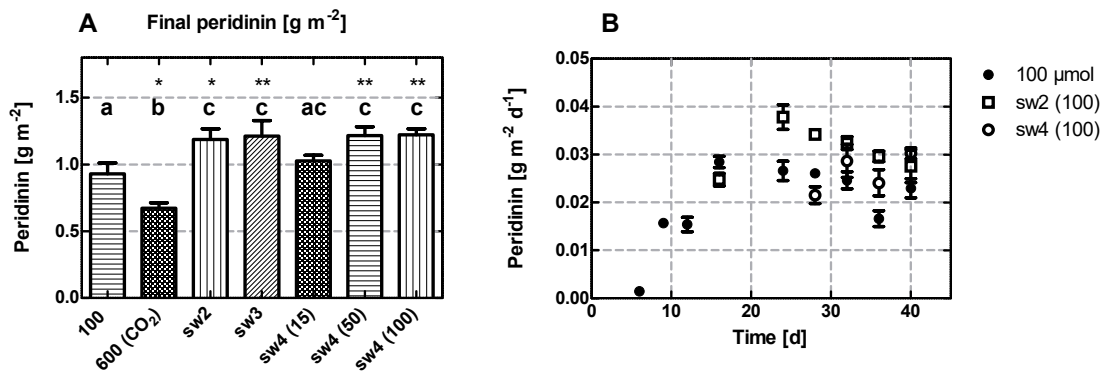


Figure 3.25: **A** Final peridinin amount of day 40 in the two-step approach. As statistical analysis a one-way ANOVA with Tukey’s multiple comparison test has been performed. **B** Average peridinin production over the time course of the experiment. Indicated by 100 μmol: data from the control for the continuous peridinin production at 100 μmol photons m⁻² s⁻¹, sw2 (100) and sw4 (100): biofilm with a growth promoting phase of two and four weeks. Shown are mean ± SD for n = 3.

the highest peridinin productivity P_P is observed after a growth promoting phase of two and four weeks (Fig. 3.24 D, H) their average productivity of peridinin per day is compared to the control conditions for peridinin enhancement (100 μmol photons m⁻² s⁻¹, ambient air, Fig. 3.25 B). The average peridinin production increases until day 24 and is maximal in the *S. voratum* biofilm with the growth enhancing phase of two weeks (Fig. 3.25 B, sw2 (100)). Furthermore on day 24 of the experiment the value of peridinin per area [g m⁻²] in the biofilm with the growth phase of two weeks

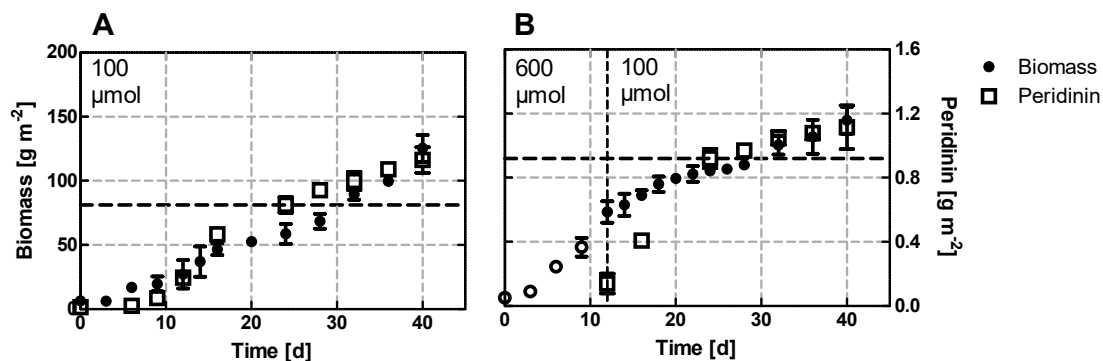


Figure 3.26: Combination of biomass and peridinin production in the *S. voratum* biofilm grown constantly at 100 μmol photons m⁻² s⁻¹ and ambient air in comparison to the biofilm with a two week growth promoting phase at 600 μmol photons m⁻² s⁻¹ and 2 % CO₂. Shown are mean ± SD for n = 3.

(Fig. 3.26 B) is increased by over 40 % to 0.92 g m^{-2} in comparison to 0.65 g m^{-2} in the biofilm grown constantly at $100 \mu\text{mol photons m}^{-2} \text{ s}^{-1}$ (Fig. 3.26 A).

In summary the step-wise production of peridinin is maximal after growth promotion of two weeks and enables a 57 % increase in the pigment productivity P_P in comparison to the control conditions at $100 \mu\text{mol photons m}^{-2} \text{ s}^{-1}$.

Form the documentation of the biofilm over the time course of the experiment (Fig. 3.27) it can be seen, that in peridinin promoting conditions ($100 \mu\text{mol photons m}^{-2} \text{ s}^{-1}$, ambient air) colouration of the biofilm increases strongly while the uppermost cell layer remains loosely connected (Fig. 3.27 A-C). In comparison the immobilised *S. voratum* culture at the growth enhancing conditions ($600 \mu\text{mol photons m}^{-2} \text{ s}^{-1}$, 2 % CO_2), appears lighter in colour and the cells are densely packed

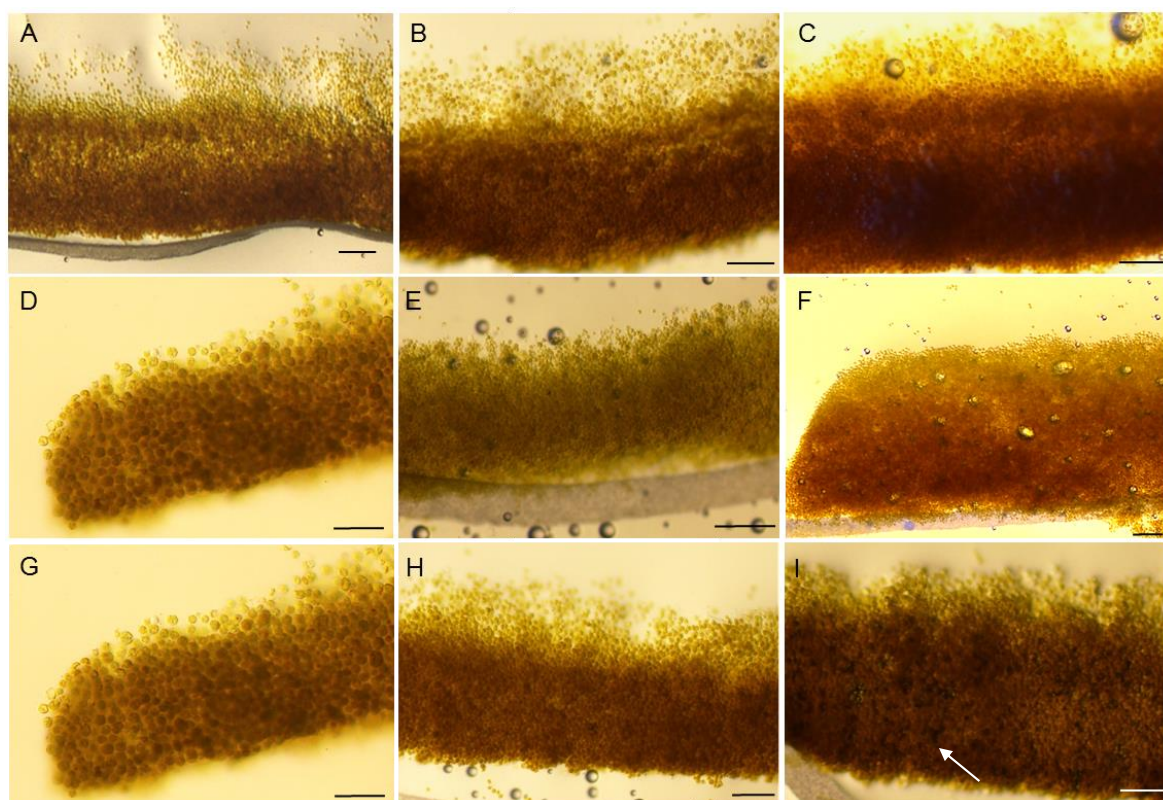


Figure 3.27: Cross-section of the *S. voratum* biofilm in the two-step approach. **A-C** $100 \mu\text{mol photons m}^{-2} \text{ s}^{-1}$, ambient air on day 9, 18 and 24. **D-F** $600 \mu\text{mol photons m}^{-2} \text{ s}^{-1}$, 2 % CO_2 on day 9, 18 and 24. **G-I** Two-Step Approach: Biofilm during the growth promoting phase ($600 \mu\text{mol photons m}^{-2} \text{ s}^{-1}$, 2 % CO_2) on day 9 and after the shift to $100 \mu\text{mol photons m}^{-2} \text{ s}^{-1}$, ambient air on day 18 **H** and 24 **I** Indicated by the white arrow are cell aggregations

within the complete biofilm (Fig. 3.27 D-F). The shift of the immobilised culture from growth to peridinin promoting conditions affects the morphology as well, since the uppermost cell layer becoming less dense and colouration increases within the duration of three weeks (Fig. 3.27 H). On day 24 dark spots within the biofilm (Fig. 3.27 I, white arrow) can be detected, which are absent in either of the control conditions (Fig. 3.27 C, F).

3.7 Media Experiment for up-scale systems (Exp. M)

Besides light, CO₂ and temperature, nutrient supply strongly affects the growth of microalgae and therefore six different media were analysed upon their impact on the growth and peridinin production of the *S. voratum* biofilm (Fig. 3.28 and Fig. 3.29). For this purpose the immobilised culture has been grown at the light intensity of 100 μmol photons m⁻² s⁻¹ and ambient air at 23 °C for 21 days, in bench-scale TL PSBRs. To mimic conditions of large scale operations, the media were not sterilised. Since artificial f/2 and ASP 12 have been used in previous experiments (Section 3.1 - 3.7), they functioned as control media. Additionally to these standardised media original f/2 and three seawater modifications were employed. These variations consisted of seawater enriched solely on phosphate and nitrate (SW1), seawater with enhanced concentrations of all macro and micro nutrients (SW2) and seawater treated with commercial fertiliser (SW3). Composition of the media are given in section 2.1.1.

The growth rate of the immobilised cultures of *S. voratum* maintained in the control media ASP 12 (Fig. 3.28 A) and artificial f/2 (Fig. 3.28 B) were in accordance to previous experiments (Fig. 3.16 A, C, section 3.4). However, f/2 based on natural seawater (Fig. 3.28 C) could enhance the productivity by 25 %. Despite an initial lag phase, the use of seawater modifications (Fig. 3.28 D, E) enhanced the growth of *S. voratum* by 67 to 73 % (SW1, SW2, respectively) compared to the control media. However, biofilms grown on the fertilised SW3 stopped growth on day 13 and creased in biomass from day 17 on (Fig. 3.28 F). With respect to the peridinin productivity P_P the control media (Fig. 3.29 A, B) obtain similar results at 100 μmol photons m⁻² s⁻¹ as

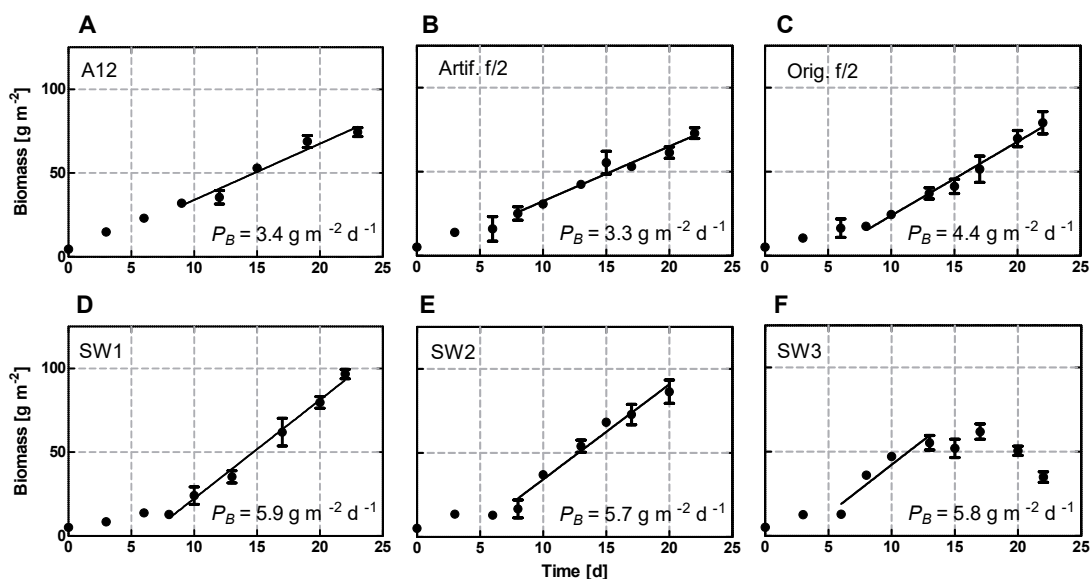


Figure 3.28: Biomass production in the *S. voratum* biofilm in six different media. Applied were **A** ASP 12 (A12), **B** artificial f/2 (artif.f/2), **C** original f/2 (orig. f/2), **D** SW(Seawater)1: Seawater + nitrogen and phosphate levels as in ASP 12. **E** SW2: Seawater as NaCl source with all ASP 12 stocks. **F** SW3: Seawater + fertiliser. The detailed composition of the media is given in 2.1.1. Shown are mean \pm SD for $n = 3$ and the correlating linear regression. P_B = Biomass growth rate from the linear fit in $\text{g m}^{-2} \text{d}^{-1}$.

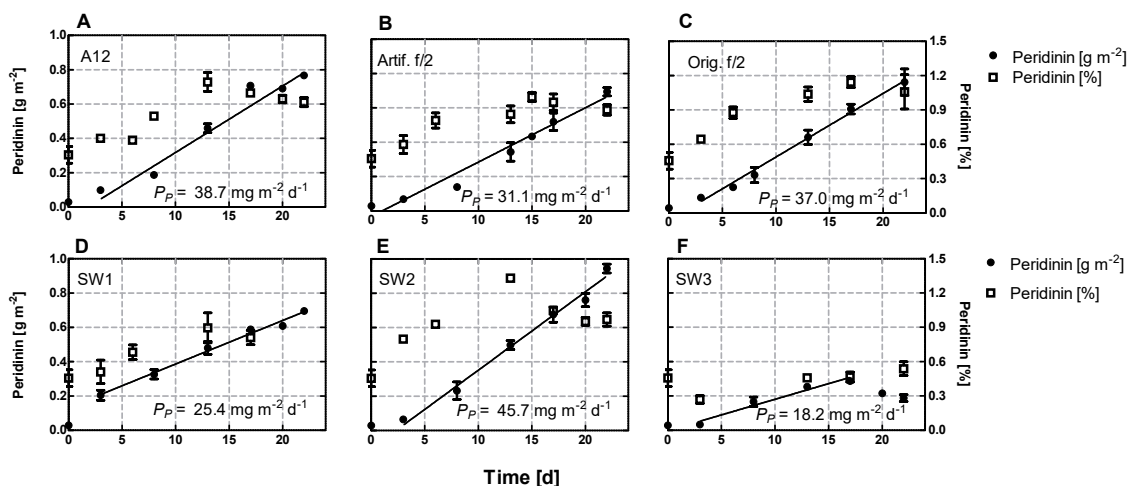


Figure 3.29: Peridinin production in the *S. voratum* biofilm in six different media. Applied were **A** ASP 12 (A12), **B** artificial f/2 (artif.f/2), **C** original f/2 (orig. f/2), **D** SW(Seawater)1: Seawater + nitrogen and phosphate levels as in ASP 12. **E** SW2: Seawater as NaCl source with all ASP 12 stocks. **F** SW3: Seawater + fertiliser. The detailed composition of the media is given in 2.1.1. Shown are mean \pm SD for $n = 3$ and the correlating linear regression. P_P = Peridinin productivity from the linear fit in $\text{mg m}^{-2} \text{d}^{-1}$.

previously recorded (Fig. 3.17 A, C). The highest production rate P_P is recorded in the SW2 with an increase of 15 % . For the other two modifications the pigment accumulation decreases. SW3 overall presents the lowest peridinin amount [g m^{-2}], which even ceases to the end of the experiment (Fig. 3.29 F). In summary the utilisation of the medium SW2 gains a 73 % increase in biomass production and a 25 % higher peridinin productivity in comparison the the control media (Fig. 3.28 E and 3.29 E).

3.8 Up-scaling of the Twin-Layer PSBR

Besides enhancement of growth and peridinin production of *S. voratum*, further development on the Twin-Layer PSBR has been conducted and an up-scaling of the culture system was performed. For comparison of different setups, investigation of *S. voratum* biofilm growth was performed on a vertical Twin-Layer PSBR (Section 3.8.1) and horizontal Twin-Layer PSBR (Section 3.8.2). Details on the technical composition of the cultivation systems are given in section 2.3.

3.8.1 Performance of *S. voratum* in the vertical up-scale TL PSBR

After a prolonged lag phase of seven days, growth of the *S. voratum* biofilm on the vertical up-scale TL PSBR was linear (Fig. 3.30 A) and thereby reproduced the growth behaviour on bench-scale systems (Sections 3.1.1).

The growth rate of biomass is determined to be $1.96 \text{ g m}^{-2} \text{ d}^{-1}$, which is over 30 % lower than in the bench-scale TL experiments under comparable conditions (Fig. 3.30 B). Besides the measurement of biofilm growth, the running Twin-Layer PSBR was closely observed over the time course of the experiment to identify potential contaminations or system failures (Fig. 3.31 A - C). Detailed observation of the *S. voratum* biofilm (Fig. 3.31 D) did not identify any contamination with other algae. However, fungi have been identified on the backside of the vertical paper TL module after four weeks, but no affect on the functionality of the reactor has been noted. Similar to previous experiments (Section 3.2), the *S. voratum* biofilm growing on the

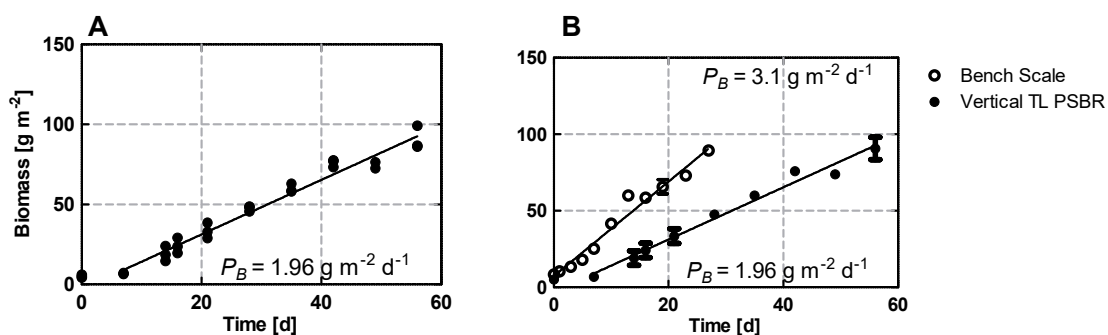


Figure 3.30: Biofilm growth of *S. voratum* in the vertical up-scale TL PSBR. **A** Biomass growth at $130 \mu\text{mol photons m}^{-2} \text{s}^{-1}$. **B** Comparison of biomass growth in vertical up-scale (\bullet) with bench-scale (\circ) TL PSBR (Section 3.1.1, figure 3.1 D). Shown are mean \pm SD for $n = 3$ and the correlating linear regression. P_B = Biomass growth rate from the linear fit in $\text{g m}^{-2} \text{d}^{-1}$.

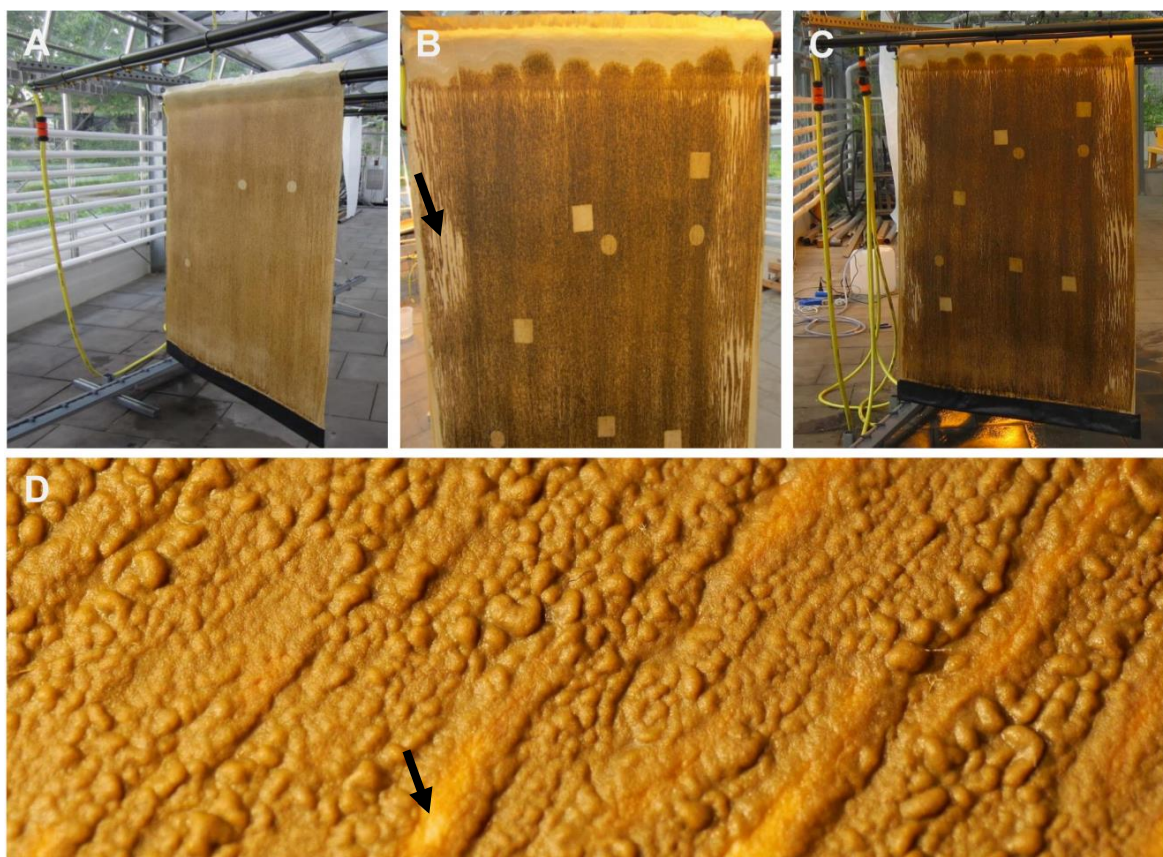


Figure 3.31: Documentation of a *S. voratum* biofilm grown on a vertical up-scale TL PSBR. Biofilm of *S. voratum* **A** on the day of the inoculation, **B** on day 16 **C** and day 30. **D** Close up to the biofilm surface on the final day of the experiment. Indicated by the black arrows are detachments of the paper substrate layer.

vertical up-scale TL PSBR develop a rough surface of hills and grooves (Fig. 3.31 D). In summary, the vertical up-scale TL PSBR has been shown to maintain the qualitative properties from the bench-scale experiments. However, the growth rate is significantly reduced.

3.8.2 Performance of *S. voratum* in the horizontal up-scale TL PSBR

To further investigate the performance of the *S. voratum* in an up-scale Twin-Layer system a second, simpler reactor design has been applied. For this purpose the *S. voratum* biofilm has been cultivated in a horizontal up-scale TL PSBR (Section 2.3.2). For comparability with previous experiments (Section 3.1 - 3.7) the initial horizontal up-scale TL PSBR system consisted of glass fibre as source layer and paper as substrate layer. Furthermore a TL setup with a fleece-based substrate layer was tested.

3.8.3 Paper as substrate layer in the horizontal TL PSBR

As the horizontal system consists of two cultivation areas (Section 2.3.2) the growth of the *S. voratum* biofilm on the "left" and the "right" side were analysed separately (Fig. 3.32). The biomass growth on both areas was linear on average (Fig. 3.32 A, C), but the *S. voratum* biofilm on the left area grew very inhomogeneously. On the bottom and middle part on the left side of the system, the *S. voratum* biofilm grow slower than on the top part (Fig. 3.32 C). While the growth rate P_B of the *S. voratum* biofilm of the right side of the horizontal system was $2.9 \pm 0.6 \text{ g m}^{-2} \text{ d}^{-1}$, which is similar to the growth of bench-scale TL systems with $3.1 \text{ g m}^{-2} \text{ d}^{-1}$ (Fig. 3.32 B), the inhomogeneous growth on the left side only reaches $2.0 \text{ g m}^{-2} \text{ d}^{-1}$ on average (Fig. 3.32 C). Even so the TL system is based on paper no fungal contamination has been recorded.

The peridinin production of the *S. voratum* biofilm on the horizontal up-scale TL PSBR was generally affected by the localisation within the growth area of the system (Fig. 3.33 A, B). While on both sides of the paper-based horizontal TL PSBR different peridinin productivities, $3.96 \text{ mg m}^{-2} \text{ d}^{-1}$ on the left and $5.27 \text{ mg m}^{-2} \text{ d}^{-1}$ on the right

side, have been recorded (Fig. 3.33 A,B), the peridinin concentration [% of dw] of both *S. voratum* biofilms were similar. However, the peridinin concentration decreases to the end of the experiment on both sides of the TL PSBR (Fig. 3.33 C, D).

The comparison of the total horizontal up-scale PSBR (left and right side combined) with the bench-scale TL PSBR shows a decrease in peridinin production by 80 % in the horizontal up-scale TL system (Fig. 3.34 A). Additionally, a decrease in peridinin concentration is not observed in bench-scale TL PSBR (Fig. 3.34 B). In summary, biomass growth rates of *S. voratum* on a paper-based horizontal up-scale TL PSBR were comparable with those achieved on bench-scale systems, while the peridinin production of bench-scale systems could not be reached.

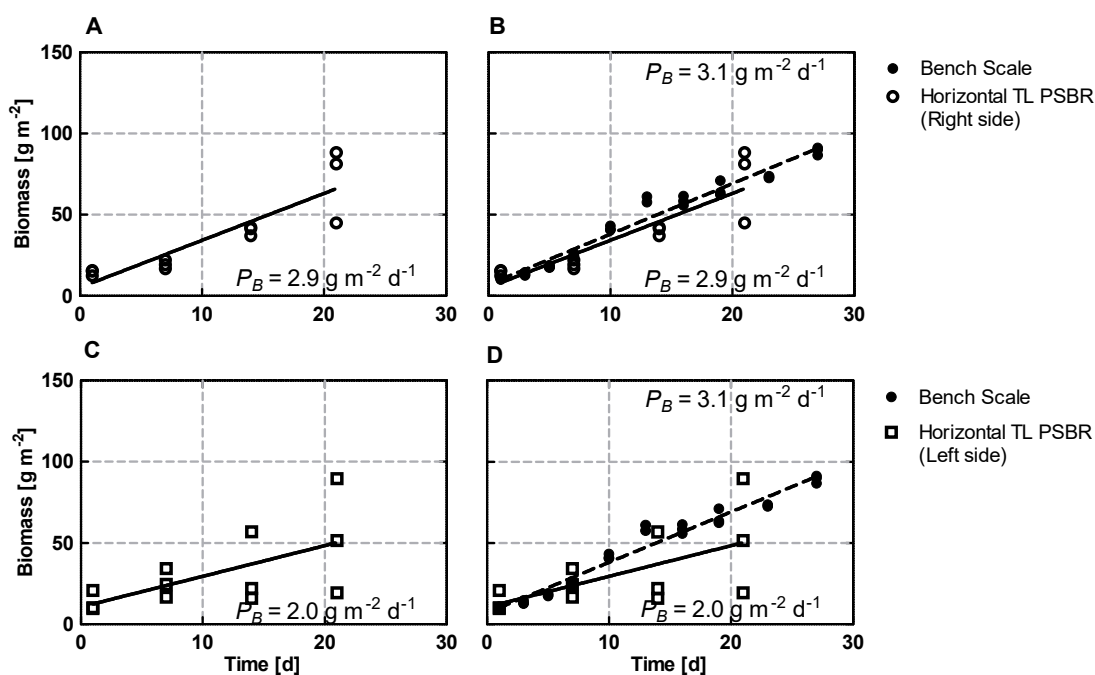


Figure 3.32: Growth of *S. voratum* in a paper-based horizontal up-scale TL PSBR. Presented are the biomass growth **A** on the right and **C** left side of the paper-based TL PSBR. The comparison to a bench-scale TL PSBR to the **B** right and **D** left side is given as well. Shown are mean \pm SD for $n = 3$ and the correlating linear regression. P_B = Biomass growth rate from the linear fit in $\text{g m}^{-2} \text{ d}^{-1}$.

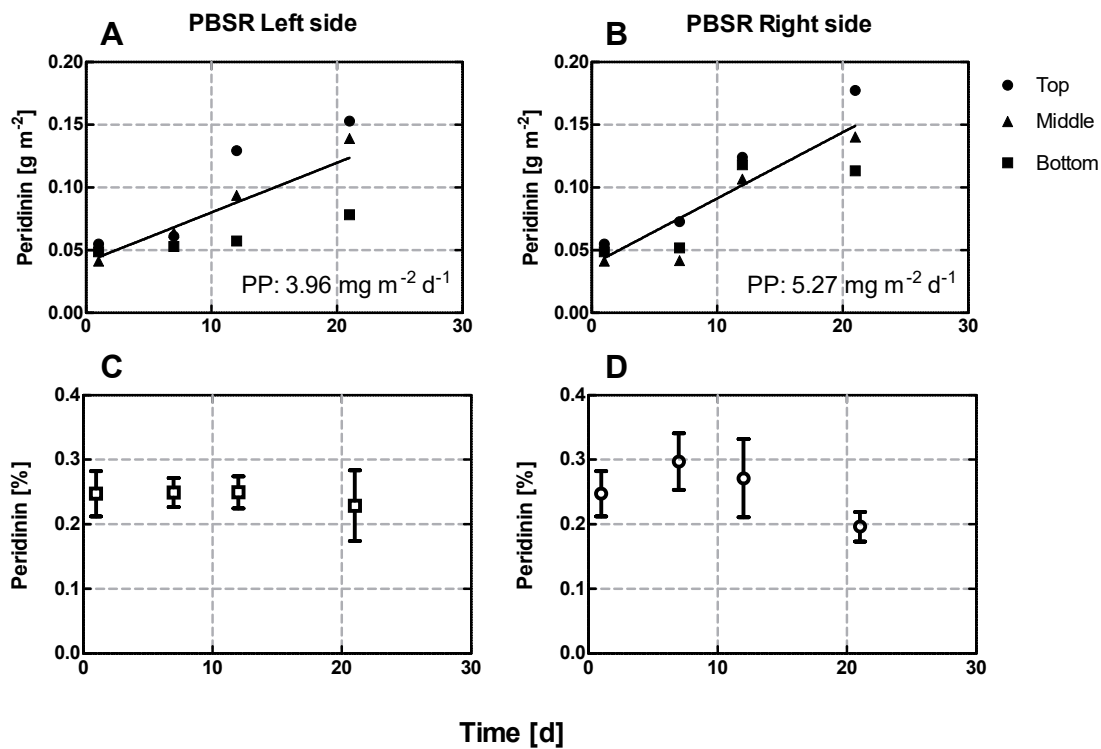


Figure 3.33: Peridinin production of *S. voratum* in a paper-based horizontal up-scale TL PSBR. Presented are peridinin amount per area (closed symbols) on the **A** left and **B** right side of the paper-based horizontal TL PSBR as well as the peridinin concentration per biomass (open symbols) on the **C** left and **D** right side of reactor. Shown are mean \pm SD for $n = 3$ and the correlating linear regression. P_P = Peridinin productivity from the linear fit in $\text{mg m}^{-2} \text{ d}^{-1}$.

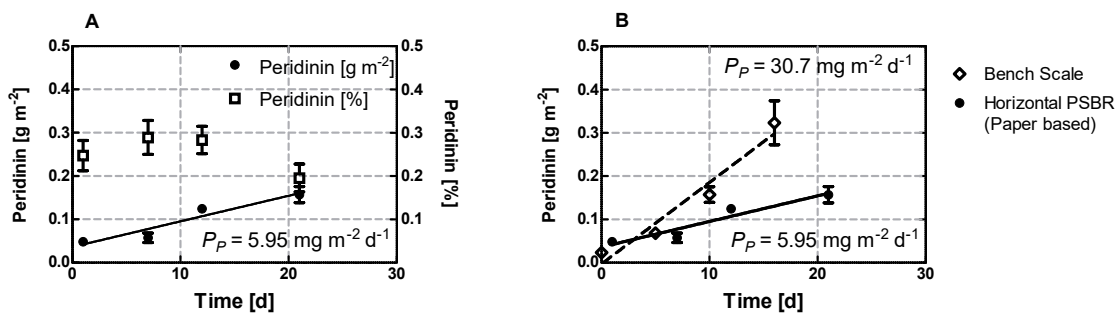


Figure 3.34: Peridinin productivity of *S. voratum* grown on a paper-based horizontal up-scale TL PSBR in comparison to the bench-scale TL PSBR. **A** Peridinin amount (●) and peridinin concentration (□) in the paper-based horizontal up-scale TL PSBR. **B** Comparison of bench and up-scale paper-based TL PSBR. The data present five replicates for the horizontal TL PSBR and three replicates for the bench-scale experiments. P_P = pigment productivity from the linear fit in $\text{mg m}^{-2} \text{ d}^{-1}$.

3.8.4 Fleece as substrate layer in the horizontal TL PSBR

First to gain comparable results to the bench-scale TL PSBRs the next horizontal up-scale TL PSBR has been constructed by the combination of the fleece material with the glass fibre as source layer. Secondly the fleece is kept as substrate layer, while a coarse grid functions as source layer in order to simply the setup.

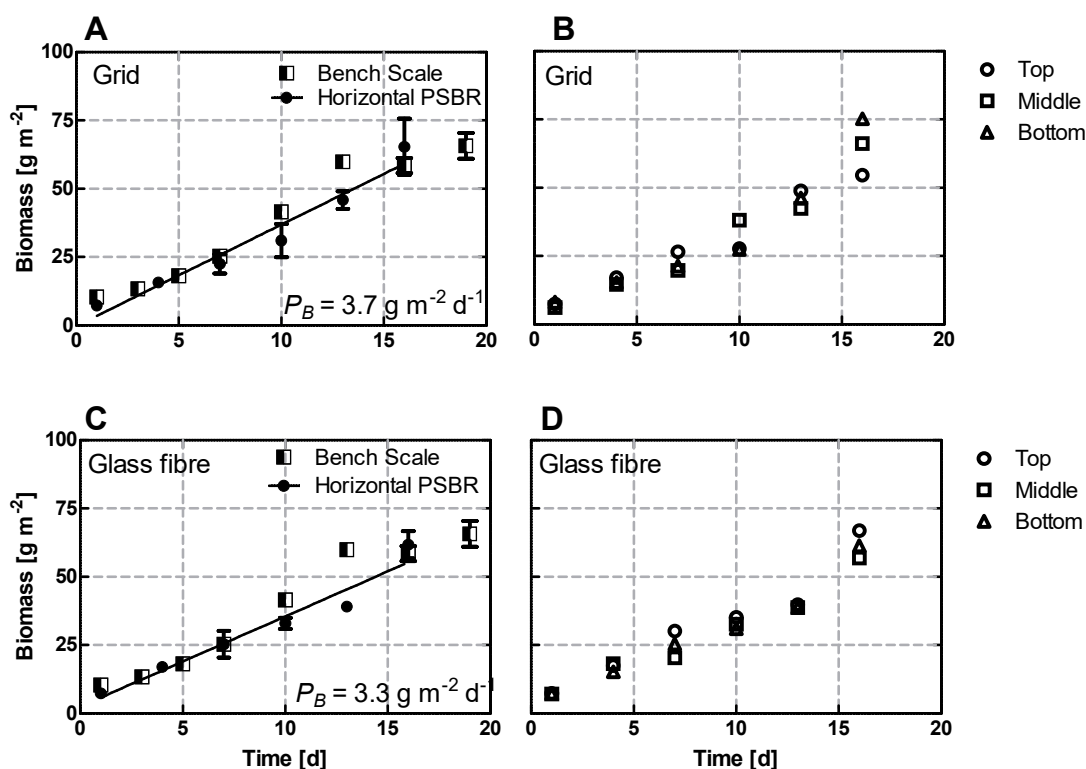


Figure 3.35: Biomass growth of *S. voratum* in a fleece-based horizontal up-scale TL PSBR in comparison to the bench-scale TL PSBR. **A, C** Presented is the comparison of the two fleece TL systems to the bench-scale TL PSBR (Section 3.1.1, figure 3.1 D). Shown are mean \pm SD for $n = 3$ and the correlating linear regression. P_B = Biomass growth rate from the linear fit in $\text{g m}^{-2} \text{ d}^{-1}$. For this three replicates each were analysed. In addition harvested sample locations with respect to the biomass are presented for the TL PSBR with **B** grid or **D** glass fibre as source layer.

The application of fleece in a horizontal up-scale TL PSBR with conventional composition (glass fibre as source layer) enabled growth of a *S. voratum* biofilm with $3.298 \pm 0.38 \text{ g m}^{-2} \text{ d}^{-1}$ (Fig. 3.35 D), while omitting the conventional source layer (fleece on the grid) generated a growth rate of $3.710 \pm 0.40 \text{ g m}^{-2} \text{ d}^{-1}$ (Fig. 3.35 B). However, both recorded growth rates do not differ significantly (ANCOVA, $p = 0.2774$).

A direct comparison of the growth in the immobilised culture of *S. voratum* on fleece as substrate with the paper-based bench-scale TL PSBR (Fig. 3.35 A, C) do not show a significant difference (ANCOVA, $p = 0.0974$). Over the time course no fungal or protist contaminations have been recorded. Therefore the cultivation of the dinoflagellate *S. voratum* in the horizontal up-scale TL PSBR with respect to biomass growth is comparable to bench-scale TL PSBR (Section 3.1.1, figure 3.1 D).

The peridinin production of the *S. voratum* biofilm, utilising fleece as substrate layer in a conventional horizontal TL PSBR was about $22.74 \text{ mg m}^{-2} \text{ d}^{-1}$ (Fig. 3.36 D), while in the fleece system omitting the source layer a peridinin production of $24.7 \text{ mg m}^{-2} \text{ d}^{-1}$ was reached (Fig. 3.36 B). Therefore both systems do not differ significantly in terms of peridinin production (ANCOVA, $p = 0.1033$) and are not distinguishable from peridinin production rates reached on bench-scale TL PSBR at the same conditions ($100 \mu\text{mol photons m}^{-2} \text{ s}^{-1}$, ambient air) (Fig. 3.36 A and C; ANCOVA, $p = 0.641$).

From the documentation of the fleece-based horizontal up-scale TL PSBRs it can be seen, that upon the inoculation an evenly distributed biofilm in both setups could be established (Fig. 3.37 A). In the first week of the experiment the biofilm grew denser and darker (Fig. 3.37 A, B) and until the end of the experiment the surface remained smooth and showed very little accumulation spots of biomass (Fig. 3.37 C, D). Even though minor detachments of the substrate layer towards the end of the experiment have been observed, the biofilm growth is not affected (Fig. 3.37 C). Observations of the *S. voratum* biofilm gave the impressions, that the horizontal system which is omitting the conventional source layer generates a wetter biofilm, that is easier to scrape of the substrate layer (Fig. 3.37 D). This finding was supported as sampling and harvesting of the conventional horizontal system was hindered by the tight connection of biofilm and fleece.

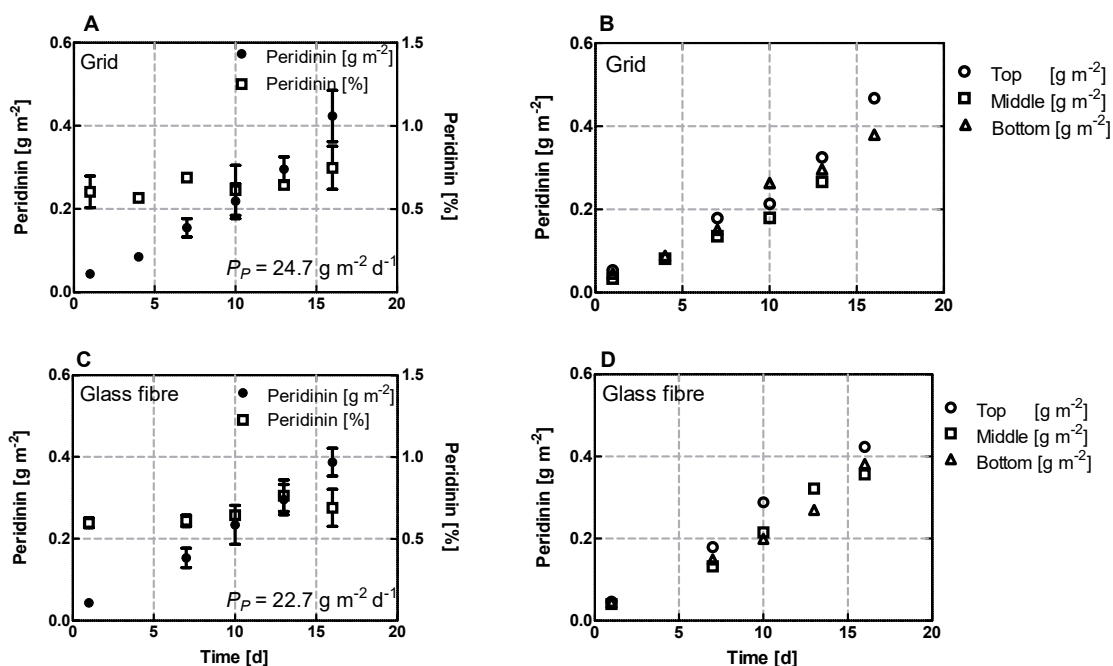


Figure 3.36: Peridinin production in an fleece-based horizontal up-scale TL PSBR. Presented is the peridinin amount per area (●) and peridinin per biomass (□) in the TL PSBR **A** grid or **C** glass fibre as source layer. Shown are mean \pm SD for $n = 3$ and the correlating linear regression. P_p = pigment productivity from the linear fit in $\text{mg m}^{-2} \text{ d}^{-1}$. In addition harvested sample locations with respect to the peridinin amount are presented for the TL PSBR with **B** grid or **D** glass fibre as source layer.

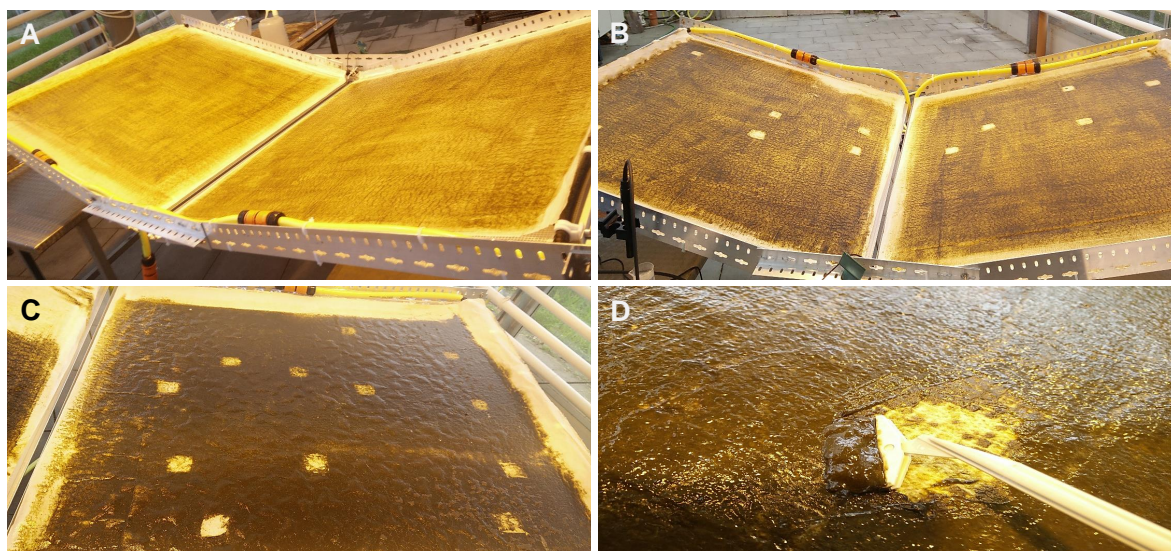


Figure 3.37: Documentation of the *S. voratum* biofilm on the horizontal up-scale TL PSBR. Depicted are the horizontal PSBRs with the TL combining fleece with grid (left) and glass fibre (right). Presented is the biofilm on **A** the inoculation day, **B** day 4 and **C** day 11. **D** Final harvesting of the *S. voratum* biofilm on day 16 in the TL PSBR composed of fleece and grid.

3.9 Comparison of the investigated up-scale TL PSBRs

While the vertical system could proof, that large cultivation of *S. voratum* in a paper-based vertical up-scale Twin-Layer PSBR is possible, the biomass growth rates observed in this system are about 35 % lower than in comparable bench-scale systems. The change from vertical to horizontal TL PSBR enhanced the growth rate of *S. voratum* to these of bench-scale systems (Fig. 3.35 A, C). With regard to the growth of the *S. voratum* biofilm the fleece-based horizontal TL PSBR gave the most profound correlation to the control data (Section 3.1.1, figure 3.1 D). The biomass productivity P_B in both horizontal fleece-based up-scale PSBRs is statistically not different from the bench-scale experiment (ANCOVA, $p = 0.097$). The highest growth rate of $3.7 \text{ g m}^{-2} \text{ d}^{-1}$ is recorded in the fleece-based horizontal TL PSBR (Tab. 3.1), which is composed of fleece as substrate layer and an underlying grid as source layer.

Table 3.1: Comparison of biomass P_B and peridinin P_P production rates of the *S. voratum* biofilms grown on different up-scale TL PSBR systems

Twin-layer PSBR	Material	P_B [$\text{g m}^{-2} \text{ d}^{-1}$]	P_P [$\text{mg m}^{-2} \text{ d}^{-1}$]	Figure
Bench-scale	Paper	3.1 ± 0.18	30.7 ± 3.0	3.1 D
Vertical	Paper	2.0 ± 0.04	n.a.	3.30 A
Horizontal	Paper *	2.9 ± 0.55	5.9 ± 1.3	3.32 B
Horizontal	Fleece	3.3 ± 0.38	24.7 ± 2.1	3.35 A
Horizontal	Fleece °	3.7 ± 0.40	22.7 ± 1.3	3.35 C

* = right reactor side (Section 3.8.3) ° = Grid as substrate layer (Section 3.8.4)

Data obtained at $100 \pm 15 \text{ } \mu\text{mol photons m}^{-2} \text{ s}^{-1}$ and $25 \pm 3 \text{ } ^\circ\text{C}$, in an outdoor green house.

In the comparison of peridinin productivities, the difference between paper and fleece-based horizontal up-scale TL PSBRs is very prominent. While the values of the fleece-based TL system are almost not distinguishable from the bench-scale TL PSBR, the peridinin production rate in the paper-based horizontal TL PSBR is three times lower. Due to the lower pigment productivity in the paper-based horizontal TL PSBR, the horizontal fleece-based reactor is the only up-scale Twin-Layer cultivation system in which the bench-scale results could be verified.

In summary, using a horizontal up-scale Twin-Layer PSBR utilising fleece as substrate layer it was possible to reproduce growth and peridinin production rates of 3.1 g m^{-2} and $30.7 \text{ mg m}^{-2} \text{ d}^{-1}$ determined under laboratory bench-scale conditions.

3.10 Photometric analysis of peridinin

An aim of the thesis has been to establish and analyse a photometrical analysis for the determination of the peridinin content. The photometric methodology is based on spectral reconstruction, which is described in more details in section 2.6. As it is indicated in figure 3.38 the correlation of the two methods is linear. The determined fit (R^2) of the linear regression equals 0.95 and is therefore significant. From the slope of the curve it can be concluded, that the peridinin concentration in the photometric analysis is consistently shifted by 20 %.

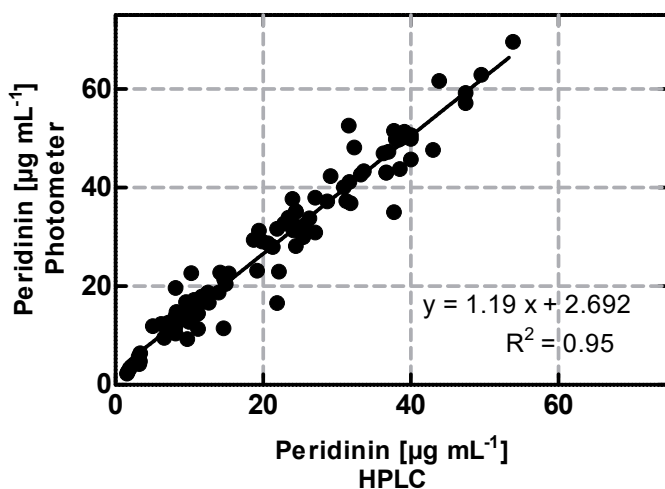


Figure 3.38: Correlation of results from the pigment analysis by HPLC and by photometer. The concentration of peridinin per area is given in $[\mu \text{ m mL}^{-1}]$. In the analysis 100 samples from various culture conditions were included.

Therefore it can be stated that a photometric, high throughput method with a overestimation of 20 % has been established.

4 Discussion

4.1 Application of dinoflagellates in biotechnology

The most prominent examples for the biotechnological application of microalgae are the halotolerant *Dunaliella salina* and the alkali-tolerant *Arthrospira (Spirulina) platensis*. Whereas these extremophiles can be grown in simple open pond systems, mass cultivation of microalgae like *Chlorella sorokiniana* [Kumar and Das, 2012; Concas et al., 2016] and *Haematococcus pluvialis* often relies on highly controlled closed suspension photobioreactors [Lopez et al., 2006; Lee et al., 2015]. Until today the utilisation of dinoflagellates in biotechnology is scarce due to the lack of suitable up-scale culturing systems and the fragility of the cultures [Shah et al., 2014; Sullivan et al., 2003]. However, dinoflagellates are, after the diatoms the second largest group in the marine phytoplankton [Field, 1998; Graham et al., 2009] and present a source for unique secondary metabolites as well as pigments. Therefore dinoflagellates have a great potential for a biotechnological application (Section 1.3).

To overcome the limitations of suspension-based systems the dinoflagellate culture in this thesis is cultivated as a biofilm in the Twin-Layer PSBR. By immobilising the dinoflagellate *Symbiodinium voratum*, in the TL system, the culture was shown to withstand exposure to osmotic stress, high light as well as high temperature, features that in general are rarely described in marine dinoflagellates. Recently also the cultivation of the symbiotic dinoflagellate *Symbiodinium microadriaticum* in the TL PSBR has been described [Kreuz, 2016], which is known to be very stress sensitive [Xiang et al., 2013; Iglesias-Prieto et al., 1992; Awai et al., 2012]. Furthermore from an elaborate screening of 90 microalgae strains it was determined that on average 80 % of all applied species were able to be cultivated in the Twin-Layer system [Nowack

et al., 2005]. Thus, the Twin-Layer system represents a very promising alternative for the mass cultivation of dinoflagellates in general.

4.2 Performance of *S. voratum* in the bench-scale Twin-Layer PSBR

4.2.1 Reproducibility of the TL experiments

Due to its biotechnological potential and the ability to grow on the Twin-Layer as an immobilised biofilm [Benstein et al., 2014], *S. voratum* has been selected in this thesis for a detailed optimisation of biomass and peridinin production.

As external factors have a strong impact on dinoflagellate physiology and growth [Fuentes-Grünewald et al., 2013], the reproducibility of the experiments was investigated by two independent light experiments. While the maxima of the obtained light curves with regard to biomass productivity differ between 100 and 200 $\mu\text{mol photons m}^{-2} \text{s}^{-1}$ (Section 3.1, figure 3.5 A), the overall trend of the curve and the peridinin productivities are identical (Fig. 3.5 B). The difference in the growth rate maxima might be related to variations in the suspension pre-culture and in growth conditions due to the location of the experiment. The used outside green house lack temperature controllability at high light intensities, which causes fluctuations of $\pm 8 \text{ }^\circ\text{C}$. However, under more controllable conditions, like in the 5th floor green house of the Biocenter of the University of Cologne, a better reproducibility of the experiments is given. This is highlighted by comparing the results at 600 $\mu\text{mol photons m}^{-2} \text{s}^{-1}$ with additional 2 % CO_2 in the CO_2 experiment (section 3.3, figure 3.11 A) and the two-step approach (section 3.6, figure 3.23 A). Here the obtained biomass growth rates P_B are identical ($7.8 \text{ g m}^{-2} \text{ d}^{-1}$) and the peridinin productivities P_P of 31.5 and 29.9 $\text{mg m}^{-2} \text{ d}^{-1}$, respectively, are statistically not distinguishable (ANCOVA, $p = 0.2697$).

4.2.2 Investigation of the lag phase in biomass and peridinin production of the *S. voratum* biofilm

The growth of *S. voratum* on bench-scale TL PSBRs often starts with a lag phase of three days after inoculation (Fig.3.1 D- H). This growth behaviour on Twin-Layer systems is in consensus with [Benstein et al., 2014; Solbach, 2016]. To investigate whether the lag phase in the beginning of Twin-Layer cultivation is caused by photo-inhibition within the immobilised culture of *S. voratum*, the impact of the inoculation density upon this lag phase was observed (Section 3.2). In fact, the enhancement of the inoculation density and, therefore, the starting biomass does decrease the lag phase in biomass and peridinin productivity of the bench-scale TL PSBRs (Fig. 3.6, 3.7). Most likely the recorded lag phase at the start of the experiments is also temperature dependent, since no lag phase in the second light experiment (Exp. L2) with the higher environmental temperature has been observed (Exp. L2, section 3.1.2, figure 3.3). Overall the lag phase is most likely associated to a light and temperature stress during the adaptation of *S. voratum* upon the transition from liquid to immobilised culture and the differentiation of the cells within the biofilm. This is supported by the fact, that in microalgae like *Halochlorella rubescens* or *Haematococcus pluvialis*, which are known to be more robust to external conditions than dinoflagellates [Fuentes-Grünwald et al., 2013], the lag phase in the TL PSBR is not observed [Schultze et al., 2015; Kiperstok, 2016].

4.2.3 Effect of biofilm physiology on biomass and peridinin production in the *S. voratum* biofilm

For all cultivation conditions measured in the bench-scale experiments the increase in biomass is linear. Thus, not the whole biofilm is growing at a constant rate, since otherwise an exponential increase of biomass would be recorded. This has been associated to the differentiation of the biofilm into two zones of different photosynthetic activity [Kiperstok, 2016; Li et al., 2015]. Depending on the penetration of light into the biofilm the presence of a layer with high photosynthetic activity, here called

"growth layer", and an underlying "dark layer" of low photosynthetic activity, has been described [Kiperstok, 2016].

With the application of a higher inoculation density the biomass productivity of the TL PSBR (Exp. D) was enhanced in ambient air to $5 \text{ g m}^{-2} \text{ d}^{-1}$ at all light intensities of $100 - 800 \text{ } \mu\text{mol photons m}^{-2} \text{ s}^{-1}$ (Fig. 3.6). These findings cannot be explained by just the differentiation of the biofilm into dark and growth layer, since the deeper light penetration into the biofilm would increase the growth layer and thereby the biomass growth rate. The obtained result by the higher inoculation density can be explained by photo-inhibition in the top layer of the *S. voratum* biofilm. Therefore a model is proposed (Fig. 4.1), in which the *S. voratum* biofilm is differentiated into three layers. These are formed in dependence to the light penetration into the biofilm. In the top layer, called "stress layer", and in the bottom layer, called "dark layer", the growth is reduced by non-optimal light conditions. According to the model the application of higher light intensities lead only to an increase of the stress layer and leave the growth layer at constant level (Fig. 4.1 B). This might be the explanation why the growth rate does not further increase at higher light intensities. At an irradiance of $45 \text{ } \mu\text{mol photons m}^{-2} \text{ s}^{-1}$ a lower growth rate is observed (Fig. 3.6 A), which indicates the absence of light stress and the reduction of the growth layer (Fig. 4.1 C). In the experiments performed with a lower inoculation density growth rates are permanently lower and do not reach the same level, even when the biofilm becomes much thicker (Fig. 3.1). This shows, that the light and stress conditions at the inoculation of the experiment are having a strong, irreversible effect on the biofilm.

Interestingly, the peridinin productivity (Fig. 3.7) and the final peridinin amount [g m^{-2}] of the *S. voratum* biofilms with higher inoculation density on the TL PSBR was found to be not significantly different at light conditions from 45 to $400 \text{ } \mu\text{mol photons m}^{-2} \text{ s}^{-1}$ (Fig. 3.8 B). Therefore the process is, up to $400 \text{ } \mu\text{mol photons m}^{-2} \text{ s}^{-1}$, not altered by input of light, which allows the conclusion, that there is also a constant production layer of peridinin as proposed for the biomass growth. However, the threshold of the light intensity generating a partitioning in the biofilm according to the model, are expected to be lower for peridinin productivity. This can be concluded

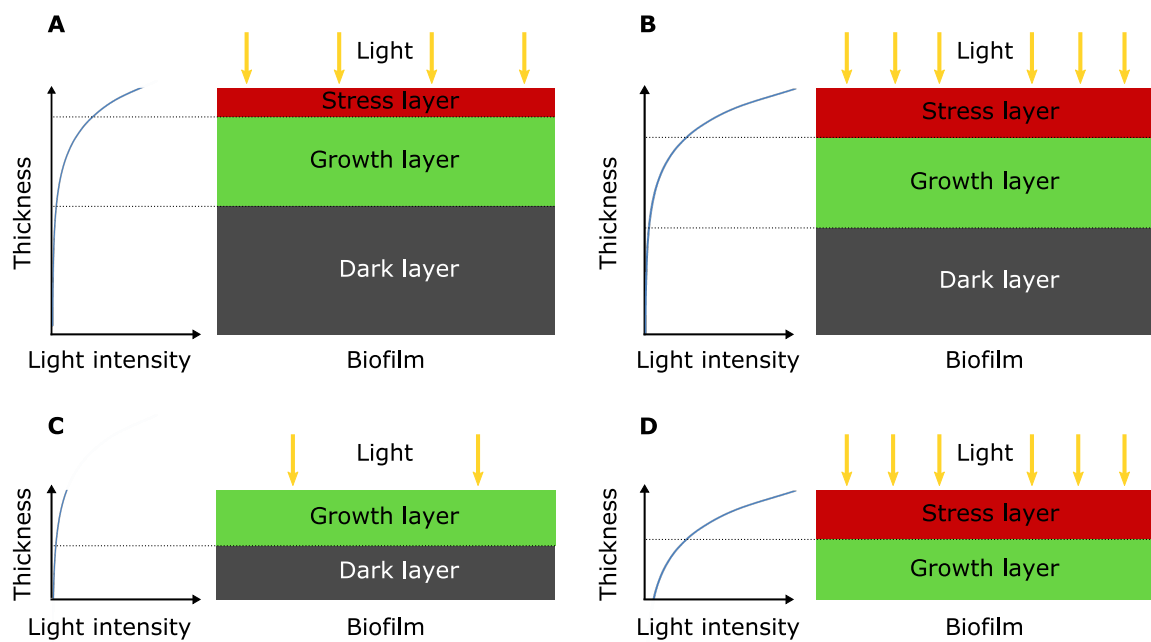


Figure 4.1: Schematic drawing of the proposed physiology in a *S. voratum* biofilm. Presented are a thicker inoculated biofilm at intermediate **A** and high **B** light intensity, as well as a thin inoculated biofilm at low **C** and high **D** light intensity.

from the fact, that very low light intensities are sufficient for peridinin accumulation but not for biomass growth. Especially with regard to peridinin being part of the antenna complex for light harvesting. The productivity of peridinin in the *S. voratum* biofilm cultivated at $800 \mu\text{mol photons m}^{-2} \text{s}^{-1}$ ($18.8 \text{ mg m}^{-2} \text{d}^{-1}$; Fig. 3.7 F) doubled in comparison to cultivation with lower inoculation density at the same light condition ($8.8 \text{ mg m}^{-2} \text{d}^{-1}$; Fig. 3.2 G). Considering this, the speculation of a permanent effect of the light stress at the inoculation can also be supported for the peridinin production.

To further investigate and characterise the biomass and peridinin productivity in *S. voratum* microsensor measurements with regard to light penetration and photosynthetic activity have to be performed.

4.3 Optimisation of the *S. voratum* biofilm in the bench-scale Twin-Layer PSBR

4.3.1 Effect of light

The optimization of the biomass and peridinin production was started by investigating the effect of light on the immobilised culture of *S. voratum* in bench-scale PSBRs. With regard to *S. voratum* the biomass productivity has been shown to be light dependent with a maximum at low light around 100 - 200 $\mu\text{mol photons m}^{-2} \text{s}^{-1}$ (Fig. 3.5). This is in agreement with the findings of [Richardson et al., 1983], which is thought to be a habitat adaptation to shaded, low light environments [Geider et al., 1987].

Due to this low light adaptation in dinoflagellates an increase in the light harvesting pigment peridinin with a lower photon input has been described [Jovine and Triplett, 1992; Khalesi and Lamers, 2010]. As expected, the maximal peridinin productivity and the highest peridinin amount per area [g m^{-2}] in both conducted light experiment have been determined at low light conditions (Fig. 3.5 B). The highest recorded peridinin concentration (1.8 % of dw) is recorded at a light intensity of 15 $\mu\text{mol photons m}^{-2} \text{s}^{-1}$. At this low irradiance only a thin biofilm of maximal 28.5 g m^{-2} is formed in which the cells in the biofilm have to produce a large number of antenna complexes to perform photosynthesis.

Since the peridinin productivity in both light experiments was maximal at the light intensity of 100 $\mu\text{mol photons m}^{-2} \text{s}^{-1}$ and ambient air, these conditions have been determined to be optimal for a efficient production of peridinin.

4.3.2 Effect of light in combination with CO₂

The limitation of CO₂ on the biomass productivity has been shown in the exposure of the *S. voratum* biofilm to 2 % CO₂ in comparison to ambient air (Section 3.3). In the utilisation of f/2 medium and 2 % CO₂ the biomass growth of *S. voratum* was only significantly increased at the light intensity of 600 $\mu\text{mol photons m}^{-2} \text{s}^{-1}$ (Fig. 3.10 C).

The significant change of the pH from 8.3 to 6.4 upon CO₂ application highlights, that the unbuffered $f/2$ is not ideal for cultivation in combination of enhanced CO₂ concentrations. However, it was previously applied, since it is in contrast to ASP 12 a low cost medium. The combination of CO₂ and ASP 12 medium increased the biomass productivities at all irradiances and the pH of setups with CO₂ was around 7.5. The acidification of the medium has a strong effect on *S. voratum*, since it is a marine organism, naturally adapted to a stable pH [Graham et al., 2009].

Additionally, the maximal biomass growth rate observed in the light experiments is shifted towards 600 $\mu\text{mol photons m}^{-2} \text{s}^{-1}$ when supplied with 2 % CO₂ (Fig. 3.16 D). Indicating, that the photosynthesis of *S. voratum* is CO₂ limited under ambient air. While the biomass growth rate is more than doubled the peridinin production is not promoted by the combination of light and CO₂ (Fig. 3.12 A, F). In the biofilm sections (Fig. 3.14 A), the reduced peridinin content of the biofilm at high light is indicated. The presence of CO₂ even reduces the peridinin amount per area which might be due to the slight pH change in ASP 12 medium.

Also the physiology of the biofilm changes. While at ambient air the biofilm possesses a top layer of loose cells at high and low light (Fig. 3.14 B, C), with the supply of 2 % CO₂ the top layer of biofilm is reduced and the cells are more densely packed (Fig. 3.14 A). This effect is stronger visible over a long cultivation period (Fig. 3.27 F). Since it has been observed, that these biofilms are not shiny, an explanation might be that the immobilised cells reduce the production of mucilage at increased CO₂ concentrations. The reason for the absence of mucilage can be correlated to the pH decrease to 7.5 or the difference in carbon availability. To improve the usability of *S. voratum* as natural resource for polysaccharides, the underlying process of mucilage production might be interesting for the utilisation in cosmetic products and the characterisation of immobilised cultivation of the microalgae in general.

Overall the peridinin accumulation at 100 $\mu\text{mol photons m}^{-2} \text{s}^{-1}$ at ambient air and 600 $\mu\text{mol photons m}^{-2} \text{s}^{-1}$ with 2 % CO₂ is identical, while the biofilm at low light has less biomass with a higher peridinin concentration [% of dw]. Thus, the quality of biomass in terms of peridinin concentration is higher when generated at a lower

light intensity. Since not only the absolute peridinin amount per area is relevant, but also the relative peridinin concentration, the low light conditions are favourable for the production of peridinin.

4.3.3 Effect of temperature

As temperature has direct impact on cell metabolism and growth of microalgae the effect on *S. voratum* in the TL PSBR was analysed. *S. voratum* has been reported to be cold water adapted and optimal growth of the strain *S. voratum* rt-383 was determined at 15 - 20°C [Jeong et al., 2014a]. However, this could not be verified in the immobilised cultivation of *S. voratum*. The temperature optimum for the biofilm cultivated at 100 $\mu\text{mol photons m}^{-2} \text{s}^{-1}$ and ambient air is at 25 °C (Fig. 3.18, Tab. 4.1), which might be correlated to the fact that the temperature optimum increases with the amount of applied light. The reduction of the growth rate above 28 °C in *S. voratum* is in accordance to literature findings [McBride et al., 2009]. This effect has been associated to an impairment of photosynthesis at high temperature [Iglesias-Prieto et al., 1992].

Table 4.1: Summary on the effect of temperature on biomass production P_B of *S. voratum* biofilms grown at 100 $\mu\text{mol photons m}^{-2} \text{s}^{-1}$ in bench-scale TL PSBR

Exp.	T [°C]	Medium	P_B [$\text{g m}^{-2} \text{d}^{-1}$]	R^2
T	20.0	A12	2.5	0.94
L1	20.5	f/2	3.1	0.96
TS	21.5	A12	2.8	0.94
CA	22.4	A12	3.3	0.99
CF	23.0	f/2	3.3	0.98
L2	24.8	f/2	4.3	0.98
T	25	A12	4.9	0.94
T	32	A12	4.4	0.94

The difference of the temperature optimum could also be due to the different cultivation systems, since the cultivation as a biofilm enables the cells to adapt to conditions, like high light exposure, which are beneficial for the growth in suspension cultures. However, it might also be a strain specific effect, since other *Symbiodinium* species, among them tropical species of *S. voratum*, have been shown to have even higher

optimal growth temperatures [McBride et al., 2009; Rogers and Davis, 2006]. Despite having the highest biomass growth rate in the *S. voratum* biofilm at 25 °C, further increase of the temperature to 32 °C enhances the maximal peridinin amount per area [g m^{-2}] by 13 % in comparison (Fig. 3.20 A, B). Similar results have been reported for *S. voratum* where the highest chlorophyll *a* content is obtained at a temperature of 30 °C [McBride et al., 2009]. It was speculated that this shows a heat-adaptation of the photosynthetic apparatus [McBride et al., 2009].

Overall the biomass productivity is strongly dependent on the applied temperature (Tab. 4.1) and maximal productivity in biomass P_B is obtained at 25 °C, while maximal peridinin concentration P_P is recorded at 32 °C.

Due to the design of the temperature experiment the biofilms were pre-grown at two light intensities, 100 and 600 $\mu\text{mol photons m}^{-2} \text{s}^{-1}$, and after a growth period of 12 days shifted in two setups to identical light and temperature condition (Exp. T., section 3.5). The biofilm pre-grown at 600 $\mu\text{mol photons m}^{-2} \text{s}^{-1}$ with 2 % CO_2 (Fig. 4.2 A, open circles), contains a 20 % higher biomass amount per area [g m^{-2}] after the shift (d 14-32) in comparison to the biofilm cultured at lower light (Fig. 4.2 A, closed circles). While this higher biomass amount is due to the previous growth promoting conditions at 600 $\mu\text{mol photons m}^{-2} \text{s}^{-1}$, the biomass productivity after the shift is identical within the two biofilms. Thus it can be concluded, that the

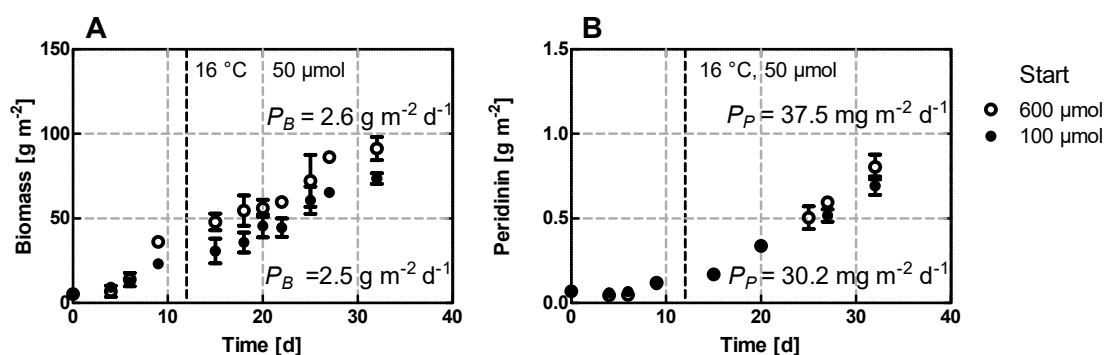


Figure 4.2: Biomass growth and peridinin accumulation in the *S. voratum* biofilm at 16 °C and 50 $\mu\text{mol photons m}^{-2} \text{s}^{-1}$. Presented are the data from the biofilms pre-grown for 12 days at either 100 $\mu\text{mol photons m}^{-2} \text{s}^{-1}$ and ambient air (\bullet) and 600 $\mu\text{mol photons m}^{-2} \text{s}^{-1}$ with 2 % CO_2 (\circ). Mean \pm SD, $n=3$ and linear regression is presented. P_B = biomass productivity in [$\text{g m}^{-2} \text{d}^{-1}$], P_P = peridinin productivity in [$\text{mg m}^{-2} \text{d}^{-1}$]

immobilized microalgae react with regard to biomass growth in a matter of days to exposed conditions independent from the previous physiology of the biofilm.

Also the obtained peridinin amount per area from the biofilm pre-grown at different light intensities are identical after the shift to 16 °C until day 20 (Fig. 4.2 B). It is further visible that after 27 days the biofilm previously grown at high light is increasing in peridinin per area [g m^{-2}] again (Fig. 4.2 B, open circles). This could indicate a long term adaptation of this thicker biofilm to the reduced light conditions. As a result the peridinin productivities show little variation (Fig. 4.2). *S. voratum* biofilms shifted from 100 and 600 $\mu\text{mol photons m}^{-2} \text{s}^{-1}$ to 4 °C and 5 $\mu\text{mol photons m}^{-2} \text{s}^{-1}$ show the same behaviour in biomass accumulation (Fig. 3.18 E, 3.19 D).

4.3.4 Combination of biomass and peridinin productivity in a two-step approach

As the growth of *S. voratum* is maximized at high light conditions while the peridinin production increases under low light, the feasibility of a two-step approach shifting from biomass growth to peridinin production was investigated. In the shift from the growth to the peridinin enhancing phase a fast adaptation of the biofilm and a strong decrease of the biomass growth rate is recorded (Fig. 3.23). From the obtained biofilm cross sections the differentiation of the cells with respect to the peridinin concentration is apparent (Fig. 3.27). While the constant growth phase (600 $\mu\text{mol photons m}^{-2} \text{s}^{-1}$, 2 % CO_2) reduces the peridinin content (Fig. 3.24 B, 3.27 F) and appears light brown due to high input of photons and photo-inhibition, the dark colouration of the biofilm at 100 $\mu\text{mol photons m}^{-2} \text{s}^{-1}$ indicates the increase of the peridinin concentration. By performing the shift from growth to peridinin phase the obtained biofilm possesses small dark spots within the cell layers, which might be an indication for the adaptation process (Fig. 3.27 I, white arrow). From the peridinin productivities the most promising conditions for an maximal pigment production are a growth promoting phase of two or four weeks before shifting to peridinin productive conditions (Fig. 3.24 D, H). Taking the amount of energy, time and consumables into account, the growth period of two weeks followed by two weeks of peridinin productive

conditions is most efficient. However, an investigation of the long term peridinin accumulation in the biofilm with a growth period of four weeks is necessary to draw more conclusions.

By the application of a two-step approach with a growth phase of two weeks a maximal peridinin productivity of $51.4 \text{ mg m}^{-2} \text{ d}^{-1}$ was gained, which is the highest value recorded in this thesis. The most efficient process for the peridinin production is to harvest the biomass after a duration of 24 days, since at this time point the highest increase of peridinin has been gained with the lowest input of time and resources (Fig. 3.25 B). A similar behaviour has been described for the microalgae *Haematococcus pluvialis*, in which nutrient stress has been shown to trigger the production of the carotenoid astaxanthin after a previous growth phase at full strength medium [Kiperstok, 2016]. In contrast to *S. voratum* and peridinin the maximal biomass and pigment production in the *Haematococcus pluvialis* can be generated simultaneously at high light [Kiperstok, 2016], since astaxanthin is a photo protective pigment [Hagen et al., 1993].

4.3.5 Media application in up-scale cultivation systems

As culture media strongly affect the growth of microalgae six different media have been investigated upon their biomass and peridinin productivity (section 3.7). In general the cultivation of marine microalgae are operated with standard media like f/2 [Wang et al., 2015; Spector, 1984], since this medium has a simple composition and is therefore very cost efficient. In contrast ASP 12 is a cultivation medium optimized for the cultivation of marine microalgae with focus on reproducibility and long time usage, as consequence the principle components of this medium are cost intensive. Since *S. voratum* is a marine organism the application of seawater is an easy and cost efficient way to maintain the microalgae in a larger cultivation scale. The highest growth rate of *S. voratum* in the media experiment was obtained in the media based on natural seawater (Fig. 3.28 C, D, E). In the application of fertiliser-based seawater medium SW3 (Fig. 3.28 F) growth ceases after two weeks. The nitrogen source of the media is solely urea, which promoted bacteria growth stronger than the algae

biomass production and does not seem to be suitable for *S. voratum*. At the end of the experiment the biomass was covered by a white top layer. The highest peridinin productivity of $45.7 \text{ mg m}^{-2} \text{ d}^{-1}$ was recorded in the most complex medium containing natural seawater and all ASP 12 stocks. The increase could be caused by the higher amount of trace metals in the marine medium, which have been shown to be beneficial for dinoflagellate growth [Spector, 1984; Anderson, 1978].

Since it has been recorded that ammonium can enhance the growth of dinoflagellates [Fuchinoue et al., 2012; Varkitzi et al., 2010; Fiore et al., 2010], the effect of the different nitrogen sources on the productivity of biomass and peridinin in *S. voratum* should be further investigated.

4.4 Conclusions from the optimisation of *S. voratum* in the bench-scale Twin-Layer PSBR

The optimisation of growth in the *S. voratum* biofilm was initially performed by the investigation of light and CO_2 . Thereby an optimal biomass productivity of $7.8 \text{ g m}^{-2} \text{ d}^{-1}$ at a light intensity of $600 \text{ } \mu\text{mol photons m}^{-2} \text{ s}^{-1}$ and 2 % CO_2 with the application of ASP 12 medium was determined. The optimisation of the bench-scale TL system for *S. voratum* could be further performed with regard to the composition of the Twin-Layer. While it has been determined, that the utilisation of different materials does not have an influence on the biomass growth at a light intensities of $200 \text{ } \mu\text{mol photons m}^{-2} \text{ s}^{-1}$ and 2 % CO_2 [Solbach, 2016]. Findings by [Benstein et al., 2014] indicate a further enhancement of biomass production by application of the high quality material polycarbonate. By the growth on a bench-scale TL system with polycarbonate as substrate layer a biomass productivity of $11 \text{ g m}^{-2} \text{ d}^{-1}$ at $400 \text{ } \mu\text{mol photons m}^{-2} \text{ s}^{-1}$ and 2 % CO_2 was determined. It becomes apparent that at higher light intensities with the application of CO_2 the performance of the paper substrate layer is not optimal. An explanation could be, that the thicker formed biofilm requires a higher diffusion of nutrients and CO_2 input through the substrate layer to the biofilm. Since paper is cellulose based and does not guarantee a certain pore size,

it is mostly not optimal for the application of high light and CO₂. By extrapolating the results from [Benstein et al., 2014] in the polycarbonate Twin-Layer the maximal growth rate of *S. voratum* would be 12.1 g m⁻² d⁻¹ at 600 μmol photons m⁻² s⁻¹. In comparison to the fast growing green algae *Haematococcus pluvialis* the maximal biomass productivity of *S. voratum* is 36 % lower in the TL PSBR [Kiperstok, 2016]. However, in this thesis a higher maximal biomass yield of 304.8 g m⁻² in *S. voratum* has been recorded (Fig. 3.23 B). With regard to the known challenges in the cultivation of dinoflagellates due to their fragility and growth limitation [Beuzenberg et al., 2011], the growth of *S. voratum* on the Twin-Layer PSBR was comparable with currently commercially grown algae. Additionally, maximal productivity was reached at high light conditions, in contrast to the previous recorded low light adaptation of the free living *Symbiodinium* and dinoflagellates in general [Richardson et al., 1983; Fuchinoue et al., 2012].

From the investigation of light and CO₂ it was concluded, that the low light and ambient air were favourable for the peridinin concentration and production. The application of the two standard media f/2 and ASP 12 at these low light conditions generate pigment productivities of 27.5 ± 3.6 g m⁻² d⁻¹ (Exp. L1 - CF; Tab. 4.2) and 29.9 ± 7.1 g m⁻² d⁻¹ (Exp. CA, TS, T; Tab. 4.2), which are not significantly different. In the further optimisation process in *S. voratum* an increase in peridinin production by temperature, medium complexity and a stepwise cultivation approach have been recorded (Tab. 4.2).

The maximal peridinin productivity recorded in this thesis was 51.4 mg m⁻² d⁻¹, which was achieved by the application of the two-step approach. This represent a 115 % increase in comparison to previously recorded data in a complete paper-based TL PSBR [Benstein et al., 2014] and an 86 % increase in comparison to the data recorded for 100 μmol photons m⁻² s⁻¹, ambient air and f/2 in this thesis (Tab. 4.2). For future investigations a potent approach would be the combination of peridinin promoting factors, like high temperatures, medium based on natural seawater and the two-step approach.

Table 4.2: Summary on peridinin productivity of *S. voratum* P_P [$\text{g m}^{-2} \text{d}^{-1}$] in the bench-scale TL PSBR

Exp.	P_P [$\text{g m}^{-2} \text{d}^{-1}$]	SD	R^2	PI ¹ [g m^{-2}]	Light	T [°C]	Medium
L2	0.0237	0.0039	0.95	0.057	100	24.8	f/2
T	0.0238	0.0029	0.94	0.069	100	20.0	A12
D	0.0282	0.0005	0.99	0.065	100	21.3	f/2
TS	0.0280	0.0023	0.96	0.012	100	21.5	A12
L1	0.0307	0.0030	0.98	0.023	100	20.5	f/2
CA	0.0377	0.0029	0.95	0.084	100	22.4	A12
T	0.0401	0.0030	0.98	0.069	100	25	A12
T	0.0424	0.0083	0.90	0.069	100	32	A12
TS	0.0456	0.0161	0.90	0.012	Sh ⁴	23	A12
M	0.0457	0.0018	0.98	0.029	100	23.4	SW2
TS	0.0514	0.0063	0.97	0.012	Sh ²	22.5	A12

PI¹ = Peridinin amount of the inoculum; Sh² = Biofilm shifted after two weeks at 600 mol to 100 $\mu\text{mol photons m}^{-2} \text{s}^{-1}$; Sh⁴ = shift after four weeks at 600 mol to 100 mol

With respect to the peridinin concentration [%] it seems that the optimization of the cultivation conditions of *S. voratum* can further be improved, since other dinoflagellates have been reported to obtain a total carotenoid content of 0.7 - 3.3 % of dry matter [Johansen et al., 1974]. In this regard, a promising approach for the increase of the peridinin content are light conditions around 15 - 25 $\mu\text{mol photons m}^{-2} \text{s}^{-1}$ which have been recorded to gain the highest peridinin content of 1.7-1.8 % [of dw] ([Benstein et al., 2014], Fig. 3.4 A). Furthermore the pigment concentration within the biofilm might be limited to a certain value by a light intensity, since the peridinin concentration at 100 $\mu\text{mol photons m}^{-2} \text{s}^{-1}$ is maximal around 1.2 % [of dw] and decreases after this threshold (Fig. 3.12 A; 3.24 A; 3.29 A, C).

4.5 Up-scaling of the *S. voratum* cultivation in the Twin-Layer PSBR

As the mass production of microalgae is not feasible in bench-scale TL systems, more industry compatible up-scale systems have been investigated regarding their

capability to cultivate *S. voratum* and subsequently peridinin production. In the application of the up-scale TL PSBR it was shown that the dinoflagellate *S. voratum* is able to grow on vertical and horizontal systems (Section 3.8.1, 3.8.2). Due to its easy handling and biomass as well as peridinin production rates as high as in the bench-scale TL experiments, the horizontal up-scale fleece-based TL PSBR proved to be the current optimum for the cultivation of *S. voratum* (Tab. 3.1). This reproducibility of laboratory scale experiments has rarely been reported for a dinoflagellate culture in general and is described for the first time in a immobilised cultivation system.

This might be due to the fact, that all previous described cultivation systems have been relying on suspension. In which the up-scaling of dinoflagellate cultures in liquid cultivation systems has not been reported to exceed a volume of 15 L [Camacho et al., 2011]. For the production of very sensitive dinoflagellates the application of suspension cultures requires high input of effort, energy and time. For example in order to gain 1.5 mg of the biomedical interesting product, gymnocin-A, over 1000 L of suspension culture had to be grown in 2 L flasks [Satake et al., 2002]. The challenge in up-scaling a cultivation system in suspension is that in a shift from Erlenmeyer flasks to open ponds and suspension PBR, a multitude of factors are altered. The setup of the system changes with respect to light penetration, due to the depth of the pond, and to shear forces, associated to the stirring and aeration of the large algae culture. In addition the temperature control in an open pond has been proven to be difficult, since such a large water body is an inert mass [Slegers et al., 2013].

Due to the two dimensional enlargement of the Twin-Layer in an up-scale, no alterations in gas exchange or light penetration of the biofilm are performed. This feature is highlighted by the shown reproduction of the bench-scale experiments with the horizontal up-scale TL PSBR. The remaining challenge of the Twin-Layer up-scaling is to ensure the small scale conditions, e.g. sufficient media supply in the source layer, which has been shown to be controllable by choosing the correct material.

4.5.1 Comparison of the applied materials in the up-scale cultivation of *S. voratum* on Twin-Layer PSBR systems

Even though the up-scaling of the Twin-Layer technology has been successful in the cultivation of *S. voratum*, the application of different materials has a great effect on culture performance of *S. voratum* with regard to biomass and peridinin productivity. While the biggest advantage of paper is the low production cost, drawbacks in the large scale application were detected. Unfortunately, the paper substrate layer tends to detach and form an uneven surface, as reported here and by [Benstein et al., 2014]. In the affected areas the medium supply can no longer be maintained and the corresponding spots dry out, along with the affected biofilm (Section 3.8.1, Fig. 3.31 B, black arrow). Furthermore, fungal growth on the backside of the vertical module was detected. It has to be noted, that the affected backside was not inoculated with algae and therefore a prone source for contamination. In a TL system with a uniform and complete inoculated growth area these type of contaminations can be avoided. With regard to the attachment of the paper more research on the Twin-Layer composition is needed to improve the TL PSBR performance. Therefore the vertical up-scale TL reactor has been shown to be less productive than in bench-scale at the same light intensity. An additional reason might be the high temperature (max. 38 °C) in the green house during the experiment. Also in the paper-based horizontal up-scale TL PSBR the performance was not optimal, since the top samples match to the control bench-scale experiments, while the middle and bottom grew not as well (Fig. 3.32). This correlates to the technical setup of the Twin-Layer system, which supplies the medium from the top of the module and can therefore be a cause for insufficient growth conditions at the lower part. In comparison to the bench-scale experiments, a 4-fold decrease in peridinin productivity was determined. This effect is most likely caused by the non optimal cultivation conditions and a high initial irradiation of the system in the outdoor greenhouse.

An improvement over the usage of paper was the utilisation of fleece, which was shown to be less prone to detachments and dessication (Fig. 3.37). Until the end of the

experiment the surface of the *S. voratum* biofilm remained smooth and even though minor detachments of the substrate layer (Fig. 3.37 C) were observed, the overlying biofilm was not affected. Due to the hydrophilic nature of the used fleece material, further improvements were achieved, using fleece material without the traditional glass fibre source layer. *S. voratum* grown on the horizontal TL PSBR composed of fleece and grid appeared to be more moist and was easier to harvest (Fig. 3.37 D). In the TL PSBR with the glass fibre the biofilm is tightly bound to the fleece and had to be removed by wetting the spatula prior to the scrapping off. A further advantage of the fleece-based TL system is the low risk of contamination which is a prerequisite for a stable biomass production. The major drawback of the fleece-based TL PSBR is the harvesting of the biofilm, since the fibres on the fleece surface tend to stick to the removed biomass, which hinders a mechanical harvesting process. However, for the peridinin extraction of the biomass samples the fleece material did not interfere with the extraction procedure. With regard to the growth of the dinoflagellate biofilm the fleece-based up-scale TL PSBR gave the most profound correlation to the control bench-scale data. Furthermore the deviation of the sample location is negligible which is an indicator for a evenly supplied biofilm. The growth of the system even slightly enhances in comparison to the bench-scale experiments, which underlines its commercial potential for effective mass cultivation.

4.5.2 Market potential of peridinin

Since it is known that dinoflagellates either possess peridinin or fucoxanthin as main carotenoid and it has been proposed that the pigments share the same origin in the synthesis pathway [Haxo et al., 1976; Yoon et al., 2002; Maeda et al., 2005; Abdel-Raouf et al., 2012; Lee et al., 2013], fucoxanthin was considered for a further comparison. With regard to fucoxanthin it can be illustrated, that the popularity and demand of a carotenoid is strongly bound to its production and availability. The carotenoid fucoxanthin has been found to have anti-carcinogenic, anti-obesity, and anti-inflammatory properties and is traditionally isolated from macroalgae, like *Sargassum fulvellum* and *Undaria pinnatifida* [D’Orazio et al., 2012; Mise et al., 2011;

Maeda et al., 2005]. Thus it was easy to obtain and fucoxanthin became available for the market. Currently fucoxanthin is applied as food additive or dietary product [Abidov et al., 2010; Peng et al., 2011; Rengarajan et al., 2013]. With the higher demand for fucoxanthin the research for alternative sources increased, since it is not possible to control and maximise the production via macroalgae. In addition the extraction of fucoxanthin from these rigid macroalgae is challenging and due to the low fucoxanthin content not optimal [Kanda et al., 2014].

Therefore the production of fucoxanthin is currently investigated in microalgae cultures. The focus is put on diatoms, which contain naturally 2.24 to 21.67 mg g [dw]⁻¹ fucoxanthin [Foo et al., 2015; Xia et al., 2013]. This is up to 20 times higher than in macroalgae [Jaswir et al., 2012; Gómez-Loredo et al., 2015]. The fucoxanthin productivity of the cultivation systems is around 5.5 - 7.96 mg L⁻¹ d⁻¹ [Guo et al., 2016; Xia et al., 2013]. The gained peridinin content of 10 mg g [dw]⁻¹ (Fig. 3.24) in the two-step approach in *S. voratum* is similar to the average fucoxanthin content (11 mg g [dw]⁻¹) of diatoms [Gómez-Loredo et al., 2015; Kim et al., 2012; Xia et al., 2013]. In *Chaetoceros calcitrans* 7.13 ± 0.01 mg g [dw]⁻¹ [Foo et al., 2015] were recorded and 15.7 mg g [dw]⁻¹ was determined in *Phaeodactylum tricornutum* [Kim et al., 2012]. However, no production rate for these species were recorded. *P. tricornutum* grown in a TL PSBR at 70 µmol photons m⁻² s⁻¹ generated a productivity of 1.8 g m⁻² d⁻¹ [Naumann et al., 2013], which is 40 % lower than the biomass growth rate recorded at 70 µmol photons m⁻² s⁻¹ (2.6 - 3.3 g m⁻² d⁻¹) for *S. voratum* (Fig. 3.1 C, 3.3 C). In an immobilised "attached cultivation bioreactor" applying *Trentepohlia arborum* a carotenoid productivity of 67.7 mg m⁻² d⁻¹ was recorded [Cheng et al., 2015], considering that it is a total of all carotenoids it is similar to the maximal productivity of 51.4 mg m⁻² d⁻¹ obtained for peridinin in this thesis (Fig. 3.24 D). With respect to the functionality of the two pigments, peridinin has even been described to have stronger anti-oxidant and anti-inflammatory properties than fucoxanthin [Onodera et al., 2014].

As it was observed in the application of fucoxanthin, the market size of peridinin, as anti-oxidant, anti-cancerous and anti-inflammatory agent or for *S. voratum*, in

aquaculture, is very likely to grow immensely with the availability of the product. With successful biotechnological application of other microalgae like the astaxanthin producing *Haematococcus pluvialis*, it has been possible to generate a market of 400 million US \$ in 2014 which is still growing [BBC Research, 2015].

4.5.3 Biotechnological application of *S. voratum*

For *S. voratum* two potential biotechnological applications are very promising. First scenario is the production of smaller amounts of biomass for the extraction of high value products, while the second scenario is focused on the mass cultivation of biomass for applications in aquaculture and food supplements.

Next to peridinin, *S. voratum* has been described to contain a variety of products with application in medicine (i.e. symbioimine), cosmetics (i.e. mycosporine-like amino acids) and biomedical research (i.e peridinin-chlorophyll *a*-protein complexes (PCPs)). For the biotechnological production of these components the aim of this scenario would be to produce biomass from which the desirable products can be extracted and purified. To ensure a stable system performance a high quality material has to be applied. If the fleece material is further improved with respect to the surface structure it would be well suited. With regard to the production of peridinin a feasible biomass growth with maximal peridinin concentration [% of dw] would be optimal. From the optimization process the growth at 100 $\mu\text{mol photons m}^{-2} \text{s}^{-1}$, ambient air and 25 °C or the application of two-step approach with a two week growth phase, at 600 $\mu\text{mol photons m}^{-2} \text{s}^{-1}$ and 2 % CO₂ and subsequently peridinin enhancement of two weeks should be applied.

Most suitable for the cultivation at low light would be a vertical TL PSBR, which has a high surface productivity in relation to the needed footprint area due to the small distance of the vertical "sheet-like" modules [Schultze et al., 2015]. For the application of the two-step approach the vertical system is also well suited, since the required shift from high to low light can easily be obtained by altering the distance of the vertical modules. In general the TL PSBR should be completely monitored

with regard to temperature, light intensity and humidity in order to ensure the high quality of the products.

For the second scenario *S. voratum* would be applied in aquaculture or as a food supplement. Since the focus would lie on a fast production of biomass on a larger scale, the growth promoting conditions of $600 \mu\text{mol photons m}^{-2} \text{ s}^{-1}$, and 2 % CO_2 should be applied. It would be advisable to grow the biofilm on the horizontal TL-PSBR due to the simplified technical design and the high light diffusion of the system. With respect to the material paper represents a very cost-efficient material, but further investigation in the Twin-Layer composition is needed to ensure uniform culture conditions and to minimize the detachment of the substrate layer.

Most promising for the commercial application of *S. voratum* is farming of bivalves, since dinoflagellates have been described to meet the nutritional requirements of the mussels [Budge et al., 2001], and are a potential food source for oysters [Hata and Hata, 1982]. Also possible is the application of dinoflagellates in larvae feed for fish hatcheries [Rodriguez and Hirayama, 1997]. If a higher peridinin concentration [% of dw] of the biomass is wanted the two-step cultivation with two weeks of growth phase and two weeks for peridinin enhancement should be performed. To further enhance the quality of the *S. voratum* biomass the optimization of the fatty acid production has to be studied closer.

4.6 Spectral reconstruction as photospectrometric method for peridinin analysis

The advantage of a photometer based method is that it is less time and cost consuming and allows high throughput applications. In order to test the established method of spectral reconstruction spectra of 100 samples were analysed photospectrometrically and for comparison their peridinin concentration was determined by HPLC. In total an overestimation of 20% has been determined from the correlation of the obtained results (Fig. 3.38). The detected deviation of the linear fit is probably due to a systematic error, since it is consistently present in the majority of the 100 applied samples. A

possible reason could be that the spectra diadinoxanthin and dinoxanthin, which are present in minor amounts within dinoflagellates [Johansen et al., 1974], have not been taken into account. Due to the low concentration of the pigments in the dinoflagellate *S. voratum* a sufficient isolation via TLC has not been successful. As improvement for the method the separation of diadinoxanthin and dinoxanthin should be performed by an accordingly equipped HPLC.

5 Conclusions and Outlook

In the present study the advantages of the immobilised cultivation of dinoflagellates on the TL PSBR have been demonstrated. While the highest biomass productivity of *S. voratum* was determined at high light and additional CO₂, peridinin production was highest at low light and ambient air. Even during long term cultivation of *S. voratum* on bench- and up-scale TL systems no saturation of growth and therefore very high biomass yields were obtained. To better understand the performance of *S. voratum* in the TL system a detailed study of light penetration and photosynthetic activity in the immobilised culture by microsensor measurements have to be performed.

From the optimisation of the peridinin productivity in the biofilm of *S. voratum* the most favourable conditions were low light, high temperature, no additional CO₂ and a complex medium. However, the maximal production rate was obtained in the application of a two-step cultivation process which combined the enhancement of biomass and peridinin accumulation. A further optimisation of peridinin production should focus on the combination of the found peridinin promoting factors. Overall more basic research on the synthesis pathways of peridinin in dinoflagellates is essential to identify and enhance this cellular process.

Next to optimisation with regard to light, CO₂, temperature and medium the biomass and peridinin production was found to be interchangeable to up-scale TL systems. This reproducibility of laboratory scale experiments has rarely been reported for a dinoflagellate culture in general and is described for the first time in a immobilised cultivation system. The highest production rates of biomass and peridinin were achieved by the application of a horizontal fleece-based TL PSBR. For an elaborated analysis on the feasibility of the biomass and peridinin production in *S. voratum* with regard to energy and cost input the performance of a large scale pilot reactor at natural light conditions has to be investigated. To enable the commercial cultivation

of *S. voratum* in aquaculture an analysis of the fatty acid composition and production on the TL PSBR is crucial.

In this thesis also a photospectrometric method for a fast and reliable analysis of peridinin was established. By a further improvement of the spectrum acquisition the method could be applied for the simultaneous determination of all pigments present in *S. voratum*. Thereby more profound conclusions on the biofilm physiology and adaptation of immobilised cells within the dinoflagellate culture could be made.

6 Appendix

Python Script for the spectral reconstruction method

```
import csv
import pylab
import os
import scipy.optimize

# definitions of functions
def readfile_num(filename, cols, head, foot):
    # head gives the number of headlines and foot number of footlines
    zielfdatei=open(filename, 'rb')
    reader = csv.reader(zielfdatei, delimiter="\t")
    rows = [row for row in reader]
    rows = filter(lambda x: len(x) == cols, rows)
    numericrows=[]
    for i in range(head, len(rows)-foot):
        numericrows.append(rows[i])

Data = [[float(row[col]) for row in numericrows] for col in range(
    cols)]
zielfdatei.close()
return Data

def read_header(filename, cols, head):
    zielfdatei=open(filename, 'rb')
    reader = csv.reader(zielfdatei, delimiter="\t")
```

```
rows = [row for row in reader]
header=[]
for i in range(head):
header += [rows[i]]

Data = [[str(row[col]) for row in header] for col in range(cols)]
zielfdatei.close()

return Data

#definition of size and color of figures
phi = (1+pylab.sqrt(5))/2
padratio = 1.03
figsize_full_double = [32/2.54, 16/phi/2.54*padratio]
axrect_full_left=[0.1, 0.22, 0.375, 0.75/padratio]
axrect_full_right=[0.6,0.22, 0.375, 0.75/padratio]

rainbow=['black', 'red', 'green', 'red', 'orange']

#here starts the actual script
#import of data
path_totalspec= ">Insert_path_name_here<"
filename_totalspec = ">Insert_file_name_here<" #Name of the file
containing the total Spectrum that should be analysed
totalspec = readfile_num(path_totalspec+filename_totalspec, 101, 7,
0) #loads the file, last numbers are: number of columns, number
of header lines, number of footer lines
totalspec_head = read_header(path_totalspec+filename_totalspec,
101, 7)
Row_HPLC_result=1
Row_real_name=5
path_singlespec=">Insert_path_name_here<"
```

```

filename_singlespec = ">Insert_file_name_here<" #Name of the file
    containing the single spectra that are used for fitting the
    total spectrum
singlespec_temp = readfile_num(path_singlespec+filename_singlespec ,
    5, 2, 0) #loads the file , last numbers are: number of columns ,
    number of header lines , number of footer lines
singlespec_head = read_header(path_singlespec+filename_singlespec ,
    5, 2)
single_400=singlespec_temp[0].index(400)
Beschreibung=filename_totalspec[:-4]+>Insert_description_here<
Outputfolder=>Insert_path_name_here<+Beschreibung+"\
if not os.path.exists(Outputfolder):
os.makedirs(Outputfolder)

singlespec=singlespec_temp
Col_s=[1,2,4] #Column of the single spectra , that should be used
    for fitting the total spectrum (In column 0 are the wavelength)
Pos_per=2 #Gives the position of Peridinin in Col_s
Col_chl_a=3 #Column of Chl. a

#a quick check whether the wavelengths of the files are the same
if totalspec[0]!=singlespec[0]:
import sys
sys.exit("Error , Wavelength_of_ " + filename_totalspec + "_and_" +
    filename_singlespec+ " _are_not_the_same")

Absorption_data=["Sample" ,"Name" ,"Dilution_factor"]
Absorption_index=[]
for i in Col_s:
Absorption_data=Absorption_data+[singlespec_head[i][0]+"_" +
    singlespec_head[i][1]]

```

```
Absorption_index=Absorption_index+[singlespec[0].index(int(
    singlespec_head[i][1]))]
Absorption_data=Absorption_data+["Peridinin_content_Photo",
    Peridinin_content_HPLC"]
Absorption_data = [Absorption_data]
```

```
Per_con_Photo=[]
Per_con_Hplc=[]
```

```
#Defining fit and error function for the fitting of all spectra
    apart from Chl. a
```

```
def fitfunc(x, p):
ind=singlespec[0].index(x)
y=singlespec[Col_chl_a][ind]*p_fit2[0]
for i in range(len(Col_s)):
y += singlespec[Col_s[i]][ind]*p[i]
return y
```

```
def fehlerfunc(p, xx, yy):
fehler = [y - fitfunc(x,p) for x, y in zip(xx,yy)]
#fehler = fehler + (p[3]-0)*1000000
for i in range(len(p)):
if p[i]<0:
fehler = fehler + (0-p[i])*1000000
return fehler
```

```
#Defining fit and error function for fitting only Chl. a
```

```
def fitfunc2(x, p):
ind=singlespec[0].index(x)
y=singlespec[Col_chl_a][ind]*p[0]
return y
```

```
def fehlerfunc2(p, xx, yy):
```

```

fehler = [y - fitfunc2(x,p) for x, y in zip(xx,yy)]
return fehler

#Here start the loop to calculate the best fit for every spectrum
for j in range(1,len(totalspec),1):
Col_t=j #Column of the total spectrum (In column 0 are the
        wavelength)
fitx2=totalspec[0][totalspec[0].index(660):totalspec[0].index(675)]
        #Defining the fitted regime of Chl. a from 660-675
fity2=totalspec[Col_t][totalspec[0].index(660):totalspec[0].index
        (675)]
p0_2=[1]
# the fitting of Chl. a:
p_fit2, cov2, info2, mesg2, ier = scipy.optimize.leastsq(
        fehlerfunc2, p0_2, args = (fitx2, fity2), full_output=1)

fitx=totalspec[0][totalspec[0].index(400):totalspec[0].index(550)]#
        Defining the fitted regime of all other pigments from 400-550
fity=totalspec[Col_t][totalspec[0].index(400):totalspec[0].index
        (550)]

p0=[] # p0 contains the start values for the fitting
for i in range(len(Col_s)):
p0=p0+[1] #this sets the start value for all spectra
        to 1

# the fitting of all other spectra:
p_fit, cov, info, mesg, ier = scipy.optimize.leastsq(fehlerfunc, p0
        , args = (fitx, fity), full_output=1)

dilution_factor= float(totalspec_head[Col_t][2])+1
Absorption_temp=[totalspec_head[Col_t][0], totalspec_head[Col_t][
        Row_real_name], totalspec_head[Col_t][2]]

```

```
for l in range(len(Col_s)):
Absorption_temp= Absorption_temp + [dilution_factor*p_fit[l]*
    singlespec[Col_s[l]][Absorption_index[l]]]
Absorption_temp= Absorption_temp + [dilution_factor*p_fit[l]*
    singlespec[Col_s[Pos_per]][Absorption_index[Pos_per]] *1E6
    /(1360*100)]
Absorption_temp= Absorption_temp + [totalspec_head[Col_t][
    Row_HPLC_result]]
Per_con_Photo=Per_con_Photo+[dilution_factor*p_fit[l]*singlespec[
    Col_s[Pos_per]][Absorption_index[Pos_per]] *1E6/(1360*100)]
Per_con_Hplc=Per_con_Hplc+[totalspec_head[Col_t][Row_HPLC_result]]
Absorption_data = Absorption_data+[Absorption_temp]

y_fit = [fitfunc(x, p_fit) for x in totalspec[0]] # creates the
    fitted spectrum using the fitparameter p_fit and the single
    spectra
Outputfile=Outputfolder+ totalspec_head[Col_t][0] + '.pdf' #name of
    Ouputfile

#creating the first figure with the single spectra
fig = pylab.figure(figsize=figsize_full_double)
ax = fig.add_axes(axrect_full_left)
ax.set_xlabel(r"Wavelength_/_nm")
ax.set_ylabel(r"Absorbance")
ax.set_axisbelow(True)
singlesresultspec=singlespec
for j in range(len(singlespec[0])):
singlesresultspec[Col_chl_a][j]=singlespec[Col_chl_a][j]*p_fit2[0]
for i in range(len(Col_s)):
singlesresultspec[Col_s[i]][j]=singlespec[Col_s[i]][j]*p_fit[i]
for i in Col_s:
```

```

ax.plot(singlespec[0], singleresultspec[i], linestyle="-", lw=2,
        marker="", color= rainbow[i%len(rainbow)] ,markersize = 2, label=
        singlespec_head[i][0])
ax.plot(singlespec[0], singleresultspec[Col_ch1_a], linestyle="-",
        lw=2,marker="", c= (23/255, 156/255, 125/255) ,markersize = 2,
        label= singlespec_head[Col_ch1_a][0])
ax.set_ylim(0,)

#creating the second figure with the full spectrum and the result
of the fit
ax2 = fig.add_axes(axrect_full_right)
ax2.plot(totalspec[0], totalspec[Col_t], linestyle="-", lw=2,marker
        = "", color= 'green' ,markersize = 2, label= totalspec_head[Col_t
        ][0])
ax2.plot(totalspec[0], y_fit , linestyle="-", lw=2,marker="", color=
        'red' ,markersize = 2, label= 'Fit')
ax2.set_xlabel(r"Wavelength□/□nm")
ax2.set_ylabel(r"Absorbance")
ax2.set_axisbelow(True)
ax2.set_ylim(0,)
ax.legend( loc= 'upper_□right')#, borderaxespadd=0.,numpoints = 1 )
ax2.legend( loc= 'upper_□right') #, borderaxespadd=0.,numpoints = )

#saving and showing the figures
pylab.savefig(Outputfile)
os.startfile(Outputfile)

#Saving the data
Outputfile=Outputfolder + Beschreibung + '.txt'
opened= open((Outputfile), 'wb')
resultswriter = csv.writer(opened, delimiter='\t', quotechar='|',
        quoting=csv.QUOTE_MINIMAL)
for ind in range(len(Absorption_data)):

```

```
resultswriter.writerow(Absorption_data[ind])
opened.close()
os.startfile(Outputfile)
Outputfile=Outputfolder + Beschreibung + '.pdf'
figsize_full = [16/2.54, 16/phi/2.54]
axrect_full=[0.15, 0.15, 0.7, 0.7]
fig = pylab.figure(figsize=figsize_full)
ax = fig.add_axes(axrect_full)
ax.plot(Per_con_Hplc,Per_con_Photo, linestyle="", lw=2,marker="o",
        color= 'orange' ,markersize = 4, label= "Peridinin□concentration
        ")
ax.set_xlabel(r"Peridinin□measured□with□HPLC")
ax.set_ylabel(r"Peridinin□measured□Photometrically")
ax.set_axisbelow(True)
pylab.savefig(Outputfile)
os.startfile(Outputfile)
```

LIST OF TABLES

2.1	ASP 12 Medium	16
2.2	Artificial f/2 Medium	16
2.3	SW1 Medium	17
2.4	SW2 Medium	17
2.5	SW3 Medium	18
3.1	Summary of biomass and peridinin production on TL PSBR	66
4.1	Effect of temperature on biomass production	76
4.2	Summary on peridinin productivity	82

LIST OF FIGURES

2.1	The bench-scale Twin-Layer PSBR.	18
2.2	Horizontal up-scale TL PSBR.	22
2.3	Chromatogram of <i>S. voratum</i>	26
2.4	Measured and simulated absorption spectrum of <i>S. voratum</i>	27
3.1	Biomass growth in dependence of light intensity (Exp. L1).	29
3.2	Peridinin production in dependence of light intensity (Exp. L1).	30
3.3	Biomass growth in dependence of light intensity (Exp. L2).	31
3.4	Peridinin production in dependence of light intensity (Exp. L2).	32
3.5	Comparison of biomass and peridinin productivity in dependence of light intensity.	32
3.6	Biomass growth in a biofilm with a higher inoculation density.	33
3.7	Peridinin production in a biofilm with a higher inoculation density.	34
3.8	Maximal amount of biomass and peridinin in Exp. D.	35
3.9	Documentation of <i>S. voratum</i> inoculated with a density of 10 g m ⁻²	36
3.10	Biomass growth on f/2 medium in 2 % CO ₂ and ambient air.	38
3.11	Biomass growth on ASP 12 medium in 2 % CO ₂ and ambient air.	39
3.12	Pigment production on ASP 12 medium in 2 % CO ₂ and ambient air.	40

3.13	Maximal amount of biomass and peridinin in Exp. CA.	40
3.14	Biofilm cross-sections from Exp. CA.	42
3.15	Biofilm performance with CO ₂ in dependence of light in f/2 and ASP 12.	42
3.16	Summary of the biomass production of <i>S. voratum</i> in the TL PSBR.	44
3.17	Summary of the peridinin production with <i>S. voratum</i> in the TL PSBR.	45
3.18	Impact of temperature on biofilm grown at low light.	47
3.19	Impact of temperature on biofilm grown at high light and CO ₂	48
3.20	Impact of temperature on peridinin production at low light.	49
3.21	Impact of temperature on peridinin production at high light and CO ₂	49
3.22	Summary of biomass and peridinin productivity from Exp. T.	50
3.23	Biomass growth in a two-step approach.	51
3.24	Pigment production in the two-step approach.	53
3.25	Final pigment amount and average peridinin productivity in the two-step approach.	54
3.26	Combination of biomass and peridinin production in the two-step approach.	54
3.27	Documentation of the cross-section in the two-step approach.	55
3.28	Effect of growth media on biomass production.	57
3.29	Effect of growth media on peridinin production.	57
3.30	Biofilm growth in the vertical up-scale TL PSBR.	59
3.31	Documentation of a biofilm grown on a vertical up-scale TL PSBR.	59
3.32	Growth in a paper-based horizontal up-scale TL PSBR.	61
3.33	Peridinin production in a paper-based horizontal up-scale TL PSBR.	62
3.34	Comparison of peridinin production in up-scale and bench-scale TL PSBR.	62

3.35	Comparison of biomass growth in a fleece-based up-scale and a paper-based bench-scale TL PSBR.	63
3.36	Peridinin production in an fleece-based horizontal up-scale TL PSBR.	65
3.37	Documentation of the horizontal up-scale TL PSBR.	65
3.38	Correlation of results from the pigment analysis by HPLC and photometer.	67
4.1	Schematic drawing of the proposed physiology in a biofilm.	73
4.2	Biomass and peridinin production at 16 °C and 50 $\mu\text{mol photons m}^{-2} \text{s}^{-1}$.	77

REFERENCES

- Abdel-Raouf, N., Al-Homaidan, A. A., and Ibraheem, I. B. M. (2012). Microalgae and wastewater treatment. *Saudi Journal of Biological Sciences*, 19(3):257–275.
- Abidov, M., Ramazanov, Z., Seifulla, R., and Grachev, S. (2010). The effects of Xanthigen in the weight management of obese premenopausal women with non-alcoholic fatty liver disease and normal liver fat. *Diabetes, Obesity and Metabolism*, 12(1):72–81.
- Alexandre, M. T. a., Lührs, D. C., van Stokkum, I. H. M., Hiller, R., Groot, M.-L., Kennis, J. T. M., and van Grondelle, R. (2007). Triplet state dynamics in peridinin-chlorophyll-a-protein: a new pathway of photoprotection in LHCs? *Biophysical Journal*, 93(6):2118–28.
- Anderson, D. M. (1978). Copper sensitivity of *Gonyaulax tamarensis*. *Limnology and Oceanography*, 23(2):283–295.
- Anderson, D. M. (1995). Toxic red tides and harmful algal blooms: A practical challenge in coastal oceanography. *Reviews of Geophysics*, (95):1189–1200.
- Avron, M. and Ben-Amotz, A. (1992). *Dunaliella: physiology, biochemistry, and biotechnology*. CRC press.
- Awai, K., Matsuoka, R., and Shioi, Y. (2012). Lipid and fatty acid compositions of *Symbiodinium* strains. *Proceedings of the 12th International Coral Reef Symposium*.
- Baker, M. (1753). Of luminous water insects. In *Employment for the Microscope*. Dodsley, R., London.

- Banaszak, A. T., Barba Santos, M. G., LaJeunesse, T. C., and Lesser, M. P. (2006). The distribution of mycosporine-like amino acids (MAAs) and the phylogenetic identity of symbiotic dinoflagellates in cnidarian hosts from the Mexican Caribbean. *Journal of Experimental Marine Biology and Ecology*, 337(2):131–146.
- Bandaranayake, W. M. (1997). Mycosporines : are they nature ' s sunscreens ? *Natural Product Reports*, (3):159–172.
- Barros, M. P., Pinto, E., Colepicolo, P., and Pedersén, M. (2001). Astaxanthin and peridinin inhibit oxidative damage in Fe²⁺-loaded liposomes: scavenging oxyradicals or changing membrane permeability? *Biochemical and Biophysical Research Communications*, 288(1):225–32.
- BBC Research (2015). Boom in Astaxanthin supplements boosting global carotenoid market. Technical report, BBC Research.
- Becker, E. W. (2007). Micro-algae as a source of protein. *Biotechnology Advances*, 25(2):207–210.
- Beijerinck, M. (1890). Culturversuche mit Zoochlorellen, Lichenengonidien und anderen niederen Algen. *Botanische Zeitung*, 48:726–740.
- Benstein, R. M. (2010). *Twin-Layer Kultivierung von Symbiodinium sp. und Isolation von Peridinin*. Bachelor thesis, University of Cologne.
- Benstein, R. M., Cebi, Z., Podola, B., and Melkonian, M. (2014). Immobilized Growth of the Peridinin-Producing Marine Dinoflagellate *Symbiodinium* sp. in a Simple Biofilm Photobioreactor. *Marine Biotechnology*.
- Beuzenberg, V., Mountfort, D., Holland, P., Shi, F., and MacKenzie, L. (2011). Optimization of growth and production of toxins by three dinoflagellates in photobioreactor cultures. *Journal of Applied Phycology*, 24(5):1023–1033.
- Bínová, B. J., Tichý, V., and Lívanský, K. (1998). Bacterial contamination or microalgal biomass during outdoor production and downstream processing. *Algological Studies*, 89:151–158.

- Bjørnland, T. (1990). Chromatographic separation and spectrometric characterization of native carotenoids from the marine dinoflagellate *Thoracosphaera heimii*. *Biochemical Systematics and Ecology*, 18(5):307–316.
- Blanken, W., Janssen, M., Cuaresma, M., Libor, Z., Bhajji, T., and Wijffels, R. H. (2014). Biofilm growth of *Chlorella sorokiniana* in a rotating biological contactor based photobioreactor. *Biotechnology and Bioengineering*, 111(12):2436–2445.
- Boelee, N. C., Janssen, M., Temmink, H., Shrestha, R., Buisman, C. J. N., and Wijffels, R. H. (2014). Nutrient removal and biomass production in an outdoor pilot-scale phototrophic biofilm reactor for effluent polishing. *Applied Biochemistry and Biotechnology*, 172(1):405–422.
- Boelee, N. C., Temmink, H., Janssen, M., Buisman, C. J. N., and Wijffels, R. H. (2011). Nitrogen and phosphorus removal from municipal wastewater effluent using microalgal biofilms. *Water Research*, 45(18):5925–5933.
- Borowitzka, M. A. (1995). Microalgae as sources of pharmaceuticals and other biologically active compounds. *Journal of Applied Phycology*, 7(1):3–15.
- Bowden, B. F. (2006). Yessotoxins - Polycyclic Ethers From Dinoflagellates: Relationships To Diarrhetic Shellfish Toxins. *Toxin Reviews*, 25(2):137–157.
- Brennan, L. and Owende, P. (2010). Biofuels from microalgae-A review of technologies for production, processing, and extractions of biofuels and co-products. *Renewable and Sustainable Energy Reviews*, 14(2):557–577.
- Budge, S., Parrish, C., and McKenzie, C. (2001). Fatty acid composition of phytoplankton, settling particulate matter and sediments at a bivalve culture site. *Marine Chemistry*, 76:285–303.
- Burkholder, J. M., Glibert, P. M., and Skelton, H. M. (2008). Mixotrophy, a major mode of nutrition for harmful algal species in eutrophic waters. *Harmful Algae*, 8(1):77–93.
- Bustillos-Guzman, J., Garate-Lizarraga, I., Lopez-Cortes, D., and Hernandez-Sandoval, F. (2004). The use of pigment "fingerprints" in the study of harmful algal blooms. *Revista de Biología Tropical*, 52(1):17–26.

References

- Callaway, E. (2015). Lab staple agar runs low. *Nature*, 258:172.
- Camacho, F. G., Rodríguez, J. G., Mirón, a. S., Belarbi, E., Chisti, Y., and Grima, E. M. (2011). Photobioreactor scale-up for a shear-sensitive dinoflagellate microalga. *Process Biochemistry*, 46(4):936–944.
- Carbonera, D., Di Valentin, M., Spezia, R., and Mezzetti, A. (2014). The unique photophysical properties of the Peridinin-Chlorophyll-*a*-Protein. *Current Protein and Peptide Science*, 15(4):332–350.
- Carlos, A. A., Baillie, B. K., Kawachi, M., and Maruyama, T. (1999). Phylogenetic position of *Symbiodinium* (Dinophyceae) from Tridacnids (Bivalvia), Cardiids (Bivalvia), a sponge (Porifera), a soft Coral (Anthozoa), and a free-living strain. *Journal of Phycology*, 35(5):1054–1062.
- Carvalho, A. P., Meireles, L. A., and Malcata, F. X. (2006). Microalgal reactors: A review of enclosed system designs and performances. *Biotechnology Progress*, 22(6):1490–1506.
- Chen, C. Y., Yeh, K. L., Aisyah, R., Lee, D. J., and Chang, J. S. (2011). Cultivation, photobioreactor design and harvesting of microalgae for biodiesel production: A critical review. *Bioresource Technology*, 102(1):71–81.
- Cheng, P., Ji, B., Gao, L., Zhang, W., Wang, J., and Liu, T. (2013). The growth, lipid and hydrocarbon production of *Botryococcus braunii* with attached cultivation. *Bioresource Technology*, 138:95–100.
- Cheng, P., Wang, J., and Liu, T. (2015). Effect of cobalt enrichment on growth and hydrocarbon accumulation of *Botryococcus braunii* with immobilized biofilm attached cultivation. *Bioresource technology*, 177:204–8.
- Chevalier, P. and de la Noüe, J. (1985). Efficiency of immobilized hyperconcentrated algae for ammonium and orthophosphate removal from wastewaters. *Biotechnology Letters*, 7(6):395–400.

- Concas, A., Malavasi, V., Costelli, C., Fadda, P., Pisu, M., and Cao, G. (2016). Autotrophic growth and lipid production of *Chlorella sorokiniana* in lab batch and BIOCOIL photobioreactors: Experiments and modeling. *Bioresource Technology*, 211:327–338.
- Craggs, R. J., Adey, W. H., Jenson, K. R., John, M. S. S., Green, F. B., and Oswald, W. J. (1996). Phosphorus removal from wastewater using an algal turf scrubber. *Water Science and Technology*, 33(7):191–198.
- Daranas, A. H., Norte, M., and Fernández, J. J. (2001). Toxic marine microalgae. *Toxicon*, 39(8):1101–1132.
- de la Noüe, J. and Basseres, A. (1989). Biotreatment of anaerobically digested swine manure with microalgae. *Biological Wastes*, 29(1):17–31.
- Del Campo, J. A., Garcia-Gonzalez, M., and Guerrero, M. G. (2007). Outdoor cultivation of microalgae for carotenoid production: Current state and perspectives. *Applied Microbiology and Biotechnology*, 74(6):1163–1174.
- Dixon, G. and Syrett, P. (1988). The growth of dinoflagellates in laboratory culture. *New Phytologist*, 109(3):297–302.
- D’Orazio, N., Gemello, E., Gammone, M. A., De Girolamo, M., Ficoneri, C., and Riccioni, G. (2012). Fucoxanthin: A treasure from the sea. *Marine Drugs*, 10(3):604–616.
- Echigoya, R., Rhodes, L., Oshima, Y., and Satake, M. (2005). The structures of five new antifungal and hemolytic amphidinol analogs from *Amphidinium carterae* collected in New Zealand. *Harmful Algae*, 4(2):383–389.
- Fensome, R., Taylor, F., Norris, G., Sarjeant, W., Wharton, D., and Williams, G. (1993). A classification of fossil and living dinoflagellates. *Micropaleontology Press Special Paper*, 7:351.
- Field, C. B. (1998). Primary Production of the Biosphere: Integrating Terrestrial and Oceanic Components. *Science*, 281(5374):237–240.

References

- Fiore, C. L., Jarett, J. K., Olson, N. D., and Lesser, M. P. (2010). Nitrogen fixation and nitrogen transformations in marine symbioses. *Trends in Microbiology*, 18(10):455–63.
- Foo, S. C., Yusoff, F. M., Ismail, M., Basri, M., Khong, N. M. H., Chan, K. W., and Yau, S. K. (2015). Production of fucoxanthin-rich fraction (FxRF) from a diatom, *Chaetoceros calcitrans* (Paulsen) Takano 1968. *Asian Pacific Journal of Tropical Biomedicine*, 5(10):834–840.
- Freudenthal, H. D. (1962). *Symbiodinium* gen. no. and *Symbiodinium microadriaticum* ap.nov., a zooxantella: Taxonomy, Life Cycle, and Morphology. *Journal of Protozoology*, 9:848–851.
- Fritsch, F. E. (1945). *The Structure and Reproduction of the Algae. Vol. 1*. Cambridge University Press, Cambridge.
- Fuchinoue, Y., Katayama, T., Obata, M., Murata, A., Kinzie, R., and Taguchi, S. (2012). Growth, biochemical properties, and chlorophyll fluorescence of symbiotic and free-living dinoflagellates in response to ammonium enrichment. *Journal of Experimental Marine Biology and Ecology*, 438:1–6.
- Fuentes-Grünewald, C. (2015). *Dinoflagellates and Raphidophytes as Feedstock for Biofuel Production*. Lambert Academic Publishing, Saarbrücken.
- Fuentes-Grünewald, C., Garces, C., Rossi, S., and Camp, J. (2009). Use of the dinoflagellate *Karlodinium veneficum* as a sustainable source of biodiesel production. *Journal of Industrial Microbiology*, 36:1215–1224.
- Fuentes-Grünewald, C., Garces, E., Alacid, E., Rossi, S., and Camp, J. (2013). Biomass and Lipid Production of Dinoflagellates and Raphidophytes in Indoor and Outdoor Photobioreactors. *Marine Biotechnology*, 15(1):37–47.
- Gallardo Rodríguez, J., Sánchez Mirón, a., García Camacho, F., Cerón García, M., Belarbi, E., and Molina Grima, E. (2010). Culture of dinoflagellates in a fed-batch and continuous stirred-tank photobioreactors: Growth, oxidative stress and toxin production. *Process Biochemistry*, 45(5):660–666.

- Gallardo Rodríguez, J. J., Ceron Garcia, M. d. C., Garcia Camacho, F., Sanchez Miron, A., Belarbi, E. H., and Grima, E. M. (2007). New culture approaches for yessotoxin production from the dinoflagellate *Protoceratium reticulatum*. *Biotechnology Progress*, 23(2):339–350.
- Ganuza, E., Benítez-Santana, T., Atalah, E., Vega-Orellana, O., Ganga, R., and Izquierdo, M. S. (2008). *Cryptocodinium cohnii* and *Schizochytrium* sp. as potential substitutes to fisheries-derived oils from seabream (*Sparus aurata*) microdiets. *Aquaculture*, 277(1-2):109–116.
- García Camacho, F., Gallardo Rodríguez, J., Sánchez Mirón, a., Cerón García, M., Belarbi, E., and Molina Grima, E. (2007). Determination of shear stress thresholds in toxic dinoflagellates cultured in shaken flasks. *Process Biochemistry*, 42(11):1506–1515.
- Garrido, R., Lagos, N., Lattes, K., Abedrapo, M., Bocic, G., Cuneo, A., Chiong, H., Jensen, C., Azolas, R., Henriquez, A., and Garcia, C. (2005). Gonyautoxin: New treatment for healing acute and chronic anal fissures. *Diseases of the Colon and Rectum*, 48(2):335–340.
- Garthwaite, I. (2001). Keeping shellfish safe to eat : a brief review of shellfish toxins , and methods for their detection. *Trends in Food Science & Technology*, 11(2000).
- Geider, R. J., Url, S., and Geider, J. (1987). Light and temperature dependence of the carbon to chlorophyll *a* ratio in microalgae and cyanobacteria. *Deep Sea Research Part B. Oceanographic Literature Review*, 34(12):1064.
- Gibson, C. H. and Thomas, W. H. (1995). Effects of turbulence intermittency on growth inhibition of a red tide dinoflagellate , *Gonyaulax polyedra* Stein. *Journal of Geophysical Research*, 100(95):841–846.
- Gladue, R. M. and Maxey, J. E. (1994). Microalgal feeds for aquaculture. *Journal of Applied Phycology*, 6(2):131–141.
- Gómez-Loredo, A., Benavides, J., and Rito-Palomares, M. (2015). Growth kinetics and fucoxanthin production of *Phaeodactylum tricornutum* and *Isochrysis galbana*

References

- cultures at different light and agitation conditions. *Journal of Applied Phycology*, 28(2):849–860.
- Gottschling, M. and McLean, T. I. (2013). New home for tiny symbionts: dinophytes determined as Zooxanthella are Peridinales and distantly related to *Symbiodinium*. *Molecular Phylogenetics and Evolution*, 67(1):217–22.
- Graham, L. E., Graham, J. M., and Wilcox, L. W. (2009). *Algae, 2nd editon*. Benjamin Cummings (Pearson), San Francisco.
- Gross, M., Jarboe, D., and Wen, Z. (2015). Biofilm-based algal cultivation systems. *Applied Microbiology and Biotechnology*, 99(14):5781–5789.
- Gross, M. and Wen, Z. (2014). Yearlong evaluation of performance and durability of a pilot-scale Revolving Algal Biofilm (RAB) cultivation system. *Bioresource Technology*, 171:50–58.
- Guillard, R. R. L. and Ryther, J. H. (1962). Studies of marine planktonic diatoms: I. *Cyclotella nana* Hustedt, and *Detonula confervacea* (Cleve) gran. *Canadian Journal of Microbiology*, 8(2):229–239.
- Guo, B., Liu, B., Yang, B., Sun, P., Lu, X., Liu, J., and Chen, F. (2016). Screening of Diatom Strains and Characterization of *Cyclotella cryptica* as A Potential Fucoxanthin Producer. *Marine Drugs*, 14(125):1–14.
- Hagen, C., Braune, W., Brickner, E., and Nüske, J. (1993). Functional in aspects of secondary *Haematococcus lacustris* Rostafinski I. The accumulation period as an active metabolic process. *New Phytologist*, 125(3):625–633.
- Haidak, D. J., Mathews, C. K., and Sweeney, B. M. (1966). Pigment Protein Complex from *Gonyaulax*. *Science*, 152:212–213.
- Hansford, G. S., Andrews, J. F., Grieves, C. G., and Carr, A. D. (1978). A steady-state model for the rotating biological disc reactor. *Water Research*, 12(10):855–868.

- Hata, M. and Hata, M. (1982). Isolation and properties of peridinin-chlorophyll-a-protein complex from the brick-red-colored oyster, *Crassostrea gigas*. *Comparative Biochemistry and Physiology* -, 72(4):631–635.
- Haxo, F. T., Kycia, J. H., Somers, G. F., Benneit, A., and Harold, W. (1976). Peridinin-Chlorophyll *a* Proteins of the Dinoflagellate *Amphidinium carterae* (Plymouth 450). *Plant Physiology*, pages 297–303.
- Heilbron, I. M., Jackson, H., and Jones, R. (1935). The Lipochromes of Sea Anemones. I. Carotenoid Pigments of *Actinia equina*, *Anemonia sulcata*, *Actinoloba dianthus* and *Tealia felina* . *Biochemical Journal*, 29:1384.
- Hejazi, M. A., Holwerda, E., and Wijffels, R. H. (2004). Milking Microalga *Dunaliella salina* for β -Carotene Production in Two-Phase Bioreactors. *Biotechnology and Bioengineering*, 85(5):475–481.
- Holland, P. T., Shi, F., Satake, M., Hamamoto, Y., Ito, E., Beuzenberg, V., McNabb, P., Munday, R., Briggs, L., Truman, P., Gooneratne, R., Edwards, P., and Pascal, S. M. (2012). Novel toxins produced by the dinoflagellate *Karenia brevisulcata* . *Harmful Algae*, 13:47–57.
- Hu, H., Chen, W., Shi, Y., and Cong, W. (2006). Nitrate and phosphate supplementation to increase toxin production by the marine dinoflagellate *Alexandrium tamarense*. *Marine Pollution Bulletin*, 52(7):756–760.
- Iglesias-Prieto, R., Matta, J. L., Robins, W. A., and Trench, R. K. (1992). Photosynthetic response to elevated temperature in the symbiotic dinoflagellate *Symbiodinium microadriaticum* in culture. *Proceedings of the National Academy of Sciences of the United States of America*, 89(21):10302–10305.
- Jaswir, I., Noviendri, D., Salleh, H. M., and Miyashita, K. (2012). Fucoxanthin Extractions of Brown Seaweeds and Analysis of Their Lipid Fraction in Methanol. *Journal of Food Science and Technology Research*, 18(2):251–257.
- Jeffery, S. W. and Haxo, F. T. (1968). Photosynthetic Pigments of Symbiotic Dinoflagellates (Zooxanthellae) From Corals and Clams. *The Biological Bulletin*, 135(1):149–165.

- Jeffrey, S. W. (1968). Quantitative thin layer chromatography of chlorophylls and carotenoids from marine algae. *Biochimica et Biophysica Acta*, 162:271–285.
- Jeong, H. J., Lee, S. Y., Kang, N. S., Yoo, Y. D., Lim, A. S., Lee, M. J., Kim, H. S., Yih, W., Yamashita, H., and LaJeunesse, T. C. (2014a). Genetics and morphology characterize the dinoflagellate *Symbiodinium voratum*, n. sp., (Dinophyceae) as the sole representative of *Symbiodinium* Clade E. *The Journal of Eukaryotic Microbiology*, 61(1):75–94.
- Jeong, H. J., Lim, A. S., Yoo, Y. D., Lee, M. J., Lee, K. H., Jang, T. Y., and Lee, K. (2014b). Feeding by heterotrophic dinoflagellates and ciliates on the free-living dinoflagellate *Symbiodinium* sp. (clade E). *Journal of Eukaryotic Microbiology*, 61(1):27–41.
- Jeong, H. J., Yoo, Y. D., Kang, N. S., Lim, a. S., Seong, K. a., Lee, S. Y., Lee, M. J., Lee, K. H., Kim, H. S., Shin, W., Nam, S. W., Yih, W., and Lee, K. (2012). Heterotrophic feeding as a newly identified survival strategy of the dinoflagellate *Symbiodinium*. *PNAS*, 109(31):12604–12609.
- Ji, B., Zhang, W., Zhang, N., Wang, J., Lutz, G. A., and Liu, T. (2014a). Biofilm cultivation of the oleaginous microalgae *Pseudochlorococcum* sp. *Bioprocess and Biosystems Engineering*, 37(7):1369–1375.
- Ji, C., Wang, J., Zhang, W., Liu, J., Wang, H., Gao, L., and Liu, T. (2014b). An applicable nitrogen supply strategy for attached cultivation of *Aucutodesmus obliquus*. *Journal of Applied Phycology*, 26(1):173–180.
- Johansen, J. E., Svec, W. A., Liaaen-Jensen, S., and Haxo, F. T. (1974). Carotenoids of the dinophyceae. *Phytochemistry*, 13(10):2261–2271.
- Jovine, R. and Triplett, E. (1992). Quantification of chromophore pigments, apoprotein abundance and isoelectric variants of peridinin-chlorophyll *a*-protein complexes (PCPs) in the dinoflagellate *Heterocapsa pygmaea* grown under variable light conditions. *Plant and Cell Physiology*, 33(6):733–741.

- Kanazawa, A., Blanchard, G. J., Szabo, M., Ralph, P. J., and Kramer, D. M. (2014). The site of regulation of light capture in *Symbiodinium*: Does the peridinin-chlorophyll *a*-protein detach to regulate light capture? *Biochimica et Biophysica Acta - Bioenergetics*, 1837(8):1227–1234.
- Kanda, H., Kamo, Y., Machmudah, S., Wahyudiono, E. Y., and Goto, M. (2014). Extraction of fucoxanthin from raw macroalgae excluding drying and cell wall disruption by liquefied dimethyl ether. *Marine drugs*, 12(5):2383–96.
- Karp-Boss, L., Boss, E., and Jumars, P. a. (2000). Motion of dinoflagellates in a simple shear flow. *Limnology and Oceanography*, 45(7):1594–1602.
- Khalesi, M. K. and Lamers, P. (2010). Partial quantification of pigments extracted from the zooxanthellate octocoral *Sinularia flexibilis* at varying irradiances. *Biologia*, 65(4):681–687.
- Kim, S. M., Jung, Y. J., Kwon, O. N., Cha, K. H., Um, B. H., Chung, D., and Pan, C. H. (2012). A potential commercial source of fucoxanthin extracted from the microalga *Phaeodactylum tricornutum*. *Applied Biochemistry and Biotechnology*, 166(7):1843–1855.
- Kiperstok, A. C. (2016). *Optimizing immobilised cultivation of Haematococcus pluvialis for astaxanthin production*. Ph.D. thesis, University of Cologne.
- Kita, M., Kondo, M., Koyama, T., Yamada, K., Matsumoto, T., Lee, K. H., Woo, J. T., and Uemura, D. (2004). Symbioimine Exhibiting Inhibitory Effect of Osteoclast Differentiation, from the Symbiotic Marine Dinoflagellate *Symbiodinium* sp. *Journal of the American Chemical Society*, 126(15):4794–4795.
- Kita, M., Ohishi, N., Konishi, K., Kondo, M., Koyama, T., Kitamura, M., Yamada, K., and Uemura, D. (2007). Symbiodinolide, a novel polyol macrolide that activates N-type Ca²⁺ channel, from the symbiotic marine dinoflagellate *Symbiodinium* sp. *Tetrahedron*, 63(27):6241–6251.
- Kita, M., Ohishi, N., Washida, K., Kondo, M., Koyama, T., Yamada, K., and Uemura, D. (2005). Symbioimine and neosymbioimine, amphoteric iminium metabolites

References

- from the symbiotic marine dinoflagellate *Symbiodinium* sp. *Bioorganic & Medicinal Chemistry*, 13(17):5253–8.
- Klebs, G. (1896). Die Bedingungen der Fortpflanzung bei einigen Algen und Pilzen. In *Über die Fortpflanzungs-Physiologie der niederen Organismen, der Protobionten*. Gustav Fischer, Jena.
- Kneeland, J., Hughen, K., Cervino, J., Hauff, B., and Eglinton, T. (2013). Lipid biomarkers in *Symbiodinium* dinoflagellates: New indicators of thermal stress. *Coral Reefs*, 32(4):923–934.
- Kobayashi, J. (2008). Amphidinolides and its related macrolides from marine dinoflagellates. *The Journal of Antibiotics*, 61(5):271–284.
- Kofoed, C. A. and Swezy, O. (1921). *The free-living unarmored Dinoflagellata*. Memoirs of the University of California.
- Kreuz, F. (2016). *Symbiontische Dinoflagellaten und Peridininbiosynthese*. Bachelor, University of Cologne.
- Kumar, K. and Das, D. (2012). Growth characteristics of *Chlorella sorokiniana* in airlift and bubble column photobioreactors. *Bioresource Technology*, 116:307–313.
- Küster, E. (1907). *Anleitung zur Kultur der Mikroorganismen*. B. G. Teubner, Leipzig.
- Kyle, D. J., Reeb, S. E., and Sicotte, J. (1998). Dinoflagellate biomass, methods for its production and compositions containing the same. U.S. Patent; Nr. 5711983.
- Lee, J.-C., Hou, M.-F., Huang, H.-W., Chang, F.-R., Yeh, C.-C., Tang, J.-Y., and Chang, H.-W. (2013). Marine algal natural products with anti-oxidative, anti-inflammatory, and anti-cancer properties. *Cancer Cell International*, 13(1):55.
- Lee, J. Y., Hong, M. E., Chang, W. S., and Sim, S. J. (2015). Enhanced carbon dioxide fixation of *Haematococcus pluvialis* using sequential operating system in tubular photobioreactors. *Process Biochemistry*, 50(7):1091–1096.

- Leupold, M., Hindersin, S., Kerner, M., and Hanelt, D. (2013). The effect of discontinuous airlift mixing in outdoor flat panel photobioreactors on growth of *Scenedesmus obliquus*. *Bioprocess and Biosystems Engineering*, 36(11):1653–1663.
- Li, T. (2011). *Removal of Zn from wastewater with a continuous treatment system based on Microalgae immobilized on Twin-Layer*. Master thesis, University of Cologne.
- Li, T., Podola, B., de Beer, D., and Melkonian, M. (2015). A method to determine photosynthetic activity from oxygen microsensor data in biofilms subjected to evaporation. *Journal of Microbiological Methods*, 117:100–107.
- Lippemeier, S., Frampton, D. M. F., Blackburn, S. I., Geier, S. C., and Negri, a. P. (2003). Influence of phosphorus limitation on toxicity and photosynthesis of *Alexandrium minutum* (Dinophyceae) monitored by in-line detection of variable chlorophyll fluorescence. *Journal of Phycology*, 39(2):320–331.
- Liu, C. H., Chang, C. Y., Liao, Q., Zhu, X., Liao, C. F., and Chang, J. S. (2013). Biohydrogen production by a novel integration of dark fermentation and mixotrophic microalgae cultivation. *International Journal of Hydrogen Energy*, 38(35):15807–15814.
- Lopez, M. C. G. M., Sanchez, E. D. R., Casas Lopez, J. L., Fernandez, F. G. A., Sevilla, J. M. F., Rivas, J., Guerrero, M. G., and Grima, E. M. (2006). Comparative analysis of the outdoor culture of *Haematococcus pluviialis* in tubular and bubble column photobioreactors. *Journal of Biotechnology*, 123(3):329–342.
- López-Rosales, L., García-Camacho, F., Sánchez-Mirón, A., Contreras-Gómez, A., and Molina-Grima, E. (2015). An optimisation approach for culturing shear-sensitive dinoflagellate microalgae in bench-scale bubble column photobioreactors. *Biore-source Technology*, 197:375–382.
- Maeda, H., Hosokawa, M., Sashima, T., Funayama, K., and Miyashita, K. (2005). Fucoxanthin from edible seaweed, *Undaria pinnatifida*, shows antiobesity effect through UCP1 expression in white adipose tissues. *Biochemical and Biophysical Research Communications*, 332(2):392–397.

References

- Mallick, N. (2002). Biotechnological potential of immobilized algae for wastewater N, P and metal removal: A review. *BioMetals*, 15(4):377–390.
- Mansour, M. P., Volkman, J. K., Jackson, A. E., Blackburn, S. I., and Hirasaki, G. (1999). The fatty acid composition and sterol composition of five marine dinoflagellates. *Journal of Phycology*, 720:710–720.
- Markou, G. and Georgakakis, D. (2011). Cultivation of filamentous cyanobacteria (blue-green algae) in agro-industrial wastes and wastewaters: A review. *Applied Energy*, 88(10):3389–3401.
- McBride, B. B., Muller-Parker, G., and Jakobsen, H. H. (2009). Low thermal limit of growth rate of *Symbiodinium californium* (Dinophyta) in culture may restrict the symbiont to southern populations of its host anemones (*Anthopleura* spp.; Anthozoa, Cnidaria). *Journal of Phycology*, 45(4):855–863.
- McFadden, G. I. and Melkonian, M. (1986). Use of Hepes buffer for microalgal culture media and fixation for electron microscopy. *Phycologia*, 25(4):551–557.
- McLachlan, J. (1973). Growth media - marine. In *Handbook of Phycological Methods, Culturing Methods Growth Measures*, pages 25–52. Cambridge University Press, London.
- Melkonian, M. and Podola, B. (2003). Method and device for cultivating eucaryotic microorganisms or blue algae, and biosensor with cultivated eucaryotic microorganisms or blue algae. U.S. Patent. Nr. 7745201.
- Michels, M. H., Slegers, P. M., Vermuë, M. H., and Wijffels, R. H. (2014). Effect of biomass concentration on the productivity of *Tetraselmis suecica* in a pilot-scale tubular photobioreactor using natural sunlight. *Algal Research*, 4:12–18.
- Mise, T., Ueda, M., and Yasumoto, T. (2011). Production of fucoxanthin-rich powder from *Cladosiphon okamuranus*. *Advance Journal of Food Science and Technology*, 3(1):73–76.

- Morowvat, M. H. and Ghasemi, Y. (2016). Culture medium optimization for enhanced β -carotene and biomass production by *Dunaliella salina* in mixotrophic culture. *Biocatalysis and Agricultural Biotechnology*, 7:217–223.
- Mulbry, W., Kondrad, S., Pizarro, C., and Kebede-Westhead, E. (2008). Treatment of dairy manure effluent using freshwater algae: Algal productivity and recovery of manure nutrients using pilot-scale algal turf scrubbers. *Bioresource Technology*, 99(17):8137–8142.
- Müller, O. F. (1773). *Vermivm terrestrium et fluviatilium, seu, Animalium infusoriorum, helminthicorum et testaceorum, non marinorum, succincta historia*. In *Voluminis Imi pars Ima*, volume I. Heineck et Faber.
- Murray, S., Flø Jørgensen, M., Ho, S. Y. W., Patterson, D. J., and Jermiin, L. S. (2005). Improving the analysis of dinoflagellate phylogeny based on rDNA. *Protist*, 156(3):269–286.
- Naqvi, K. R., Hassan, T. H., and Naqvi, Y. A. (2004). Expeditious implementation of two new methods for analysing the pigment composition of photosynthetic specimens. *Spectrochimica Acta - Part A: Molecular and Biomolecular Spectroscopy*, 60(12):2783–2791.
- Naqvi, K. R., Melar, T. B., and Raju, B. B. (1997). Assaying the chromophore composition of photosynthetic systems by spectral reconstruction : application to the light-harvesting complex (LHC II) and the total pigment content of higher plants. *Spectrochimica Acta Part A*, 53:2229–2234.
- Naumann, T. (2003). *Entwicklung von Dünnschichtkulturverfahren für Mikroalgen auf Basis gaspermeabler Kunststofffolien und Verbundschichten*. Diploma thesis, University of Cologne.
- Naumann, T., Çebi, Z., Podola, B., and Melkonian, M. (2013). Growing microalgae as aquaculture feeds on twin-layers: A novel solid-state photobioreactor. *Journal of Applied Phycology*, 25(5):1413–1420.

References

- Nowack, E. C. M., Podola, B., and Melkonian, M. (2005). The 96-well Twin-Layer system: A novel approach in the cultivation of microalgae. *Protist*, 156(2):239–251.
- Ogbonna, J. C., Yada, H., and Tanaka, H. (1995). Kinetic study on light-limited batch cultivation of photosynthetic cells. *Journal of Fermentation and Bioengineering*, 80(3):259–264.
- Onodera, K. I., Konishi, Y., Taguchi, T., Kiyoto, S., and Tominaga, A. (2014). Peridinin from the marine symbiotic dinoflagellate, *Symbiodinium* sp., regulates eosinophilia in mice. *Marine Drugs*, 12(4):1773–1787.
- Ozkan, A., Kinney, K., Katz, L., and Berberoglu, H. (2012). Reduction of water and energy requirement of algae cultivation using an algae biofilm photobioreactor. *Bioresource Technology*, 114:542–548.
- Parker, N. S., Negri, A. P., Frampton, D. M. F., Rodolfi, L., Tredici, M. R., and Blackburn, S. I. (2002). Growth of the toxic dinoflagellate *Alexandrium minutum* (Dinophyceae) using high biomass culture systems. *Journal of Applied Phycology*, 14(5):313–324.
- Peng, J., Yuan, J. P., Wu, C. F., and Wang, J. H. (2011). Fucoxanthin, a marine carotenoid present in brown seaweeds and diatoms: Metabolism and bioactivities relevant to human health. *Marine Drugs*, 9(10):1806–1828.
- Perez-Garcia, O., Bashan, Y., and Esther Puente, M. (2011). Organic carbon supplementation of sterilized municipal wastewater is essential for heterotrophic growth and removing ammonium by the microalga *Chlorella vulgaris*. *Journal of Phycology*, 47(1):190–199.
- Podola, B., Li, T., and Melkonian, M. (2016). Porous substrate bioreactors - a paradigm shift in microalgal biotechnology? *Trends in Biotechnology*, (In press).
- Polívka, T., Hiller, R. G., and Frank, H. a. (2007). Spectroscopy of the peridinin-chlorophyll-a protein: insight into light-harvesting strategy of marine algae. *Archives of Biochemistry and Biophysics*, 458(2):111–20.

- Ponmani, T., Guo, R., and Ki, J.-S. (2016). Analysis of the genomic DNA of the harmful dinoflagellate *Prorocentrum minimum*: a brief survey focused on the noncoding RNA gene sequences. *Journal of Applied Phycology*, 28:335–344.
- Radmann, E. M., Reinehr, C. O., and Costa, J. A. V. (2007). Optimization of the repeated batch cultivation of microalga *Spirulina platensis* in open raceway ponds. *Aquaculture*, 265(1-4):118–126.
- Recktenwald, D. (1987). Peridinin-chlorophyll complexes as fluorescent label. U.S. Patent; Nr. 4876190.
- Rengarajan, T., Rajendran, P., Nandakumar, N., Balasubramanian, M. P., and Nishigaki, I. (2013). Cancer preventive efficacy of marine carotenoid fucoxanthin: Cell cycle arrest and apoptosis. *Nutrients*, 5(12):4978–4989.
- Richardson, K., Beardall, J., and Raven, J. a. (1983). Adaption of unicellular algae to irradiance: an analysis of strategies. *New Phytologist*, 93:157–191.
- Robinson, P., a.L. Dainty, Goulding, K., Simpkins, I., and Trevan, M. (1985). Physiology of alginate-immobilized *Chlorella*. *Enzyme and Microbial Technology*, 7(5):212–216.
- Rodriguez, E. M. and Hirayama, K. (1997). Semi-mass culture of the dinoflagellate *Gymnodinium splendens* as a live food source for the initial feeding of marine finfish larvae. In *Developments in Hydrobiology*. Kluwer Academic Publisher.
- Rodriguez-Navarro, A. J., Lagos, N., Lagos, M., Braghetto, I., Csendes, A., Hamilton, J., Figueroa, C., Truan, D., Garcia, C., Rojas, A., Iglesias, V., Brunet, L., and Alvarez, F. (2007). Neosaxitoxin as a Local Anesthetic. *Anesthesiology*, 106(2):339–345.
- Roeselers, G., Loosdrecht, M. C. M. V., and Muyzer, G. (2008). Phototrophic biofilms and their potential applications. *Journal of Applied Phycology*, 20(3):227–235.
- Rogers, J. and Davis, R. (2006). Application of a new micro-culturing technique to assess the effects of temperature and salinity on specific growth rates of six *Symbiodinium* isolates. *Bulletin of Marine Science*, 79(1):113–126.

References

- Rogers, J. E. and Marcovich, D. (2007). A simple method for the extraction and quantification of photopigments from *Symbiodinium* spp. *Journal of Experimental Marine Biology and Ecology*, 353(2):191–197.
- Rosic, N. N. and Dove, S. (2011). Mycosporine-like amino acids from coral dinoflagellates. *Applied and Environmental Microbiology*, 77(24):8478–86.
- Satake, M., Shoji, M., Oshima, Y., Naoki, H., Fujita, T., and Yasumoto, T. (2002). Gymnocin-A, a cytotoxic polyether from the notorious red tide dinoflagellate, *Gymnodinium mikimotoi*. *Tetrahedron Letters*, 43(33):5829 – 5832.
- Sausen, N. (2016). *Phylogenie der Dinoflagellaten: Stammbäume im Vergleich*. Ph.D. thesis, University of Cologne.
- Schnepf, E. and Elbrächter, M. (1992). Nutritional strategies in dinoflagellates: A review with emphasis on cell biological aspects. *European Journal of Protistology*, 28(1):3–24.
- Schnurr, P. J., Molenda, O., Edwards, E., Espie, G. S., and Grant Allen, D. (2016). Improved biomass productivity in algal biofilms through synergistic interactions between photon flux density and carbon dioxide concentration. *Bioresource Technology*, 219:72–79.
- Schulte, T., Johanning, S., and Hofmann, E. (2010). Structure and function of native and refolded peridinin-chlorophyll-proteins from dinoflagellates. *European Journal of Cell Biology*, 89(12):990–7.
- Schultze, L. K. P., Simon, M. V., Li, T., Langenbach, D., Podola, B., and Melkonian, M. (2015). High light and carbon dioxide optimize surface productivity in a twin-layer biofilm photobioreactor. *Algal Research*, 8:37–44.
- Schütt, F. (1890). Über Peridineenfarbstoffe. *Berichte der Deutschen Botanischen Gesellschaft*, 8(1):9–32.
- Sebestyén, P., Blanken, W., Bacsa, I., Tóth, G., Martin, A., Bhaiji, T., Dergez, Á., Kesserü, P., Koós, Á., and Kiss, I. (2016). Upscale of a laboratory rotating disk biofilm reactor

- and evaluation of its performance over a half-year operation period in outdoor conditions. *Algal Research*, 18:266–272.
- Shah, M. M. R., Kalpa, W. S., Ju-Young, K., H., H. C. L., Ji-Hyeok, L., So-Jeong, A., You-Jin, J., and Joon-Baek, L. (2014). Potentiality of benthic dinoflagellate cultures and screening of their bioactivities in Jeju Island, Korea. *African Journal of Biotechnology*, 13(6):792–805.
- Shi, J. (2005). *Nitrogen and Phosphorus removal from municipal wastewater by immobilized Chlorella vulgaris and Scenedesmus rubescens*. Master thesis, University of Cologne.
- Shi, J., Podola, B., and Melkonian, M. (2007). Removal of nitrogen and phosphorus from wastewater using microalgae immobilized on twin layers: An experimental study. *Journal of Applied Phycology*, 19(5):417–423.
- Shi, J., Podola, B., and Melkonian, M. (2014). Application of a prototype-scale twin-layer photobioreactor for effective N and P removal from different process stages of municipal wastewater by immobilized microalgae. *Bioresource Technology*, 154:260–266.
- Shi, X.-M., Liu, H.-J., Zhang, X.-W., and Chen, F. (1999). Production of biomass and lutein by *Chlorella protothecoides* at various glucose concentrations in heterotrophic cultures. *Process Biochemistry*, 34(4):341–347.
- Shoguchi, E., Shinzato, C., Kawashima, T., Gyoja, F., Mungpakdee, S., Koyanagi, R., Takeuchi, T., Hisata, K., Tanaka, M., Fujiwara, M., Hamada, M., Seidi, A., Fujie, M., Usami, T., Goto, H., Yamasaki, S., Arakaki, N., Suzuki, Y., Sugano, S., Toyoda, A., Kuroki, Y., Fujiyama, A., Medina, M., Coffroth, M. A., Bhattacharya, D., and Satoh, N. (2013). Draft assembly of the *Symbiodinium minutum* nuclear genome reveals dinoflagellate gene structure. *Current Biology*, 23(15):1399–1408.
- Slegers, P. M., Lösing, M. B., Wijffels, R. H., van Straten, G., and van Boxtel, A. J. B. (2013). Scenario evaluation of open pond microalgae production. *Algal Research*, 2(4):358–368.

References

- Smayda, T. J. (1997). Harmful algal blooms: Their ecophysiology and general relevance to phytoplankton blooms in the sea. *Limnology and Oceanography*, 42:1137–1153.
- Solbach, M. D. (2016). *Vergleich von Mikroalgen nach Wachstum auf Biofilmen unterschiedlicher Substrate*. Bachelor thesis, University of Cologne.
- Spector, D. L. (1984). *Dinoflagellates*. Academic Press, INC.
- Stein, F. (1883). Der Organismus der Infusionstiere. III. Abt. Der Organismus der Arthrodelen Flagellaten. Einleitung und Erklärung der Abbildungen. In *Der Organismus der arthrodelen Flagellaten*. W. Engelmann, Leipzig.
- Strain, H. (1976). Algal carotendoids. Structural studies on peridinin. *Acta Chemica Scandinavica B*, 30:109–120.
- Strain, H. H., Manning, W. M., and Hardin, G. (1944). Xanthophylls and Carotenes of Diatoms, Brown Algae, Dinoflagellates, and Sea-anemones. *Biological Bulletin*, 86(3):169–191.
- Sugawara, T., Yamashita, K., Sakai, S., Asai, A., Nagao, A., Shiraishi, T., Imai, I., and Hirata, T. (2007). Induction of apoptosis in DLD-1 human colon cancer cells by peridinin isolated from the dinoflagellate, *Heterocapsa triquetra*. *Bioscience, Biotechnology, and Biochemistry*, 71(4):1069–72.
- Sullivan, J. M., Swift, E., Donaghay, P. L., and Rines, J. E. B. (2003). Small-scale turbulence affects the division rate and morphology of two red-tide dinoflagellates. *Harmful Algae*, 2(3):183–199.
- Takahashi, S., Whitney, S. M., and Badger, M. R. (2009). Different thermal sensitivity of the repair of photodamaged photosynthetic machinery in cultured *Symbiodinium* species. *Proceedings of the National Academy of Sciences of the United States of America*, 106(9):3237–3242.
- Tam, N. F. Y. and Wong, Y. S. (2000). Effect of immobilized microalgal bead concentrations on wastewater nutrient removal. *Environmental Pollution*, 107(1):145–151.

- Tampion, J. and Tampion, M. D. (1987). *Immobilized cells: Principles and Applications. Cambridge Studies in Biotechnology.* Cambridge University Press, Cambridge.
- Taylor, F. J. R. (1980). On dinoflagellate evolution. *Biosystems*, 13(1-2):65–108.
- Tobias, R. D. and Lariree, V. M. (2013). *Dinoflagellates Biology, geographical Distribution and Economic Importance.* Nova Biomedical, New York.
- Tsunematsu, Y., Ohno, O., Konishi, K., Yamada, K., Suganuma, M., and Uemura, D. (2009). Symbiospirols: Novel long carbon-chain compounds isolated from symbiotic marine dinoflagellate *Symbiodinium* sp. *Organic Letters*, 11(10):2153–2156.
- Uduman, N., Qi, Y., Danquah, M. K., Forde, G. M., and Hoadley, A. (2010). Dewatering of microalgal cultures: A major bottleneck to algae-based fuels. *Journal of Renewable and Sustainable Energy*, 2(1):012701.
- Ugwu, C. U., Aoyagi, H., and Uchiyama, H. (2008). Photobioreactors for mass cultivation of algae. *Bioresource Technology*, 99(10):4021–4028.
- Varkitzi, I., Pagou, K., Granéli, E., Hatzianestis, I., Pyrgaki, C., Pavlidou, A., Montesanto, B., and Economou-Amilli, A. (2010). Unbalanced N:P ratios and nutrient stress controlling growth and toxin production of the harmful dinoflagellate *Prorocentrum lima* (Ehrenberg) Dodge. *Harmful Algae*, 9(3):304–311.
- Wan, M., Wang, Z., Zhang, Z., Wang, J., Li, S., Yu, A., and Li, Y. (2016). A novel paradigm for the high-efficient production of phycocyanin from *Galdieria sulphuraria*. *Bioresource Technology*, 218:272–278.
- Wang, S., Chen, J., Li, Z., Wang, Y., Fu, B., Han, X., and Zheng, L. (2015). Cultivation of the benthic microalga *Prorocentrum lima* for the production of diarrhetic shellfish poisoning toxins in a vertical flat photobioreactor. *Bioresource Technology*, 179:243–8.
- Warner, M. E. and Berry-Lowe, S. (2006). Differential xanthophyll cycling and photochemical activity in symbiotic dinoflagellates in multiple locations of three species of Caribbean coral. *Journal of Experimental Marine Biology and Ecology*, 339(1):86–95.

References

- Wegmann, K. and Metzner, H. (1971). Synchronization of *Dunaliella* cultures. *Archiv für Mikrobiologie*, 78(4):360–367.
- Wilkie, A. C. and Mulbry, W. W. (2002). Recovery of dairy manure nutrients by benthic freshwater algae. *Bioresource Technology*, 84(1):81–91.
- WWF Australia, Hoegh-Guldberg, O., Hoegh-Guldberg, H., Veron, J., Green, A., Gomez, E. D., Lough, J., King, M., Ambariyanto, Hansen, L., Cinner, J., Dews, G., Russ, G., Schuttenberg, H. Z., Peñaflor, E., Eakin, C. M., Christensen, T. R. L., Abbey, M., Areki, F., Kosaka, R. A., Tewfik, A., and Oliver, J. (2009). *The Coral Triangle and Climate Change: Ecosystems, People and Societies at Risk*. Technical report, WWF Australia, Brisbane.
- Xia, S., Wang, K., Wan, L., Li, A., Hu, Q., and Zhang, C. (2013). Production, characterization, and antioxidant activity of fucoxanthin from the marine diatom *Odontella aurita*. *Marine Drugs*, 11(7):2667–2681.
- Xiang, T., Hambleton, E. A., Denofrio, J. C., Pringle, J. R., and Grossman, A. R. (2013). Isolation of clonal axenic strains of the symbiotic dinoflagellate *Symbiodinium* and their growth and host specificity. *Journal of Phycology*, 49(3):447–458.
- Yoon, H. S., Hackett, J. D., and Bhattacharya, D. (2002). A single origin of the peridinin- and fucoxanthin-containing plastids in dinoflagellates through tertiary endosymbiosis. *Proceedings of the National Academy of Sciences of the United States of America*, 99(18):11724–9.
- Yoshida, J., Nakagawa, M., Seki, H., and Hino, T. (1992). Total synthesis of symbio-ramide, a novel Ca²⁺-ATPase activator from *Symbiodinium* sp. *Journal of the Chemical Society, Perkin Transactions 1*:343–350.
- Yoshida, T., Maoka, T., Das, S. K., Kanazawa, K., Horinaka, M., Wakada, M., Satomi, Y., Nishino, H., and Sakai, T. (2007). Halocynthiaxanthin and peridinin sensitize colon cancer cell lines to tumor necrosis factor-related apoptosis-inducing ligand. *Molecular Cancer Research*, 5(6):615–25.

- Zeng, X., Danquah, M. K., Zheng, C., Potumarthi, R., Chen, X. D., and Lu, Y. (2012). NaCS-PDMDAAC immobilized autotrophic cultivation of *Chlorella* sp. for wastewater nitrogen and phosphate removal. *Chemical Engineering Journal*, 187:185–192.
- Zhang, W., Wang, J., Wang, J., and Liu, T. (2014). Attached cultivation of *Haematococcus pluvialis* for astaxanthin production. *Bioresource Technology*, 158:329–335.

Acknowledgements

First of all I would like to thank my thesis advisor Prof. Dr. Michael Melkonian for his support and guidance in the last 7 years. I am grateful for the opportunity to work on this thesis and at the University of Cologne. I would like to thank Prof. Dr. Burkard Becker not only for the second review of this thesis, but his input and help during my work at the AG Melkonian. Thank you to Dr. Björn Podola for his advise during Bachelor, Master and PhD thesis and providing me with knowledge and help on biotechnological experiments, discussions and the preparation of the perfect cup of coffee. I am also thankful to Professor Dr. Michael Bonkowski for being the chairman of the defence committee and to Lenka Caisova for taking part in this committee.

It was a great time to work with the Biotechnology Group of Professor Melkonian. For this and all their support I thank Dr. Alice Kiperstok, Dr. Alice Ekelhof, Bastian Piltz, Frederik Koepsell, Dr. Tong Li and last but not least Zehra Cebi. I would like to thank all members of the CCAC, especially Dr. Barbara Melkonian and Nicole Feja for their advise and help as well as the supply of my now favourite species *Symbiodinium voratum*. Thanks for the support from the workshop and the gardeners at the Biozentrum Cologne. In general I would like to thank all the members of the AG Melkonian and AG Becker for creating a most welcoming working environment and providing me with inspirations for my scientific work or distractions from it as needed. Thanks to Martin Rippin for about 200 km of entertainment and friendship and Tanja Reeder for tons of good times and million of lunches. Thank you to Nicole Sausen who has been my saviour in more than one situation. A big thank you is dedicated to Ruben M. Benstein for introducing me to this topic and helping me to proof read this thesis, I certainly had less work with yours. However I am most grateful for every single concert and beer we shared.

Thank you to my family and friends for never quite understanding what I do all day and still supporting me every step of the way. Especially thanks to Stephan Fieberg for the IT, LateX, Tech support and taking care of my every need for the last 15 years.

It would not been possible or not as much fun without any of you - thank you.

Erklärung

Ich versichere, dass ich die von mir vorgelegte Dissertation selbständig angefertigt, und die benutzten Quellen und Hilfsmittel vollständig angegeben und die Stellen der Arbeit (einschließlich Tabellen, Karten und Abbildungen), die anderen Werken im Wortlaut oder dem Sinn nach entnommen sind, in jedem Einzelfall als Entlehnung kenntlich gemacht habe; dass diese Dissertation noch keiner anderen Fakultät oder Universität zur Prüfung vorgelegen hat; dass sie (abgesehen von unten angegebenen Teilpublikationen) noch nicht veröffentlicht worden ist sowie, dass ich eine solche Veröffentlichung vor Abschluss des Promotionsverfahrens nicht vornehmen werde. Die Bestimmungen der Promotionsordnung sind mir bekannt.

Die von mir vorgelegte Dissertation ist von Prof. Dr. Michael Melkonian betreut worden.

Köln, den 05.09.2016

Dorothee Langenbach